(2)

NAVAL POSTGRADUATE SCHOOL
Monterey, California

THESIS

SHORT TERM TELECONNECTIONS
ASSOCIATED WITH
AN INDIVIDUAL TROPICAL CYCLONE

by

Stephen C. Woll

December, 1993

Thesis Advisor: James Thomas Murphree

Approved for public release; distribution is unlimited.

REPORT DOCUMENTATION PAGE

Form Approved OMB No. 0704

1. AGENCY USE ONLY *(Leave blank)*	2. REPORT DATE December 1993	3. REPORT TYPE AND DATES COVERED Master's Thesis

4. TITLE AND SUBTITLE *SHORT TERM TELECONNECTIONS ASSOCIATED WITH AN INDIVIDUAL TROPICAL CYCLONE

5. FUNDING NUMBERS

6. AUTHOR(S) *Stephen C. Woll

7. PERFORMING ORGANIZATION NAME(S) AND ADDRESS(ES)
Naval Postgraduate School
Monterey CA 93943-5000

8. PERFORMING ORGANIZATION REPORT NUMBER

9. SPONSORING/MONITORING AGENCY NAME(S) AND ADDRESS(ES)

10. SPONSORING/MONITORING AGENCY REPORT NUMBER

11. SUPPLEMENTARY NOTES The views expressed in this thesis are those of the author and do not reflect the official policy or position of the Department of Defense or the U.S. Government.

12a. DISTRIBUTION/AVAILABILITY STATEMENT
Approved for public release; distribution is unlimited.

12b. DISTRIBUTION CODE
*A

13. ABSTRACT *(maximum 200 words)*

The short term teleconnections associated with an individual western Pacific tropical cyclone have been investigated using an atmospheric general circulation model. The general strategy was to use the GCM, in combination with several tropical cyclone bogusing procedures, to isolate the effects on the global circulation of the tropical cyclone. The bogusing procedures were used to alter the tropical cyclone in the initial conditions for the model.

The primary modeling experiments involved using the tropical cyclone bogusing procedures to include or exclude the tropical cyclone from the initial conditions. The difference between model results that contained the tropical cyclone and those that did not were used to analyze the global response to the tropical cyclone.

These results showed a strong and persistent teleconnection response in the extratropical northern hemisphere. This response was mainly evident in slowly propagating Rossby waves in the 200 mb height field. Examinations of the teleconnection mechanisms showed that the east Asian-north Pacific jet played a major role in the development of the teleconnection. In particular: (1) the 200 mb height responses showed a consistent relationship with the jet; (2) the jet acted as a waveguide for the Rossby wave energy; and (3) the regions of potential barotropic instability which flank the jet were often colocated with areas of wave amplilfication.

14. SUBJECT TERMS *Teleconnections; Tropical Cyclones; Tropical Cyclone Bogusing; Jet Stream.

15. NUMBER OF PAGES * 138

16. PRICE CODE

17. SECURITY CLASSIFICATION OF REPORT	18. SECURITY CLASSIFICATION OF THIS PAGE	19. SECURITY CLASSIFICATION OF ABSTRACT	20. LIMITATION OF ABSTRACT
Unclassified	Unclassified	Unclassified	UL

NSN 7540-01-280-5500

Standard Form 298 (Rev. 2-89)
Prescribed by ANSI Std. 239-18

Approved for public release; distribution is unlimited.

Short Term Teleconnections Associated With An Individual Tropical Cyclone

by

Stephen C. Woll
Lieutenant, United States Navy
B.S., Duke University, 1983

Submitted in partial fulfillment
of the requirements for the degree of

MASTER OF SCIENCE IN METEOROLOGY AND PHYSICAL OCEANOGRAPHY

from the

NAVAL POSTGRADUATE SCHOOL
December 1993

Author: _____
Stephen C. Woll

Approved by: _____
James Thomas Murphree, Thesis Advisor

_____
Ronald Gelaro, Second Reader

_____
Robert L. Haney, Chairman
Department of Meteorology

ABSTRACT

The short term teleconnections associated with an individual western Pacific tropical cyclone have been investigated using an atmospheric general circulation model. The general strategy was to use the GCM, in combination with several tropical cyclone bogusing procedures, to isolate the effects on the global circulation of the tropical cyclone. The bogusing procedures were used to alter the tropical cyclone in the initial conditions for the model.

The primary modeling experiments involved using the tropical cyclone bogusing procedures to include or exclude the tropical cyclone from the initial conditions. The difference between model results that contained the tropical cyclone and those that did not were used to analyze the global response to the tropical cyclone.

These results showed a strong and persistent teleconnection response in the extratropical northern hemisphere. This response was mainly evident in slowly propagating Rossby waves in the 200 mb height field. Examinations of the teleconnection mechanisms showed that the east Asian/North Pacific jet played a major role in the development of the teleconnection. In particular: (1) the 200 mb height responses showed a consistent relationship with the jet; (2) the jet acted as a waveguide for the Rossby wave energy; and (3) the regions of potential barotropic instability which flank the jet were often colocated with areas of wave amplification.

TABLE OF CONTENTS

LIST OF TABLES

LIST OF FIGURES

LIST OF ACRONYMS AND SYMBOLS

BTI	barotropic instability
β	total derivative of the Coriolis parameter
EA	ensemble average
Forecast 1	15 day NOGAPS model run started from 26 November 1991 00Z initial conditions
Forecast 2	15 day NOGAPS model run started from 27 November 1991 12Z initial conditions
Forecast 3	15 day NOGAPS model run started from 29 November 1991 00Z initial conditions
FNOC	Fleet Numerical Oceanography Center
GCM	general circulation model
gpm	geopotential meter
H1	first positive (anticyclonic) 200 mb geopotential height difference; i.e., a "high" in the height differences
H2	second positive (anticyclonic) 200 mb geopotential height difference; i.e., a "high" in the height differences
IDEA Lab	Interactive Digital Environmental Analysis Laboratory
L1	first negative (cyclonic) 200 mb geopotential height difference; i.e., a "low" in the height differences
m	meter
mb	millibar
NCAR	National Center for Atmospheric Research
NEGATIVE	bogusing procedure which applies modified tropical cyclone bogusing procedure to remove storm; also used to refer to runs with initial conditions produced by this bogusing procedure

NO	bogusing procedure which does not apply any tropical cyclone bogus to data assimilation; also used to refer to runs with initial conditions produced by this bogusing procedure
NOGAPS	Navy Operational Global Atmospheric Prediction System
NRL	Naval Research Laboratory
OLR	outgoing longwave radiation
PNA	Pacific-North American
POSITIVE	bogusing procedure which applies standard tropical cyclone bogus to data assimilation; also used to refer to runs with initial conditions produced by this bogusing procedure
QG	quasi-geostrophic
s	second
SLP	sea level pressure
T79	triangular 79 truncation
u_{yy}	second meridional derivative of the zonal wind component
W	watt
Z	Zulu time (Greenwich Mean Time)

ACKNOWLEDGEMENTS

I would like to thank Professor Tom Murphree and Dr. Ron Gelaro for their energy, guidance, and explanations. Dr. Jim Goerss also assisted in designing the procedures and conducting the model runs upon which this study is based. Most importantly, I would like to thank my wife Sue for her patience, support, and understanding.

I. INTRODUCTION

A. OVERVIEW

A tremendous amount of effort has been directed in the past forty years at improving atmospheric forecasts. These efforts have produced current forecasts of synoptic scale weather systems that are fairly accurate and useful to about 72 hours. The improvement of our *extended range* (e.g., one to two week) forecasts has been a major focus of study for the last twenty years.

Many of these studies have indicated that useful extended range forecasts of large scale, quasistationary systems may be possible (e.g., Chelliah et al. 1988). These large scale systems remain in approximately the same location for days or weeks at a time and strongly influence the strength and location of the smaller scale synoptic systems.

These quasi-stationary systems, or low frequency waves, are especially evident in large scale views of time mean circulations and circulation anomalies. Figure 1(a) shows an example of such anomalies from November 1991. Note the large scale pattern of cyclonic and anticyclonic anomalies extending from the tropical northwestern Pacific across the north Pacific and North American region.

Associated with these circulation anomalies were strong negative outgoing longwave radiation (OLR) anomalies extending from the equator and dateline northwestward toward Japan (Figure 1(b)). These areas of negative OLR anomalies correspond to increased convective cloudiness and tropospheric heating. The negative OLR anomaly in the western Pacific lies along the paths taken by the two major tropical cyclones of November 1991. These were supertyphoon Seth, which did not recurve and made landfall on the coast of China, and supertyphoon Yuri, which did recurve and passed to the east of Japan before dissipating in the north Pacific.

By improving our forecasts of large scale, low frequency waves such as those shown in Figure 1(a), we may be able to improve extended range forecasts of the synoptic systems which are steered by these larger scale waves. One area of research that has contributed to the prediction of these quasi-stationary waves is the study of atmospheric teleconnections.

A **teleconnection** is a statistically significant correlation between time-varying atmospheric parameters at widely separated locations (cf. Horel and Wallace 1981, Wallace and Gutzler 1981). Certain teleconnections, if carefully used, may be useful predictors of large scale quasi-stationary waves (cf. Chelliah et al. 1988).

Many teleconnection studies have been conducted using observational data. While these have produced many important insights, they have been limited by, among other things, sparse data in many regions and the inability to vary experimental conditions.

Modeling studies of teleconnections can overcome both of these limitations. A numerical general circulation model (GCM) can give high temporal and spatial resolution and allow manipulation of initial and boundary conditions.

However, in order to be useful, a model must give a realistic simulation of both the background atmosphere in which the model teleconnections occur and the specific atmospheric processes involved in producing the teleconnections. If a model is unsuccessful in simulating these features of the atmosphere, then its usefulness is severely limited.

Consequently, a model that is to be used for teleconnection studies must first pass several simulation tests. Once it has been demonstrated that the model provides realistic simulations, it can then be used to evaluate specific hypotheses.

This study uses the U.S. Navy's operational global forecast model to examine short term teleconnections associated with individual tropical cyclones.

B. REVIEW OF PREVIOUS TELECONNECTION STUDIES

1. INTERANNUAL TELECONNECTIONS

The Southern Oscillation is a global scale shift in atmospheric mass that may be seen in variations of sea level pressure. The centers of this shift, where the sea level pressure anomalies are largest, are over the southeastern Pacific and the tropical western Pacific and Indian Oceans. During years when sea level pressures in the southeastern Pacific have been higher than the climatological values, the sea level pressures in the tropical western Pacific and Indian Oceans have been lower than the climatological values. Thus, the pressure anomalies in these two regions have tended to vary out of phase with each other.

The sign of these pressure anomalies (positive or negative) have tended to remain the same for a year or more and then reverse. Thus, these anomaly variations have a distinct interannual time scale.

In the first modern teleconnection study, Walker and Bliss (1932) correlated this oscillation in sea level pressures with other atmospheric fluctuations throughout the world. Later researchers, with far more data and processing capability, linked the Southern Oscillation to additional fluctuations in the tropical and global atmosphere and ocean. The most well known event linked to the Southern

Oscillation is the ocean-atmosphere phenomenon known as El Niño.

El Niño is characterized by the appearance of a pool of relatively warm surface water off the tropical west coast of South America. Bjerknes (1966) linked the appearance of this warm pool with a number of physically remote events, including weakened equatorial easterlies, stronger midlatitude westerlies, a deepening of the Aleutian low, and a weakening of the Icelandic low.

Later papers by Bjerknes also connected El Niño with heavy precipitation in the tropical Pacific, stronger westerlies in the central and northeastern Pacific, and the appearance of twin upper tropospheric anticyclones straddling the equator (Bjerknes 1969, 1972).

In his pioneering series of studies, Bjerknes identified widely scattered yet related events. But he could only suggest some possible mechanisms that might link them all together.

In the years following Bjerknes' papers, a large number of research efforts identified several teleconnection patterns that appeared repeatedly in different data sets. Many of these were found to originate over the Pacific Ocean, and some of the strongest were found to occur during the northern hemisphere winter.

Wallace and Gutzler (1981) reviewed a number of previously identified interannual teleconnection patterns

found during the northern hemisphere winter. Using more complete and up to date data sets, they were able to verify several of these patterns, including the Pacific-North America (PNA) pattern. Horel and Wallace (1981) also found significant correlations at an interannual time scale between the sea surface temperature in the equatorial Pacific and the 700 mb geopotential heights in the extratropical northern hemisphere.

2. INTRASEASONAL TELECONNECTIONS

Nitta (1987) examined the correlation during the northern hemisphere summer between tropical western Pacific convection and the strength of the midlatitude westerlies in a study that examined both interannual and intraseasonal teleconnections. On the interannual time scale, Nitta compared years in which sea surface temperatures in the tropical western Pacific were warmer or colder than usual. At the intraseasonal time scale, he compared periods of stronger and weaker OLR in the region between the Philippines and Japan.

In general, Nitta found geopotential height patterns similar to those seen in earlier works (e.g., Wallace and Gutzler 1981, Horel and Wallace 1981), in which northern hemisphere geopotential heights were strongly linked to variations in tropical convection. The shape, spacing, and tilt of these height patterns indicated that quasi-

stationary Rossby wave energy was being propagated poleward and eastward out of the tropical western Pacific (cf. Hoskins and Karoly 1981). A schematic of the pattern found by Nitta is shown in Figure 2.

Nitta's calculations showed that the magnitude of the intraseasonal variation was more than twice that of the interannual variation, especially in years for which tropical sea surface temperatures were warmer than normal.

Teleconnection mechanisms were investigated by Murphree (1994), who used a simple global circulation model to study the role of the background jet stream in the teleconnection process. Murphree used the quasi-geostrophic wave activity flux vector (Plumb 1985) to track the wave energy associated with the model's teleconnections. He found that the north Pacific jet stream served as a barrier to Rossby wave energy propagating away from the tropical forcing region. In effect, the jet acted as a waveguide that focused energy emanating from the tropics.

Murphree (1994) also hypothesized that the regions of barotropic instability which flank the exit regions of the jet may have an amplifying effect on the wave energy propagating out of the tropics and along the jet.

In order to test this hypothesis, Gelaro and Murphree (1994) used a general circulation model to investigate the midlatitude response to an increase in tropical sea surface temperatures in the eastern Pacific. They focused on the

sensitivity of the midlatitude quasi-stationary wave response to variations in the midlatitude background flow. Their results were in basic agreement with those from Murphree (1994). However, they found that the intraseasonal variation in the model's north Pacific jet had a profound impact on tropical-extratropical teleconnections.

Intraseasonal variations in the midlatitude westerly jet were evaluated in a modeling study by Neith (1992), who found that the north Pacific jet was well correlated at intraseasonal time scales with the amount of convection found over the tropical Indian and western Pacific oceans. A stronger jet was associated with increased deep convection and tropospheric heating over the tropical western Pacific and reduced convection and heating over the Indian Ocean.

3. SHORT TERM TELECONNECTIONS

Chang and Lum (1985) used observations of the northern hemisphere winter circulation to examine the response of the midlatitude jet to variations in tropical convection. They focused on tropical convection events that lasted from several days to a week. They examined, in particular, convection variations associated with cold surges and tropical cyclones.

Their higher frequency data showed a strong positive correlation between increased tropical convection and the strength of the east Asian jet stream maximum, which was

found approximately 25 degrees to the north of the convective activity. The response of the westerly jet to the tropical forcing showed no discernable time lag. However, Chang and Lum's examination of the convection events led them to conclude that the convection forced the acceleration in the winds, and not vice versa.

Chang and Lum (1985) proposed that the stronger tropical convection led to an increase in upper level divergent outflow over the area of convection which, through Coriolis turning, intensified the upper tropospheric westerlies.

Hurrell and Vincent (1990) found similar high frequency teleconnection results in the southern hemisphere during January to March 1979. In their study, they found the subtropical jet stream near Australia strengthened within a day after convection near Indonesia intensified.

Hurrell and Vincent (1991) showed that this jet strengthening involved the conversion of the divergent kinetic energy of the upper level outflow from the tropical convective areas into the rotational kinetic energy of the extratropical jet.

Both the Chang and Lum (1985) and Hurrell and Vincent (1990, 1991) studies showed observationally that there were periods when tropical atmospheric heating was linked to the strength of the midlatitude westerly jet stream. This linkage took place on short time scales (less than a week).

Harr et al. (1991) also looked at high frequency events in a study of extratropical circulation anomalies associated with observed tropical cyclones in the western Pacific. They showed that tropical cyclones that recurved into the northern subtropics were associated with strong flow anomalies over the north Pacific. Further, the anomaly pattern was similar to the apparent Rossby wave train found by Nitta (1987), Murphree (1994), and Gelaro and Murphree (1994). The extratropical flow anomalies associated with tropical cyclones that remained in the tropics were much weaker and less coherent.

Building on this work, Miller (1993) examined the impact of an individual tropical cyclone on the global atmosphere in a GCM study. Miller showed that the presence of supertyphoon Yuri in November and December 1991 resulted in significant changes in the 200 mb heights and jet over the north Pacific and North America.

4. SUMMARY

Teleconnections between widely separated atmospheric events have been documented for more than half a century. Walker and Bliss (1932) correlated the Southern Oscillation with events throughout the world, while Bjerknes (1966, 1969, 1972) connected the Southern Oscillation and El Niño to northern winter circulation anomalies.

The studies of Nitta (1987), Chang and Lum (1985), and Harr et al. (1991) examined teleconnections occurring at intraseasonal time scales. Miller (1993) linked an individual tropical cyclone to changes in the midlatitude westerly jet stream.

At the same time, other investigators searched for physical mechanisms to explain these observed teleconnections. The results of Horel and Wallace (1981), Hoskins and Karoly (1981), Nitta (1987), and Harr et al. (1991) indicated that the propagation of Rossby wave energy was involved in establishing teleconnections.

Murphree (1994) and Gelaro and Murphree (1994) demonstrated the role of the midlatitude jet as a waveguide which channelled along the jet the wave energy associated with teleconnections. They also found that this wave energy was often greatly enhanced in areas which had the potential for barotropic instability.

This study, like those of Harr et al. (1991) and Miller (1993), focuses on the short term teleconnections associated with individual tropical cyclones. A particular focus of this study are the physical mechanisms involved in producing such teleconnections.

C. DESIGN OF THIS STUDY

This study builds on the methodology and analyses used by Miller (1993), Murphree (1994), and Gelaro and Murphree

(1994) to examine the impacts of supertyphoon Yuri on the global atmosphere. A preliminary examination of a second case study, involving typhoons Gay and Hunt during November 1992, was also conducted for this study.

This study investigates two main hypotheses, developed from several previous studies (especially Miller 1993, Murphree 1994, and Gelaro and Murphree 1994):

- Hypothesis 1: Individual tropical cyclones can produce strong teleconnections.
- Hypothesis 2: The development of the teleconnection is strongly influenced by the waveguiding and amplification effects of the midlatitude westerly jet.

The basic strategy of this study was to use a GCM in conjunction with variations of a tropical cyclone bogusing procedure to simulate the global impacts of an individual tropical cyclone. Various tropical cyclone bogusing procedures were used, during the data assimilation process, in order to:

1. retain the tropical cyclone in the model atmosphere, and
2. remove the tropical cyclone from the model atmosphere.

The methods used are described in Chapter II. The results are presented in Chapter III. Conclusions and recommendations are given in Chapter IV.

II. METHODS

A. TROPICAL CYCLONE SELECTION

For our initial study of the teleconnections arising from an individual tropical cyclone, we wanted to model a tropical cyclone that appeared likely to produce strong teleconnections. Previous investigations have found that strong teleconnections might be expected:

- during the northern hemisphere winter (Wallace and Gutzler 1981, Chang and Lum 1985), and
- when the tropical cyclone track extends poleward into regions of westerly flow, which is most likely to occur if the tropical cyclone recurves (Harr et al. 1991).

In addition, we anticipated that a strong tropical cyclone would be more likely than a weak one to produce strong teleconnections.

Based on these criteria, we chose to examine supertyphoon Yuri, which occurred in November and December 1991. This was a very strong tropical cyclone, maintaining typhoon status for 8 days (24 November - 1 December 1991) and supertyphoon status (winds greater than 70 m/s) for more than two days (26-29 November 1991).

A second set of model runs was carried out to simulate typhoons Gay and Hunt, which took place in November and December 1992. Because of problems with the model's representation of these tropical cyclones, results for these

tropical cyclones are not presented in detail in this study. However, Chapter IV briefly reviews how the results from the Gay and Hunt runs compared to the results for Yuri.

B. MODEL DESCRIPTION

This study was conducted using output from the U.S. Navy Global Atmospheric Prediction System (NOGAPS) general circulation model. This is a full physics spectral model used for operational weather prediction by the U.S. Navy. It uses triangular 79 (T79) truncation, corresponding to a horizontal resolution of 1.5 degrees. It has 18 levels and a time step of 30 minutes. The NOGAPS model is described more fully in Hogan and Rosmond (1991).

The model runs for this study were conducted by Dr. R. Gelaro and Dr. J. Goerss at the Naval Research Laboratory (NRL) in Monterey, California. The model was run using the computing facilities of the Fleet Numerical Oceanography Center (FNOC). Postprocessing of the model output was done in the Interactive Digital Environmental Analysis (IDEA) Laboratory, Naval Postgraduate School, Monterey, California, using NCAR Graphics Version 3.0 software.

C. TROPICAL CYCLONE BOGUSING PROCEDURES

The spatial resolution of most general circulation models, including NOGAPS, is too coarse to allow accurate representation of tropical cyclones. In order to improve

the model's simulation of these relatively small scale tropical cyclones, synthetic data assimilation (bogusing) procedures have been added to some operational weather models. The introduction of a tropical cyclone bogus is used to produce a more realistic representation of the tropical cyclone in the forecast model's initial conditions. In particular, tropical cyclone bogusing is done to provide a more realistic tropical cyclone intensity and track, and to induce realistic impacts on the surrounding circulation. Goerss et al. (1991) includes a description of the NOGAPS tropical cyclone bogusing procedure. The effectiveness of this procedure is evaluated by Fiorino et al. (1991).

In this study, we use the tropical cyclone bogusing procedure as an experimental tool for selectively altering an individual tropical cyclone in the model's initial conditions. The standard operational tropical cyclone bogusing procedure was used to calculate a set of initial conditions with a relatively realistic representation of the tropical cyclone. A modified version of the tropical cyclone bogusing procedure was used to remove the tropical cyclone, leaving only the prevailing background circulation. This use of the tropical cyclone bogusing procedure as an experimental tool permits studies of tropical cyclone impacts that are not possible in observational studies.

In this study, three variations of the NOGAPS tropical cyclone bogusing procedure were employed. These variations

affected only the initial conditions used to start the model runs. The NOGAPS model itself was identical for all of the model results presented in this study.

1. POSITIVE BOGUS

The first variation applied the NOGAPS tropical cyclone bogusing procedure to the data assimilation when tropical cyclone wind speeds reached a prescribed level (18 m/s). This was referred to as the POSITIVE bogus. This is the procedure used by FNOC to prepare the initial conditions used for operational runs of the NOGAPS model. The POSITIVE tropical cyclone bogusing procedure tends to produce the most realistic initial strength and position for the tropical cyclone.

2. NO BOGUS

The second variation did not apply the tropical cyclone bogusing procedure at any time during the data assimilation. This was referred to as the NO bogus. This procedure tends to produce initial conditions in which the tropical cyclone exists, but with a less realistic intensity and location than those produced by the POSITIVE procedure.

3. NEGATIVE BOGUS

The third variation, the NEGATIVE tropical cyclone bogusing procedure, used a modification of the tropical cyclone bogusing procedure to remove the effects of the

tropical cyclone, leaving only the relatively large scale background circulation in the initial conditions.

D. MODEL RUNS

The three tropical cyclone bogusing procedures (POSITIVE, NO, and NEGATIVE) were used to provide initial conditions for each of three initial times. The three initial times for the supertyphoon Yuri case were 26 November 1991, 00Z; 27 November 1991, 12Z; and 29 November 1991, 00Z. The combination of three initial condition sets for three start times produced a total of nine model forecasts:

- three runs started on 26 November 1991, 00Z, called the Forecast 1 runs;
- three runs started on 27 November 1991, 12Z, called the Forecast 2 runs; and
- three runs started on 29 November 1991, 00Z, called the Forecast 3 runs.

The nine model runs may be grouped according to the tropical cyclone bogusing procedures used to develop their initial conditions. This grouping gives:

- three runs started with initial conditions produced with the POSITIVE tropical cyclone bogusing procedure, called the POSITIVE runs;
- three runs started with initial conditions produced with NO tropical bogusing procedure, called the NO runs;
- three runs started with initial conditions produced with the NEGATIVE tropical cyclone bogusing procedure, called the NEGATIVE runs;

Each run is referred to by its initialization time and the tropical cyclone bogusing procedure used to calculate its initial conditions. For example, the run started on 26 November 1991 at 00Z, using initial conditions from the POSITIVE tropical cyclone bogusing procedure, is called the Forecast 1 POSITIVE run.

Each of the nine runs lasted 15 days. Figure 3 shows these nine model runs schematically, along with the data assimilation procedures used to calculate the initial conditions for each run. Note that the nine runs differ only in their initial conditions. For any of the three start times, the differences in the runs are due solely to the different tropical cyclone bogusing procedures used to develop the initial conditions for that start time.

E. ANALYSES OF MODEL RESULTS

In order to assess the global impacts of Yuri, the output from the nine model runs was analyzed in terms of:

a) individual fields from individual runs (e.g., the 200 mb geopotential height field from the POSITIVE Forecast 1 run);

b) difference fields (e.g., the difference between the 200 mb height fields from the POSITIVE Forecast 1 and NEGATIVE Forecast 1 runs);

c) ensemble average fields (e.g., the average of the 200 mb height fields from the POSITIVE Forecast 1, POSITIVE Forecast 2, POSITIVE Forecast 3 runs at corresponding times); and

d) combinations of a & b, a & c, and b & c.

To distinguish the individual fields from the difference fields, the individual fields are referred to as **total** fields.

The difference fields were used to analyze the impacts of the different initial conditions on the model's global atmosphere. In the case of a POSITIVE - NEGATIVE difference, the difference shows the model's **response** to the presence of the tropical cyclone in the initial conditions. This is also the case for a NO - NEGATIVE difference, since the NO run contains a representation of the tropical cyclone. A POSITIVE - NO difference shows the model's response to the operational tropical cyclone bogusing procedure. In this study, we have focused on the POSITIVE - NEGATIVE differences, since they provide the most realistic simulation of the model's response to the presence of an individual tropical cyclone.

Table 1 summarizes the model runs performed with the different tropical cyclone bogusing procedures. Table 2 summarizes the differences between these runs.

F. ENSEMBLE AVERAGING OF MODEL OUTPUT

Ensemble averaging is a process in which multiple representations of a single parameter are made at the same point in time and then averaged together. This process produces a relative enhancement of the features which the different representations have in common. This process was

applied to many of the model output fields in order to highlight the model runs' consistent global responses to a tropical cyclone.

As shown in Figure 4, the output from each of the three start times overlapped in time for much of the output period. For each output time at which the runs overlapped, the output for any field may be averaged to produce an ensemble average field. The overlap period is called the ensemble average period in Figure 4. Ensemble averages were calculated for several different model fields. This averaging was applied only to Forecast 1, Forecast 2, and Forecast 3 runs that used a common tropical cyclone bogusing procedure (e.g., to the Forecast 1, Forecast 2, and Forecast 3 POSITIVE runs; or to the Forecast 1, Forecast 2, and Forecast 3 NEGATIVE runs).

G. MODEL OUTPUT FIELDS

Several standard model output fields were analyzed for this study. These fields were provided by Dr. R. Gelaro of NRL on a 2.5 degree (latitude and longitude) global horizontal grid. Model output was available at the model's 00Z and 12Z times for each of the 15 days of each model run.

The following model fields were analyzed in this study.

1. SEA LEVEL PRESSURE

The sea level pressure, in millibars, was used to investigate:

(a) the initial conditions that were used to start the various runs; and

(b) the model runs' representations of the tropical cyclone track.

2. ATMOSPHERIC HEATING

The atmospheric heating, expressed in °C/day, is the vertical integral of the model's total heating. In the vicinity of a strong convective system, such as a tropical cyclone, this heating is dominated by the release of latent heat during convective cloud formation.

3. 200 MB GEOPOTENTIAL HEIGHTS

The 200 mb geopotential height, in geopotential meters (gpm), indicates the structure of the upper troposphere. These heights may be used to infer the upper tropospheric teleconnections and quasi-geostrophic wave dynamics.

4. 200 MB WINDS

The u and v components of the 200 mb winds, in m/s, describe the flow of mass through the upper troposphere.

H. WAVE AND INSTABILITY CALCULATIONS

Hypothesis 2 addresses the development of the teleconnection process (see Chapter I, Section C). In order

to analyze the mechanisms involved in the model's teleconnections, the following diagnostic quantities were calculated from the model's 200 mb heights and winds.

1. QUASI-GEOSTROPHIC WAVE ACTIVITY FLUX VECTORS

Quasi-geostrophic wave activity flux vectors, in m^2/s^2, were used to track the propagation of quasi-geostrophic wave energy through the model's upper troposphere (Plumb 1985).

These vectors provide a means to track the propagation, sources, and sinks of wave energy associated with teleconnections. The amount of energy propagating is proportional to the length of the vector. The vector direction indicates the propagation direction. Areas from which the vectors diverge represent energy sources, while areas into which they converge indicate energy sinks.

Plumb (1985) provided the mathematical derivation of the quasi-geostrophic wave activity flux vector, while Murphree (1994) and Gelaro and Murphree (1994) provided examples of their use in analyzing teleconnection mechanisms.

2. 200 MB POTENTIAL BAROTROPIC INSTABILITY

The studies of Murphree (1994) and Gelaro and Murphree (1994) indicated that barotropic instability may be an important process in providing energy for teleconnection processes. In those studies and in this one, areas of potential barotropic instability in the model's circulation were identified using the Rayleigh-Kuo criterion (Kuo 1949):

$$\beta - u_{yy} = 0 \qquad (1)$$

Here, β is the total derivative of the Coriolis parameter, and u_{yy} is the second meridional derivative of the 200 mb zonal wind. In this study, all fields of $\beta - u_{yy}$ have been smoothed with a nine-point horizontal smoother before being plotted.

It is important to remember that (1) is a necessary, but not sufficient, condition for the presence of barotropic instability. Consequently, (1) indicates only where barotropic instability might be an energy source, not where it necessarily is an energy source.

III. RESULTS FROM SUPERTYPHOON YURI CASE STUDY

A. INTRODUCTION

This chapter explores the results obtained from using the NOGAPS global circulation model (GCM) to simulate the atmosphere during and immediately after supertyphoon Yuri. Each of the experimental runs was made using the exact same model, but each run was started from a unique set of initial conditions. Nine runs were made, combining three start times (26 November 1991 00Z; 27 November 1991 12Z; and 29 November 1991 00Z) with three tropical cyclone bogusing procedures (POSITIVE, NO, and NEGATIVE). See Chapter II, Section D for a more complete description of all nine runs and the naming conventions used to refer to them in this study.

The use of a GCM to simulate a tropical cyclone and its global impacts requires that certain prerequisites have been met. These address:

(1) the validity of the tropical cyclone bogusing procedures used;

(2) the model's simulation of the tropical cyclone;

(3) the model's representation of the global background circulation.

These modeling prerequisites are listed briefly below and are addressed in more depth later in this chapter.

- Prerequisite 1: The tropical cyclone bogusing procedures have a large effect on the model's initial conditions only in the vicinity of the tropical cyclone.

- Prerequisite 2: Model simulations based on a tropical cyclone bogusing procedure that attempts to retain the tropical cyclone in the initial conditions give a realistic simulation of the tropical cyclone. Model simulations based on a tropical cyclone bogusing procedure that attempts to remove the tropical cyclone from the initial conditions do not simulate the tropical cyclone.

- Prerequisite 3: The model produces a realistic global circulation for all of the runs.

As shown in Figure 4, there was a common 12 day period for all nine model runs, the ensemble average period. The fourth prerequisite addresses the ensemble averaging process.

- Prerequisite 4: The major features of the individual runs are preserved when an ensemble average is made of those runs.

In the following sections, we address the first three prerequisites which must be satisfied in order for the modeling methodology to be valid. We then examine the results concerned with the prerequisite that addresses the ensemble averaging process. Finally, we evaluate our two hypotheses concerning the teleconnections that are associated with supertyphoon Yuri (see Chapter I, Section C for a summary of these hypotheses).

In cases where the results from just a single forecast are presented, Forecast 2 results are used because these results tend to be close to the average of the results from

all three forecasts. Comments are provided when the results of another forecast are significantly different.

B. PREREQUISITE 1 - THE EFFECT OF BOGUSING ON THE MODEL'S INITIAL CONDITIONS

For our modeling methodology to be valid, we must ensure that the tropical cyclone bogusing procedures used to modify the tropical cyclone in the model's initial conditions affect those initial conditions only in the vicinity of the tropical cyclone. If the tropical cyclone bogusing procedure has large effects on the initial conditions away from the tropical cyclone, then the model may develop spurious teleconnections that are not due to the effects of the tropical cyclone.

This first prerequisite can be restated as:

(1) the tropical cyclone bogusing procedures have their largest effects on the initial conditions in the vicinity of the tropical cyclone (referred to as the **local** effects), and

(2) the tropical cyclone bogusing procedures have small effects on the initial conditions elsewhere in the world (referred to as the **remote** effects).

To address this prerequisite, we examine the initial conditions for sea level pressure for Forecast 2. We also examine the differences between initial conditions, using the POSITIVE - NO, NO - NEGATIVE, and POSITIVE - NEGATIVE initial sea level pressure differences. These differences allow us to analyze the relative magnitudes of the local and

remote effects of the POSITIVE, NO, and NEGATIVE tropical cyclone bogusing procedures on the initial conditions.

1. SEA LEVEL PRESSURE INITIAL CONDITIONS

Figure 5 presents the initial sea level pressure fields for the Forecast 2 POSITIVE, NO, and NEGATIVE runs. These fields showed very similar features, except near Yuri, at about 140°E 15°N. The POSITIVE and NO run initial conditions placed Yuri at the center of a deep low pressure system. In the NEGATIVE run, this strong low pressure system was replaced by a much weaker monsoon trough, a common feature at this time of year.

The effects of the tropical cyclone bogusing procedure on the initial conditions are even more obvious in Figure 6, which gives the Forecast 2 POSITIVE - NO, NO - NEGATIVE, and POSITIVE - NEGATIVE initial sea level pressure differences. The largest differences were the local differences in the vicinity of Yuri (-16 mb for the POSITIVE - NO; -11 mb for NO - NEGATIVE; and -27 mb for POSITIVE - NEGATIVE differences). The largest remote difference found anywhere was -4 mb over the midlatitude south Pacific.

The sea level pressure initial conditions for Forecast 1 and Forecast 3 (not shown) displayed similar general features.

2. CONCLUSION

Ideally, all of the remote differences would have been close to zero. The fact that there were some must be weighed in the later interpretation of results. These remote effects are likely the result of the model's limited resolution (T79). Because of the finite resolution of our model, the perturbation of the tropical cyclone initial conditions (due to the introduction of a bogus) tends to induce unwanted (but unavoidable) perturbations elsewhere. Such remote effects are especially likely given the small spatial scale at which the tropical cyclone bogusing procedure is applied.

However, Figure 6 shows that these remote differences were much smaller than the local differences near Yuri. Thus, we concluded that our first prerequisite was met. That is, the effects of the tropical cyclone bogusing procedures on the initial conditions were largest at the tropical cyclone location and small elsewhere.

C. PREREQUISITE 2 - THE MODEL'S REPRESENTATION OF THE TROPICAL CYCLONE

A second major prerequisite for this modeling study is that the tropical cyclone itself is well represented within the model. For the POSITIVE and NO runs, this means that the model must maintain an adequate representation of the tropical cyclone and its effects. For the NEGATIVE runs,

this prerequisite means that the tropical cyclone is absent in both the initial conditions and in the forecast fields.

The representation of Yuri in the different runs was evaluated by looking at Yuri's track and intensity, as indicated by the forecast sea level pressure fields.

1. TROPICAL CYCLONE TRACK

A track history provided by the Joint Typhoon Warning Center (JTWC) was used as the best estimate of the actual track for supertyphoon Yuri. The model's ability to position Yuri was then evaluated by comparing the JTWC positions with the location of the minimum sea level pressure within the model output at each output time.

It is important to keep in mind that the model output used for this study was on a coarser grid than that used within the NOGAPS model itself. As a result, the tracks presented here may be less smooth and less realistic than those actually calculated by the model.

Figures 7, 8, and 9 show the sea level pressure fields in the western Pacific at selected times during the Forecast 2 POSITIVE, NO, and NEGATIVE runs, respectively. The POSITIVE and NO run sea level pressures clearly showed a strong, organized, synoptic scale low pressure center throughout the early part of the runs (Figures 7 and 8). However, the NEGATIVE run sea level pressures showed a much

weaker and broader area of low pressure that remained within the model's monsoon trough throughout the run (Figure 9).

A tropical cyclone track was constructed using the minimum sea level pressures at each output time from the Forecast 2 POSITIVE, NO, and NEGATIVE runs. These tracks are presented in Figure 10. When compared to the JTWC best estimate of the tropical cyclone track, the POSITIVE track was the most accurate, with the NO run also providing a rather realistic track. The "track" for the NEGATIVE run did not follow the JTWC track, but instead traced an erratic path that remained confined to the tropics.

The tracks for the Forecast 1 and Forecast 3 runs (not shown) provided similar results.

2. TROPICAL CYCLONE INTENSITY

The model's representation of Yuri's strength was evaluated by comparing the model runs' minimum sea level pressures at each output time with each other and with the JTWC values. Table 3 presents these values for the Forecast 2 POSITIVE, NO, and NEGATIVE runs. The output times are the same as those used to construct the tracks seen in Figure 10.

Also presented in Table 3 are the JTWC best estimates of the actual sea level pressure at the center of Yuri. These JTWC estimates were calculated in a two step process. First, Yuri's maximum winds were estimated from satellite

imagery. Then, these winds were converted to minimum sea level pressures using a relationship derived by Atkinson and Holliday (1977).

Note that the actual JTWC sea level pressures were much lower than the model output. Some of this difference may have been due to the coarse space and time resolution of the model output, but it is also unlikely that the model was capable of reproducing the extremely low sea level pressures seen during supertyphoon Yuri.

With that limitation in mind, the Forecast 2 POSITIVE and NO runs both provided reasonable representations of the development and strength of supertyphoon Yuri. The POSITIVE run was closer to the timing and sea level pressure trends seen in the JTWC data. As expected, the sea level pressure minima from the NEGATIVE runs were much weaker and did not show the organization seen in the POSITIVE and NO run results. The NO run reached a sea level pressure of 979 mb. But this was on 1 December 1991, well after the actual tropical cyclone had entered the tropics.

The values obtained from the Forecast 1 and Forecast 3 runs (not shown) provided similar results.

3. CONCLUSION FOR PREREQUISITE 2

The POSITIVE run clearly provided a realistic tropical cyclone track and a reasonable representation of the tropical cyclone intensity. The NEGATIVE run, on the other

hand, never developed a realistic track and intensity. Thus, we concluded that our second prerequisite was met for supertyphoon Yuri. That is, the POSITIVE run realistically represented the tropical cyclone within the model, while the NEGATIVE run effectively removed the tropical cyclone from the model atmosphere.

D. PREREQUISITE 3 - THE MODEL'S GENERAL CIRCULATION

The final major prerequisite for this type of modeling study is that the model produce realistic global heating and circulation patterns in all cases. To determine how well the model results met this prerequisite, we compared the model's time averaged heating, geopotential heights, and winds to climatological values.

1. ATMOSPHERIC HEATING

Figure 11 shows the 15 day average of the vertically integrated heating for the Forecast 2 POSITIVE, NO, and NEGATIVE runs. The heating patterns for all of the runs were similar to those seen in the climatological patterns of precipitation and outgoing longwave radiation (OLR) for this time of year (e.g., Kousky 1991).

All of the runs showed the same major heating features, indicating tropical convection in the Caribbean and central and western tropical Pacific, along with relatively weak and isolated heating in the midlatitudes.

The POSITIVE and NO run time averages clearly reflected the very strong influence of supertyphoon Yuri, with the areas of greatest heating following the tropical cyclone track from the tropics up into the midlatitudes. For the NEGATIVE run, this heating from Yuri was absent.

The 15 day time averages of the Forecast 1 and Forecast 3 POSITIVE, NO, and NEGATIVE runs (not shown) showed patterns very similar to the those seen for the Forecast 2 run.

2. 200 MB GEOPOTENTIAL HEIGHTS

Figure 12 shows the 15 day time averages of the 200 mb geopotential heights for the Forecast 2 POSITIVE, NO, and NEGATIVE runs. There were only subtle differences between the runs, and the patterns for all of the runs were consistent with climatology for this time of year (e.g., Kousky 1991).

Several important features were evident in the geopotential heights. The east Asian-North Pacific jet was prominent in all of the runs, extending from the Asian coastline to the north central Pacific and reaching maximum speeds of 80 m/s. Likewise, all of the runs had a region of diffluent flow over the northeastern Pacific, a region of weakly confluent flow over western North America, and weaker (50 m/s) zonal flow over eastern North America.

The primary difference was found in the NEGATIVE run time average. In it, the east Asian-North Pacific jet exit, and the diffluent region downstream of the exit, were further to the west than in the other runs.

The 15 day time averages for the Forecast 1 and Forecast 3 POSITIVE, NO, and NEGATIVE runs (not shown) showed patterns very similar to the those seen for the Forecast 2 run.

3. 200 MB WINDS

Figure 13 shows the 15 day time averages of the 200 mb winds for the Forecast 2 POSITIVE, NO, and NEGATIVE runs. As with the heating and geopotential heights, all of the time averaged wind patterns were consistent with climatology for the season (e.g., Kousky 1991).

The same major features were seen in the winds as were seen in the geopotential heights: a strong and zonal east Asian jet, a large diffluent region over the northeastern Pacific, weak confluence over western North America, and weaker zonal flow over eastern North America and the western north Atlantic. Also evident were easterlies in the tropical western Pacific, westerlies in the tropical eastern Pacific, and a large scale anticyclone in the subtropical western Pacific, all of which were consistent with the season.

The differences between the time averaged winds for the Forecast 2 POSITIVE, NO, and NEGATIVE runs were similar to those described in Section D2, above.

The time averages of the 200 mb winds for the Forecast 1 and Forecast 3 POSITIVE, NO, and NEGATIVE runs (not shown) were much like those seen for the Forecast 2 run.

4. CONCLUSION FOR PREREQUISITE 3

The 15 day time averages of vertically integrated heating, 200 mb geopotential heights, and 200 mb winds all compared favorably with climatological values. The only major differences in the output from the varying runs were the strong heating that followed Yuri into the midlatitudes, and the stronger and more zonally elongated north Pacific jet, in the POSITIVE and NO runs.

Because all of the time averages were consistent with climatology, we concluded that Prerequisite 3 was met for supertyphoon Yuri - that each of the three boguses used with the NOGAPS model produced reasonable global heating and circulation patterns.

E. PREREQUISITE 4 - THE EFFECTIVENESS OF ENSEMBLE AVERAGING

The technique of ensemble averaging is an important tool for this type of study. By taking the average of three simultaneous runs, as described in Chapter II, the smallest perturbations are smoothed away, while larger, more consistent signals are made more apparent.

On the other hand, model results from early in a given forecast tend to be more accurate than those from later in the same forecast. By using data from three different forecasts in our ensemble average, values of differing accuracy were averaged together (see Figure 4). However, due to the relatively small differences between the initial times for the forecasts (36 and 72 hours), we believe that the resulting differences in accuracy were small enough to justify the use of ensemble averages.

However, for an ensemble average to be useful, it must be a good representation of its individual component forecasts. To determine this, we examined the POSITIVE and NEGATIVE run heating and geopotential height fields every 12 hours for Forecasts 1, 2, and 3 and for the corresponding ensemble average. These fields are shown, for every two days, in Figures 14-29. These figures also show the evolution of the heating and height fields for the six different runs. These figures depict the main area of interest for this study - the north Pacific and North American region.

The accompanying descriptions are provided specifically for the ensemble average fields, but most of the features described are also visible in the individual forecasts. Large differences between the individual forecasts and the ensemble average are noted.

1. ATMOSPHERIC HEATING

We have already seen that the time averaged atmospheric heating during the study period (e.g., Figure 10) closely matched climatological patterns for November and December. In this section, the evolution over time of this heating is shown for the Forecast 1, 2, 3:

(a) POSITIVE runs and for the ensemble averages of these runs; and

(b) NEGATIVE runs and for the ensemble averages of these runs.

a. POSITIVE RUN RESULTS

The atmospheric heating results from the POSITIVE runs are presented as follows:

- Forecast 1 results in Figure 14,
- Forecast 2 results in Figure 15,
- Forecast 3 results in Figure 16, and
- Ensemble average results in Figure 17.

At 29 November 1991, 12Z (Figures 14-17(a)), Yuri was clearly evident in the tropical western Pacific. Two small but relatively strong midlatitude weather systems were also found to the northeast of Yuri, off the east coast of Japan.

By 01 December 1991, 12Z (Figure 14-17(b)), Yuri had recurved, tracked to the northeast, and merged with the nearby midlatitude systems, creating a large area of strong heating to the east of Japan.

By 03 December 1991, 12Z (Figure 14-17(c)), this combined heating source had weakened considerably. It had also moved well to the east, and was now located to the southwest of the Aleutian Islands.

From 05 December 1991, 12Z (Figure 14-17(d)), through 07 December 1991, 12Z (Figure 14-17(e)), the weak remnants of Yuri moved northeastward into the Gulf of Alaska and rapidly dissipated.

In summary, supertyphoon Yuri, the strongest heat source during the period, tracked northwest from the tropical western Pacific, recurved, and then moved northeast into the midlatitudes. It weakened noticeably before merging with a midlatitude weather system, and the combined system moved eastward across the Pacific, rapidly dissipating as it approached western Canada. A comparison of Figures 14-16 with Figure 17 shows that the ensemble average atmospheric heating was representative of its component individual runs.

b. NEGATIVE RUN RESULTS

The atmospheric heating results from the NEGATIVE runs are presented as follows:

- Forecast 1 results in Figure 18,
- Forecast 2 results in Figure 19,
- Forecast 3 results in Figure 20, and
- Ensemble average results in Figure 21.

On 29 November 1991, 12Z (Figures 18-21(a)), there was no trace of supertyphoon Yuri in the tropical western Pacific, only two extratropical heating sources in the north Pacific east of Japan. These two sources corresponded well to the two extratropical systems seen to the north and east of Yuri in the POSITIVE run (cf. Figures 14-17(a)).

By 01 December 1991, 12Z (Figures 18-21(b)), the extratropical sources had dissipated, leaving only a weak new source in the tropical western Pacific east of the Philippines. In the POSITIVE runs the extratropical heatings east of Japan on 01 December 1991, 12Z, persisted for several more days (cf. Figures 14-17(b)). Thus, it is possible that the absence of Yuri in the NEGATIVE runs contributed to the accelerated weakening of these extratropical sources.

By 03 December 1991, 12Z (Figures 18-21(c)), there was a midlatitude heating in the central north Pacific east of southern Japan, while the weak Philippine heating had moved slowly northwest. By 05 December 1991, 12Z (Figures 18-21(d)), the midlatitude heating had weakened considerably, but the weak Philippine system had moved slightly to the north.

By 07 December 1991, 12Z (Figures 18-21(e)), no major midlatitude sources remained, while the Philippine source had split into different heating centers, scattered across the South China Sea. All of these weak sources disappeared

by 09 December 1991, 12Z (Figures 18-21(f)) and 11 December 1991, 00Z (Figures 18-21(g)).

Thus, with supertyphoon Yuri effectively removed by the NEGATIVE tropical cyclone bogusing procedure, atmospheric heating was limited to a series of much smaller, weaker, and more widely scattered sources. These sources included several weak midlatitude systems which lasted for several days and a weak tropical heating source near the Philippines. A comparison of Figures 18-20 with Figure 21 shows that the ensemble average atmospheric heating was again representative of its component individual runs.

2. 200 MB GEOPOTENTIAL HEIGHTS

In this section, we present the evolution of the major geopotential height features and the associated flow for the Forecasts 1, 2, 3:

(a) POSITIVE runs and for the ensemble averages of these runs; and

(b) NEGATIVE runs and for the ensemble averages of these runs.

a. POSITIVE RUN RESULTS

The 200 mb geopotential height results from the POSITIVE runs are presented as follows:

- Forecast 1 results in Figure 22,
- Forecast 2 results in Figure 23,
- Forecast 3 results in Figure 24, and
- Ensemble average results in Figure 25.

At 29 November 1991, 12Z (Figures 22-25(a)), several major features were evident in the upper level atmosphere. These included large scale ridges (highs) anticyclones over the tropical western Pacific, subtropical eastern Pacific, and tropical Atlantic, and large scale troughs (lows) over Siberia and western North America. Jets are evident over the east Asian-north Pacific and North American areas. The jet over Japan had a speed of approximately 80 m/s at this time (not shown).

By 01 December 1991, 12Z (Figures 22-25(b)), the ridge in the western Pacific had strengthened and extended north into the subtropics, while the northeast Pacific ridge had weakened and moved east. The east Asian-North Pacific jet had shifted to the north, and the North American jet had strengthened and developed a distinct southwest to northeast tilt.

By 03 December 1991, 12Z (Figures 22-25(c)), the northeast Pacific ridge had weakened further. The east Asian-North Pacific had jet strengthened and became much more zonal, while its exit region shifted to the east. The North American jet also strengthened, moved east, and maintained its tilt.

At 05 December 1991, 12Z (Figures 22-25(d)), all of these trends continued. The subtropical western Pacific ridge was further north and east. The east Asian-North Pacific jet had accelerated further and stretched across

most of the north Pacific. The North American jet shifted further to the east over the Atlantic and maintained its strength.

By 07 December 1991, 12Z (Figures 22-25(e)), the east Asian-North Pacific jet strengthened further, moved further to the east, and became quite zonal. The North American jet maintained its tilt, weakened a little, and approached the western edge of Europe, leaving basically zonal flow across the entire northern hemisphere (not shown).

At 09 December 1991, 12Z (Figures 22-25(f)), the east Asian-north Pacific jet had weakened slightly, extending to the west coast of North America. The North American jet had weakened and extended well into Europe (not shown). The overall flow across the northern hemisphere was even more zonal than on 07 December 1991 (not shown).

By 11 December 1991, 00Z (Figures 22-25(g)), the strong zonal flow had begun to weaken, as a weak trough-ridge-trough system developed in the north Pacific-North American region (note, for example, the ridge over the subtropical eastern Pacific in Figures 22-25 (g)).

In summary, large changes took place in the geopotential height fields over the study period which clearly affected the evolution of the 200 mb jet streams. The east Asian-north Pacific jet strengthened, became more zonal, and moved eastward. The North American jet strengthened, tilted strongly from southwest to northeast, moved eastward, and

became more zonal. This led to a predominantly zonal flow across the northern midlatitudes by about 07-09 December 1991. By 11 December 1991, this zonal flow was weakening and developing large scale waves. Comparison of Figures 22-24 with Figure 25 shows that, as seen for previous fields, the ensemble average geopotential heights were representative of the heights seen in the individual runs.

b. NEGATIVE RUN RESULTS

The 200 mb geopotential height results from the NEGATIVE runs are presented as follows:

- Forecast 1 results in Figure 26,
- Forecast 2 results in Figure 27,
- Forecast 3 results in Figure 28, and
- Ensemble average results in Figure 29.

On 29 November 1991, 12Z, the NEGATIVE run results (Figures 26-29(a)) showed features similar to those seen in the POSITIVE runs (Figures 22-25(a)). These features included the western Pacific, eastern Pacific, and Atlantic ridges and the Siberian and North American troughs.

By 01 December 1991, 12Z (Figures 26-29(b)), the east Asian-north Pacific jet had become more zonal and extended out to the international date line as the eastern Pacific ridge weakened. The North American jet strengthened significantly and acquired a southwest-northeast tilt. A comparison with the corresponding figures from the POSITIVE

runs (Figures 22-25(b)) shows that, in the NEGATIVE runs, the western Pacific ridge was less developed and located further south, leading to more zonal flow across the north Pacific.

By 03 December 1991, 12Z (Figures 26-29(c)), the northeastern Pacific ridge weakened further, and the entire north Pacific pattern had become more zonal.

By 05 December 1991, 12Z (Figures 26-29(d)), the flow across North America had become more zonal. Compared to the POSITIVE runs (Figures 22-25(d)), the tropical western Pacific ridge was weaker and centered further south and east. Thus, the east Asian-north Pacific jet did not reach as far across the Pacific.

By 07 December 1991, 12Z (Figures 26-29(e)), the eastern Pacific ridge had weakened further, and the east Asian-north Pacific jet had strengthened and extended to the east. The flow from eastern Asia to western Europe (not shown) was basically zonal, although less so than for the POSITIVE run.

By 09 December 1991, 12Z (Figures 26-29(f)), the eastern Pacific ridge had strengthened and moved east. The east Asian-north Pacific jet had extended further east. The North American jet had weakened, and a ridge had developed in the north Atlantic (not shown). This resulted in a generally more wavy flow than that seen in the POSITIVE runs, which had much a weaker eastern Pacific ridge and no north Atlantic ridge.

By 11 December 1991, 00Z (Figures 26-29(g)), the east Asian-north Pacific jet was relatively zonal across most of the north Pacific. The eastern Pacific ridge had strengthened and shifted to the east. In the eastern Pacific, there was a strong northeastward flow across southern Alaska. There was also a weaker northeastward flow around a subtropical trough and into the southwestern U.S. Over eastern North America, a trough had intensified.

In summary, the east Asian-north Pacific jet strengthened and moved eastward, as the eastern Pacific ridge slowly moved eastward and over western North America. One of the clearest differences between the POSITIVE and NEGATIVE runs was the strength of the eastern Pacific ridge and the north Atlantic ridge (not shown). These ridges tended to be stronger and more persistent in the NEGATIVE runs, leading to a much less zonal flow across the north Pacific and North America.

These differences are most evident in a comparison of the ensemble averages (Figures 25 and 29). Note in particular, the large differences in the heights over the eastern Pacific and North America on 11 December 1991 (Figures 25(g) and 29(g)). Once again, the ensemble average fields were reasonable representations of the fields for the individual runs.

3. CONCLUSION FOR PREREQUISITE 4

The ensemble averages (Figures 17, 21, 25, and 29) were smoothed versions of the individual run results which highlighted the stronger and more consistent signals in the heating and height fields. Similar results were found for the NO run results (not shown). Thus, we concluded that our fourth prerequisite was met. That is, the ensemble averages provided a valid representation of the major features in the individual runs. In light of this conclusion, most of the results presented in the following sections are ensemble averages.

F. HYPOTHESIS 1 - TELECONNECTIONS ASSOCIATED WITH A SINGLE TROPICAL CYCLONE

Our first hypothesis, originally addressed in Miller (1993), contends that an individual tropical cyclone may be capable of producing a strong teleconnection within a short period of time. We can see evidence of teleconnections in the total fields presented above, but the teleconnection patterns are much more obvious if difference fields are used.

We calculated the differences between the POSITIVE runs and the NEGATIVE runs for several fields. Remember that the POSITIVE runs represent the atmosphere with Yuri and the NEGATIVE runs represent the atmosphere without Yuri (Table

1). Thus, the POSITIVE - NEGATIVE differences represent the global atmosphere's **responses** to Yuri (Table 2).

1. DIFFERENCES IN ATMOSPHERIC HEATING AND 200 MB GEOPOTENTIAL HEIGHTS

Figure 30 shows the ensemble average POSITIVE - NEGATIVE heating and 200 mb height differences. It is important to note that the POSITIVE - NEGATIVE heating differences do not show the model's best representation of Yuri's position. These are given by the POSITIVE sea level pressures (Figures 7 and 10). However, early in the run, the heating from Yuri in the POSITIVE runs was so much larger than the heating without Yuri in the NEGATIVE runs (see Figures 14-17 and 18-21) that the heating difference does show Yuri's approximate position. This does not apply later in the run, when the amount of heating in both POSITIVE and NEGATIVE runs has dropped dramatically.

To clarify the discussion of the geopotential height differences in Figure 30, the major differences have been assigned labels. The first major positive height difference to form was labeled H1 (H for high); the first major negative height difference to form was labeled L1 (L for low); and so forth. This allowed us to track persistent height responses as they developed and propagated over time.

References to Yuri in the discussion of Figure 30, and other POSITIVE - NEGATIVE difference figures, refer to Yuri

in the POSITIVE runs, since Yuri was not present in the NEGATIVE runs.

Figure 30(a) shows the ensemble average differences on 29 November 1991, 12Z. The strong heating difference northeast of the Philippines (maximum difference ≈ 20°C/day) mainly indicates the merger of the heating associated with Yuri and the nearby midlatitude synoptic system. Just to the north of this large heating difference, there was a weak positive height difference (H1).

By 01 December 1991, 12Z (Figure 30(b)), as Yuri reached the midlatitude westerlies east of Japan, the large heating difference had weakened and elongated to the east. In marked contrast, the positive height difference, H1, had strengthened and broadened dramatically. In addition, a negative height difference, L1, had also developed over the Aleutians and was centered east of H1. Another positive height difference, H2, had formed near eastern Siberia.

By 03 December 1991, 12Z (Figure 30(c)), the heating difference associated with Yuri and the midlatitude systems had moved to the northeast of H1, near the western Aleutians, and had weakened considerably. H1 had broadened to the east but its center had moved only slightly to the east. L1 weakened and became centered between Kamchatka and the Aleutians. (L1 was too weak to be contoured at the lowest contour level in Figure 30(c)). H2 had extended eastward to the western coast of Canada.

By 05 December 1991, 12Z (Figure 30(d)), the heating differences were very small and remained so through the rest of the ensemble average period H1 had shifted eastward and become more zonal. L1 had strengthened considerably and formed two lobes straddling the Aleutians. H2 had also strengthened considerably and become centered over southwestern Canada. Note that the H1-L1-H2 centers define an arc (concave to the south) in Figure 30(d).

By 07 December 1991, 12Z (Figure 30(e)), a broad region of positive height differences, combining H1, H2, and a third difference over eastern Asia, had formed and stretched across the entire northern Pacific. H1 and H2 had moved to the east. Over Alaska, L1 had strengthened tremendously. The boundary between H1 and L1 had become very zonal in the central north Pacific.

By 09 December 1991, 12Z (Figure 30(f)), H1, L1, and H2 had moved further to the east. By 11 December 1991, 00Z (Figure 30(g)), L1 had shifted further east so that H1, L1, and H2 formed a distinct arcing pattern from the northeastern Pacific to the east coast of North America. Note that this arcing pattern resembles a "negative" version of the PNA pattern identified by Wallace and Gutzler (1981).

In summary, the H1/L1/H2 pattern of height differences was coherent, strong (with height differences of up to 700 gpm between H1 and L1), and persistent.

In addition to the H1, L1, and H2 differences, there were weaker and smaller scale differences (e.g., those over North America in Figure 30(b-c)). These differences, when traced through the ensemble averaging period (Figure 30(a-g)) were found to propagate more rapidly than the stronger, large scale differences. Analysis of the results from the individual POSITIVE and NEGATIVE runs suggest these smaller differences were mainly due to phase differences in midlatitude synoptic systems. Thus, they appear to have had a distinctly different character than the larger responses, especially the H1-L1-H2 response pattern.

2. CONCLUSION FOR HYPOTHESIS 1

A coherent, strong, and persistent pattern was clearly evident in the ensemble average 200 mb geopotential height differences. Consequently, we concluded that our first hypothesis was true. That is, an individual tropical cyclone may produce strong teleconnections within a short period of time.

The ensemble average differences in heating and heights also revealed several important points concerning the process by which teleconnections associated with Yuri developed. First, the H1 part of the H1/L1/H2 response started to form when Yuri was still in the tropics. But H1 strengthened dramatically once Yuri reached the region of westerly winds (Figure 30(a,b)).

Second, the heating and height responses did not intensify and propagate together. Instead, the height responses strengthened as the major heating response weakened, and reached their maximum intensity well after the heating response had dissipated. In addition, the heating response moved eastward across the north Pacific much more rapidly that the height responses. Thus, we infer that the height differences were **not** a simple, direct response to nearby heating differences. This indicates that some other source of energy was being tapped. The next section addresses our hypothesis for this teleconnection mechanism.

G. HYPOTHESIS 2 - THE JET'S ROLE IN TELECONNECTIONS

Several factors indicate that Yuri's heating was probably not the only source of energy for the teleconnection:

(1) the strength of the teleconnection (see Figure 30(g));

(2) the fact that the heating and height differences did not grow and propagate together; and

(3) the persistence fo the height differences long after dissipation of the major heating difference.

As proposed by Murphree (1994) and Gelaro and Murphree (1994), the strong 200 mb jet, in the vicinity of the strongest height responses, may have been an important energy source for the teleconnection process. These earlier

studies also suggest that the jet may have acted to guide wave energy associated with the teleconnection.

Thus, building on these previous studies, hypothesis 2 may be expressed as three major components which address the development of the teleconnection. These components are:

- the teleconnection pattern (as reflected in the 200 mb geopotential heights) develops with a characteristic arrangement of height responses in relation to the jet;
- the jet acts as a waveguide for the propagation of quasi-geostrophic wave energy; and
- amplification of wave energy may take place in areas of potential barotropic instability, which are likely to occur on the north and south flanks of the jet.

In this section we examine the propagation of energy through the north Pacific/North America region during the study period. Studying the energy propagation allows us to better understand the dynamics of the teleconnection. It also allows us to evaluate our second hypothesis, which concerns the role of the midlatitude jet in the development of the teleconnection.

The primary tool for our examination of energy propagation is the wave activity flux vector (Plumb 1985) which helps to describe the propagation of wave energy. These fluxes were calculated using the ensemble average POSITIVE - NEGATIVE geopotential height differences.

As discussed in Chapter II, Section H(1), the amount of propagating energy is proportional to the length of the flux vector, and the direction of propagation is the same as the

direction of the vector. Areas from which the flux vectors diverge are energy source regions, while regions into which the flux vectors converge are energy sinks.

We are primarily interested in the role played by the jet when Yuri was present, which is best represented by the jet in the ensemble average of the POSITIVE runs. Thus, in the following discussions, the ensemble average POSITIVE run 200 mb zonal winds were used to calculate the 200 mb jet and potential barotropic instability. We have compared this jet and its associated potential barotropic instability to the 200 mb height differences (Figure 30) in order to evaluate the jet's role in the teleconnection process.

1. GEOPOTENTIAL HEIGHT DIFFERENCES AND THE 200 MB JET

Our first step was to investigate the relationship between the height differences shown in the previous section and the 200 mb jet. Figure 31 presents the POSITIVE - NEGATIVE geopotential height differences overlaid with a thick line representing the POSITIVE 200 mb jet axis (u>60 m/s).

On 29 November 1991, 12Z (Figure 31(a)), Yuri and its associated heating were approaching the jet from the south (Figures 14-17 (a)). This led to a strengthening and northward shift of the western Pacific ridge (Figures 14-17(a)). In the height response, this change in the ridge was represented by the development of the H1 positive height

response over the western half of the 200 mb east Asian-north Pacific jet (Figure 31(a)).

By 01 December 1991, 12Z (Figure 31(b)), the western Pacific ridge and H1 had further strengthened and shifted north. Correspondingly, the jet also shifted to the north. The center of the much strengthened H1 positive height was just to the south of the jet.

By 03 December 1991, 12Z (Figure 31(c)), the jet had shifted and extended to the west. The center of H1 was south of the eastern end of the jet.

By 05 December 1991, 12Z (Figure 31(d)), the jet core shifted and extended back to the east, with its exit region reaching to the south of the Aleutians. The H1 positive height difference was south of the jet, while the center of the L1 negative height difference was north of the jet exit, and the H2 positive height difference was about 45 degrees east of the jet exit, over western North America.

By 07 December 1991, 12Z (Figure 31(e)), the jet had strengthened and extended further east, spanning most of the north Pacific. This very zonal jet lay between H1 to the south and L1 to the north. Both H1 and L1 were located near the eastern end of the jet.

By 09 December 1991, 12Z (Figure 31(f)), flow near the jet entrance had weakened and the jet had extended slightly further to the east. H1 and L1 still flanked the jet but

were located closer to the jet exit. H2 was about 50 degrees east of the jet exit.

By 11 December 1991, 00Z (Figure 31(g)), a second jet was evident over Japan. The jet over the northeastern Pacific had extended east into western North America, H1 remained south of the east end of the jet, L1 was north of the jet exit, and H2 was about 40 degrees east of the jet exit.

Thus, a relatively consistent relationship existed between the major height differences (H1, L1, and H2) and the 200 mb jet. This relationship pattern was most pronounced in the second half of the run, when the teleconnection pattern (as reflected in the height differences) was the strongest. The height differences formed an arcing pattern, with H1 to the south of the east end of the jet, L1 north of the jet exit, and H2 to the east of the jet exit. A schematic of this pattern is presented in Figure 32.

This pattern, with the H1 positive height difference to the south of the jet and the L1 negative height difference to the north of the jet, indicates that, near H1 and L1, the POSITIVE jet was stronger than the NEGATIVE jet. The positioning of H1 and L1 near the east end of the jet indicates that theese height differences were associated with the development of a more zonal and more zonally extensive jet in the POSITIVE runs.

2. THE 200 MB JET AS A WAVEGUIDE

The impact of the jet on the propagation of quasi-geostrophic wave energy associated with the ensemble average POSITIVE - NEGATIVE height response is shown in Figure 33. This figure shows wave activity flux vectors, calculated from the ensemble average POSITIVE - NEGATIVE geopotential height differences, overlaid with a thick line representing the POSITIVE 200 mb jet axis ($u > 60$m/s).

On 29 November 1991, 12Z (Figure 33(a)), the east Asian jet was relatively strong (maximum speed about 80 m/s) and extended from the southern coast of Japan to about 170°E. The flux vectors indicated that there was only weak energy propagation at this time.

By 01 December 1991, 12Z (Figure 33(b)), the jet had shifted to the east and the propagation of wave energy had increased. Most of the propagation was along the jet to the east-northeast, roughly parallel to the jet itself.

On 03 December 1991, 12Z (Figure 33(c)), the jet extended from east Asia to about 170°E. Energy propagated eastward along the jet core and then turned poleward at the jet exit. Energy also propagated to the southeast from a source region south of the Aleutians.

By 05 December 1991, 12Z (Figure 33(d)), the jet had moved well to the east, stretching from Japan to the central north Pacific. Energy propagation on both flanks of the jet

was, on average, parallel to the jet, with poleward propagation at the jet exit. Over the northeast Pacific and North America, the energy propagated to the east and southeast. Overall, the energy flux vectors traced an arcing path from the jet exit over the central north Pacific, across Canada, and into the eastern U.S.

By 07 December 1991, 12Z (Figure 33(e)), the jet had lengthened in the east and become more zonal. Energy propagation across the north Pacific was primarily parallel to the jet. But near the jet exit, there was considerable propagation to the northeast, on the north flank of the jet, and to the southeast, on the south flank. The energy flux on the north flank was especially strong and extended eastward and southeastward across North America. The southeastward flux west of California emanated from a source south of the east end of the jet.

By 09 December 1991, 12Z (Figure 33(f)), the jet was slightly further to the east. Energy propagated zonally along the north flank of the jet, then followed the poleward, eastward, and southeastward arcing pattern. The southeastward propagation of energy from a source south of the east end of the jet was again apparent.

At 11 December 1991, 00Z (Figure 33(g)), most of the energy propagation occurred near and to the east of the northeast Pacific jet. The weak prpagation near the west end of this jet was parallel to the jet. Near the east end

of the jet, the energy propagated poleward, eastward, and southeastward across North America. Energy also propagated southeastward from a source on the south flank of the jet.

In summary, there were relatively weak fluxes along the western end of the jet, but with an intensification of the fluxes near the eastern end and jet exit. Near the exit, most of the energy propagated poleward, before arcing to the east and then southeast. Some energy also propagated directly to the southeast from the jet exit. This basic pattern is shown schematically in Figure 34.

3. THE ROLE OF BAROTROPIC INSTABILITY

Murphree (1994) and Gelaro and Murphree (1994) outlined the possible role played by barotropic instability (BTI) in amplifying the energy propagation associated with teleconnections. Regions of potential BTI are often found on the flanks of strong midlatitude westerly jets, so that a tropical cyclone which reaches the jet may be expected to trigger the release of energy from the jet through barotropic instability processes.

In this study, areas of potential barotropic instability have been identified using the Rayleigh-Kuo criterion, in which the quantity $\beta - u_{yy}$ changes sign from positive to negative (cf. Gelaro and Murphree 1994). This sign change is a necessary, but not sufficient, condition for the occurrence of barotropically unstable flow.

Figure 35 presents the same wave activity flux vectors seen in Figure 33, but with regions of potential BTI indicated by medium gray lines. These lines indicate where $\beta - u_{yy} = 0$. Thus, they give a rough indication of where barotropic instability may have occurred. Of particular interest in this figure are the areas of divergent energy flux, indicating an energy source, or an amplification of the wave energy. The colocation of these amplification areas with areas of potential BTI is an indication that barotropic instability processes may have been involved in amplifying the teleconnection response.

On 29 November 1991, 12Z (Figure 35(a)), regions of potential BTI are scattered across the northern hemisphere including, but not limited to, the north and south flanks of the relatively strong (80 m/s) east Asian-north Pacific jet. The energy propagation at this time was uniformly weak and no source regions were readily apparent.

On 01 December 1991, 12Z (Figure 35(b)), areas of potential BTI were again found on both flanks of the jet and jet exit region. The major source region was a broad area which encompassed the jet itself, and an area just south of the jet, but did not overlap much with the areas of potential BTI.

On 03 December 1991, 12Z (Figure 35(c)), areas of potential BTI were again found on the flanks of the jet and straddling the jet exit region. Both of the major source

regions, one to the south of the jet exit and one to the north of the jet exit, were found in areas of potential barotropic instability.

At 05 December 1991, 12Z (Figure 35(d)) and 07 December 1991, 12Z (Figure 35(e)), similar patterns were evident. Note that the zonally more extensive jet and jet exit area are flanked by potentially unstable areas that extend across all of the north Pacific and much of North America. Two source regions north of the jet were in areas of potential BTI, as was a third source region to the south of the east end of the jet.

By 09 December 1991, 12Z (Figure 35(f)), the flanking regions of potential barotropic instability were again colocated with the two primary source regions, south and north of the east end of the jet.

By 11 December 1991, 00Z (Figure 35(g)), the jet over the northeast Pacific had regions of potential barotropic instability to the north and south. The major source regions occurred in these unstable areas, one to the north and one to the south of the jet.

Note from the sequence shown in Figure 35 that the areas of potential barotropic instability on the jet flanks developed into larger and more zonally extensive structures as the jet strengthened and extended eastward.

Note also that the major source regions for the quasi-geostrophic wave activity flux vectors were predominantly

found within areas of potential barotropic instability, especially later in the sequence, as the fluxes intensified. Of course, by itself, this is unremarkable, since the areas of potential barotropic instability were so widespread. However, notice from Figure 35 that the major source regions were found almost exclusively in areas of potential barotropic instability near the jet exit region.

This positioning of the source regions near the jet exits is consistent with the waveguiding and amplification mechanisms proposed at the beginning of this section. Response energy guided along the jet is guided through extensive potentially unstable regions. Previous analytical and numerical modeling studies of barotropic instabilities (e.g. Peng and Williams 1986, Crum and Stevens 1990) have indicated that this response energy tends to increase with the length of its propagation path lying within unstable regions.

Thus, the largest amplification of the response would be expected near the downstream ends of the unstable areas. However, since the jet plays a major role in confining the wave energy within the unstable areas, the largest amplification is likely to occur within the unstable areas near the jet exits. Downstream of the exits, the energy tends to propagate poleward and equatorward (cf. Hoskins and Karoly 1981) and out of the unstable areas. Thus,

downstream of the exits, amplification associated with barotropic instability tends to decrease.

A schematic representation of the energy fluxes, their association with the jet and regions of potential barotropic instability, and their major source regions is shown in Figure 36.

4. CONCLUSION FOR HYPOTHESIS 2

From the model results presented in this section, we have identified several distinct patterns associated with the model's teleconnections. These patterns relate the model's geopotential height responses to the westerly jet, the regions of potential barotropic instability along the jet, and the propagation of quasi-geostrophic wave energy associated with the height responses. These patterns are presented in Figures 32, 34, and 36.

The appearance of these relatively strong and consistent patterns in the model results strongly supports our second hypothesis. In particular, the organization of the height responses around the westerly jet and the waveguiding by the jet strongly support the first two components of the hypothesis (see Section G).

The association of the major wave energy sources regions with areas of potential barotropic instability supports the third component of our second hypothesis. However, further study is needed to clearly demonstrate the role played by

barotropic instability in the release of energy to the teleconnection waves.

IV. CONCLUSIONS

A. SUMMARY AND DISCUSSION

Much of the early work involving teleconnections (e.g., Walker and Bliss 1932; Bjerknes 1966, 1969, 1972; Horel and Wallace 1981) was conducted by sifting through large amounts of observational data to find recurring patterns that were strong, coherent, and persistent. Efforts such as these helped link the various manifestations of the El Niño phenomenon.

Later researchers, studying smaller space and time scales, were able to link intraseasonal variations in tropical heating to changes in extratropical geopotential heights (e.g., Nitta 1987, Chang and Lum 1985). Other researchers (e.g., Harr et al. 1991) studied the teleconnections associated with recurving tropical cyclones.

While observational studies were providing evidence of short term teleconnections, numerical models were being used to simulate these the teleconnections. For example, Miller (1993) used the NOGAPS model to show that teleconnections might arise from a single tropical cyclone.

However, Miller (1993) did not address the mechanisms through which such teleconnections might occur. The present study was designed to investigate the role played by the

midlatitude westerly jet in the development of these teleconnections and to conduct additional case studies. The efforts to conduct further case studies were not successful (see below), but the investigations of teleconnection mechanisms provided exciting new evidence.

This study, like Miller's (1993), used the NOGAPS general circulation model, in conjunction with tropical cyclone bogusing procedures, to compare the global atmosphere with and without the designated tropical cyclone, supertyphoon Yuri. Our data analyses had two goals. The first was to validate the numerical modeling methodology, and the second was to use the results to investigate teleconnection mechanisms.

A series of basic underlying prerequisites was addressed, each of which had to be satisfied for our modeling methodology to be valid. The first assumption dealt with the effect of the tropical cyclone bogusing procedures on the initial conditions from which the model was started. We found that the tropical cyclone bogusing procedures had a large effect on the initial conditions near the tropical cyclone and much smaller effects on the initial conditions elsewhere in the world.

The second prerequisite addressed the model's representation of the tropical cyclone. We found that, for the POSITIVE and NO runs, the model maintained a reasonable

representation of the tropical cyclone. In the NEGATIVE runs, the tropical cyclone was essentially absent.

The third prerequisite involved the global circulation patterns generated by the model. All of the forecasts produced global circulations that were consistent with November-December climatological values.

The final prerequisite examined the process of ensemble averaging. Comparison of the individual forecasts with the corresponding ensemble average showed that all major features were preserved, while smaller (and presumably less important) features were smoothed out. This allowed us to isolate the dominant features in the model's teleconnection process.

Since all of the prerequisites were satisfied for the supertyphoon Yuri forecasts, we concluded that the forecasts were suitable for testing our teleconnection hypotheses.

Our first hypothesis asserted that an individual tropical cyclone might initiate a clear teleconnection. Our examination of the model's 200 mb height responses showed that supertyphoon Yuri initiated a very strong teleconnection across the north Pacific and North America.

Our second hypothesis addressed the mechanism involved in developing the teleconnection. The teleconnection process appeared to be initiated by interactions between Yuri and the east Asian-north Pacific jet, as Yuri approached and entered the jet. This was followed by the

generation of quasi-geostrophic wave energy that propagated away from the interaction site. Analyses of the wave energy and associated height responses revealed three distinct patterns.

First, the 200 mb geopotential height responses were located in a consistent pattern near the exit region of the 200 mb westerly jet. Second, the jet tended to guide the wave energy along the jet. Third, the major regions of wave energy amplification were near the jet exit in areas of potential barotropic instability.

In summary, the NOGAPS global circulation model, used in conjunction with a set of tropical cyclone bogusing schemes, was a very useful tool for simulating the effects of supertyphoon Yuri on the global atmosphere. A very strong, coherent, and persistent teleconnection was found in the model's 200 mb geopotential height output.

The evolution of that teleconnection was consistent with our hypothesized mechanism. Rossby wave energy generated by interactions between the tropical cyclone and the background flow propagated along the jet, was amplified in areas of potential barotropic instability, and helped establish a characteristic pattern of height responses near the jet exit.

The overall process suggests that several feedbacks may be involved in teleconnections associated with tropical cyclones. In this process, the tropical cyclone interacts

with the 200 mb westerly jet over Japan and triggers the generation and propagation of Rossby wave energy. This wave energy affects the development of the downstream 200 mb geopotential height responses. These height responses, in turn, affect the subsequent evolution of the 200 mb jet, which then affects the height responses, and so on. The variations of the jet during this process would, of course, affect the interactions between the jet and subsequent tropical cyclones. This hypothesized feedback loop is depicted in Figure 37.

B. IMPLICATIONS FOR EXTENDED RANGE FORECASTING

The confirmation that strong teleconnections may be caused by an individual tropical cyclone is an important contributions to the study of the atmosphere. Beyond the scientific insights gained, knowledge of these teleconnections may have important practical benefits.

The impacts of Yuri on the jet are especially intriguing in this respect, since the jet acts as the steering flow for midlatitude synoptic weather systems. Thus, for example, the east Asian-north Pacific jet plays a large role in determining the location and amount of precipitation along the west coast of North America.

Figure 38 compares the east Asian-north Pacific jets at the end of the ensemble average POSITIVE and NEGATIVE runs. The NEGATIVE jet (representing the jet that would have

occurred if Yuri had never developed) had a split flow over the northeast Pacific. The northern branch crosses into North America in the northwestern United States, consistent with the December climatology.

The POSITIVE jet (representing the jet that developed with Yuri present) was far more zonal than the NEGATIVE jet. It crossed into North America farther south, near northern California, and was likely associated with more precipitation in this region.

We have seen that the development of these two different jets can be traced back to events (specifically, the interaction between supertyphoon Yuri and the jet) that took place, or did not take place, 10-12 days earlier and thousands of kilometers upstream. Obviously, the ability to reliably forecast such teleconnections could be very helpful in producing useful extended range forecasts. Improvements of this sort could have many important societal benefits.

C. RECOMMENDATIONS FOR FUTURE WORK

There are several aspects of this study which need further work. A few of these are discussed below.

1. ADDITIONAL CASE STUDIES

The results for supertyphoon Yuri were very exciting, showing a very strong teleconnection within a short period of time. More case studies are needed to determine whether

Yuri's impacts were unique, or whether there are other examples of similar short term teleconnections.

A second case study was attempted for this investigation, with the hope of confirming Yuri's promising results. In this second case, the same procedures used in the Yuri study were applied to typhoon Gay and Hunt. These typhoons occurred in the tropical western Pacific and recurved into the northern midlatitudes in November and December of 1992.

Unfortunately, the NOGAPS forecasts of Gay and Hunt gave very poor simulations of the tracks and intensities of both typhoons. Thus, these model runs failed to satisfy our second assumption - that the model maintain a reasonable representation of the tropical cyclone(s). Therefore, no detailed results from this case study are presented in this report.

However, the results of these model runs, while obviously not representative of the actual global atmosphere during November and December 1992, provided some evidence of short term teleconnections that were generally consistent with those seen for Yuri (not shown). As such, they inspire cautious optimism that further case studies will confirm the Yuri results. If the shortcomings in these model runs can be remedied, this case study may be presented at a later date.

2. COMPARISON OF MODEL FORECASTS TO OBSERVED DATA

An important check of the validity of this approach would be to compare the output generated by the model to the operational analyses during the designated periods. If the 200 mb jet stream did indeed develop as the POSITIVE jet did (as seen in Figures 22-25, 31, 33, 35, and 38), this would greatly support the experimental methodology and the results of this study. Unfortunately, there is no comparable real world analysis with which to verify the NEGATIVE jet.

3. STUDIES WHICH VARY TROPICAL CYCLONE AND JET PARAMETERS

Presumably, the strength of the teleconnection caused by a single typhoon is a function of both the typhoon and the background flow with which it interacts. Tropical cyclone parameters which would likely impact the development of the teleconnection include the intensity, location, duration, and number of tropical cyclones. Jet parameters that could have an impact include the strength of the jet, its location (in both the north-south and east-west directions), whether it is zonal or wavy, and the associated shear. Note that all of these jet parameters will have a strong effect on the associated potential barotropic instability. Thus, additional modeling studies in which these tropical cyclone and jet parameters are carefully varied would be very useful

in determining the robustness of the teleconnection process found in this study.

4. FURTHER INVESTIGATIONS OF THE TELECONNECTION MECHANISM

This study has provided evidence that strong, short term teleconnections may result from a tropical cyclone. Furthermore, our results indicate some possible mechanisms involving the extratropical jets that may explain these teleconnections. However, there are many details of this mechanism that must be addressed.

A partial list of dynamical questions that still need to be answered includes:

- What is the nature of the interaction between the typhoon and the background flow? How is the Rossby wave energy actually generated?
- How exactly does the jet act as a waveguide? Is a wavy jet as effective a waveguide as a zonal one?
- What are the processes by which the energy released through barotropic instability processes is converted to quasi-geostrophic wave energy? Do calculations of this conversion confirm the hypothesized role of barotropic instability?
- What is the nature of the feedbacks from the waves to the jet? What processes are operating in the energy sink regions?

Additional case studies are under way at the Naval Postgraduate School, with an emphasis on the generation and propagation of Rossby wave energy.

The results of this study hold great promise. If further studies show that such short term teleconnections

can be accurately and reliably anticipated, then it may be possible to produce more accurate predictions of the large scale steering flow. Improvements of this sort could have substantial economic and societal benefits, allowing planners more time to make informed decisions.

LIST OF REFERENCES

Atkinson, G., and C. Holliday, 1977: Tropical cyclone minimum sea-level pressure and maximum sustained wind relationship for the western North Pacific. *Mon. Wea. Rev.*, **105**, 421-427.

Bjerknes, J., 1966: A possible response of the atmospheric Hadley circulation to equatorial anomalies of ocean temperature. *Tellus*, **18**, 820-829.

-----, 1969: Atmospheric teleconnections from the equatorial Pacific. *Mon. Wea. Rev.*, **97**, 163-172.

-----, 1972: Large-scale atmospheric response to the 1964-1965 Pacific equatorial warming. *J. Phys. Oceanogr.*, **2**, 212-217.

Chang, C., and K. Lum, 1985: Tropical-midlatitude interactions over Asia and the western Pacific Ocean during the 1983/84 northern winter. *Mon. Wea. Rev.*, **113**, 1345-1358.

Chelliah, M., J.E. Schemm, and H.M. van der Dool, 1988: The impact of low latitude anomalous forcing on local and remote circulation: Winters of 1978/79 - 1986/87. *J. Climate*, **1**, 1138-1152.

Chen, T., R. Tzeng, and H. van Loon, 1988: A study on the maintenance of the winter subtropical jet streams in the northern Hemisphere. *Tellus*, **40**, 392-397.

Crum, F.X., and D.E. Stevens, 1990: Barotropic instability with downstream and asymmetric cross-steam variations: idealized calculations. *J. Atmos. Sci.*, **47**, 5-23.

Fiorino, M., J. Goerss, and J. Jensen, 1991: An evaluation of the tropical cyclone forecasting skill of the Navy Operational Global Atmospheric Prediction System. *Proceedings of the 19th Conference on Hurricanes and Tropical Meteorology*, 16-20.

Gelaro, R., and T. Murphree, 1994: Intraseasonal variations in tropical-extratropical teleconnection mechanisms. To be submitted to *J. Atmos. Sci.*, January 1994.

Goerss, J., L. Brody, and R. Jeffries, 1991: Assimilation of tropical cyclone observations into the Navy Operational Global Atmospheric Prediction System. *Proceedings of the Ninth Conference on Numerical Weather Prediction*, 638-641.

Harr, P., J. Chen, and T. Murphree, 1991: The relationship of western Pacific monsoon and tropical cyclone activity to North Pacific and North American climate anomalies. *Proceedings of the Eighth Annual Pacific Climate Workshop*, 99-106.

-----, and R. Elsberry, 1991: Tropical cyclone track characteristics as a function of large-scale circulation anomalies. *Mon. Wea. Rev.*, **119**, 1448-1468.

Hogan, T., and T. Rosmond, 1991: The description of the Navy Operational Global Atmospheric Prediction System's Spectral Forecast Model. *Mon. Wea. Rev.*, **119**, 1786-1815.

Horel, J., and J. Wallace, 1981: Planetary-scale atmospheric phenomena associated with the Southern Oscillation. *Mon. Wea. Rev.*, **109**, 813-829.

Hoskins, B., and D. Karoly, 1981: The steady linear response of a spherical atmosphere to thermal and orographic forcing. *J. Atmos. Sci.*, **38**, 1179-1196.

Hurrell, J., and D. Vincent, 1990: Relationship between tropical heating and subtropical westerly maxima in the southern Hemisphere during SOP-1, FGGE. *J. Climate*, **3**, 751-768.

-----, and -----, 1991: On the maintenance of short term subtropical wind maxima in the Southern Hemisphere during SOP-1, FGGE. *J. Climate, 4, 1009-10021.*

Kousky, V., 1991: *Climate Diagnostics Bulletin, November 1991.* Climate Analysis Center, Washington, D.C., 74 pp.

Kuo, H.-L., 1949: Dynamic instability of two-dimensional nondivergent flow in a barotropic atmosphere. *J. Meteor.*, **6**, 105-122.

Miller, E., 1993: *The Impact of a Typhoon on the Global Atmosphere.* Master's Thesis, Naval Postgraduate School, Monterey California, April 1993.

Murphree, T., 1994: Subtropical mechanisms influencing Pacific-North American teleconnections. Submitted to *J. Climate.*

Neith, M., *Intraseasonal Relationships Between Tropical Heating and Extratropical Jets*. Master's Thesis, Naval Postgraduate School, Monterey, California, December 1992.

Peng, M.S., and R.T. Williams, 1986: Spatial instability of the barotropic jet with slow streamwise variation. *J. Atmos. Sci.*, **43**, 2430-2442.

Plumb, R., 1985: On the three-dimensional propagation of stationary waves. *J. Atmos. Sci.*, **42**, 217-229.

Sardeshmukh, P., and B. Hoskins, 1988: The generation of global rotational flow by idealized tropical divergence. *J. Atmos. Sci.*, **45**, 1228-1251.

Walker, G., 1924: Correlation in seasonal variations of weather IX: a further study of world weather. *Memoirs of the Royal Meteorological Society*, **24**, 275-332.

-----, and E. Bliss, 1932: World Weather V. *Memoirs of the Royal Meteorological Society*, **4**, 53-84.

Wallace, J., and D. Gutzler, 1981: Teleconnections in the geopotential height field during the northern Hemisphere winter. *Mon. Wea. Rev.*, **109**, 784-812.

Wyrtki, K., 1975: El Niño - the dynamic response of the equatorial Pacific Ocean to atmospheric forcing. *J. Phys. Oceanogr.*, **5**, 572-584.

Model Runs	Circulation Represents	Circulation Includes
POSITIVE	atmosphere with tropical cyclone	background flow + tropical cyclone + interactions
NO	atmosphere with tropical cyclone	background flow + tropical cyclone + interactions
NEGATIVE	atmosphere without tropical cyclone	background flow

Table 1. Summary of the model runs performed with the three different tropical cyclone bogusing procedures used to calculate the initial conditions for the model runs.

Differences Between Model Runs	Circulation Represents the Effect on the Global Atmosphere of	Circulation Includes
POSITIVE - NO	POSITIVE tropical cyclone bogusing procedure	(POSITIVE-NO) tropical cyclone + (POSITIVE-NO) interactions
NO - NEGATIVE	NEGATIVE tropical cyclone bogusing procedure	NO tropical cyclone + NO interactions
POSITIVE - NEGATIVE	POSITIVE tropical cyclone and interactions	POSITIVE tropical cyclone + POSITIVE interactions

Table 2. Summary of the differences between model runs described in Table 1. These differences are used to assess impacts of the three tropical cyclone bogusing procedures on the model forecasts.

Date Time (1991)	POSITIVE SLP Position (mb)	NO SLP Position (mb)	NEGATIVE SLP Position (mb)	JTWC SLP Position (mb)
28 Nov 00Z	988 15N,140E	990 12N,140E	1005 10N,137E	892 14N,141E
28 Nov 12Z	988 15N,140E	987 15N,137E	1005 12N,132E	898 16N,140E
29 Nov 00Z	988 17N,140E	986 15N,137E	1005 12N,130E	906 18N,139E
29 Nov 12Z	987 20N,140E	983 17N,137E	1005 10N,130E	922 19N,139E
30 Nov 00Z	989 22N,142E	980 20N,137E	1005 12N,127E	938 21N,141E
30 Nov 12Z	989 27N,145E	980 22N,137E	1004 10N,130E	948 24N,144E
01 Dec 00Z	984 32N,152E	979 25N,140E	1004 12N,135E	95[illegible] 27N,149E
01 Dec 12Z	983 35N,160E	983 27N,145E	998 47N,150E	972 32N,154E

Table 3. Minimum sea level pressures (SLP) for the Forecast 2 POSITIVE, NO, and NEGATIVE runs, plus the JTWC best estimates of minimum sea level pressure for Yuri.

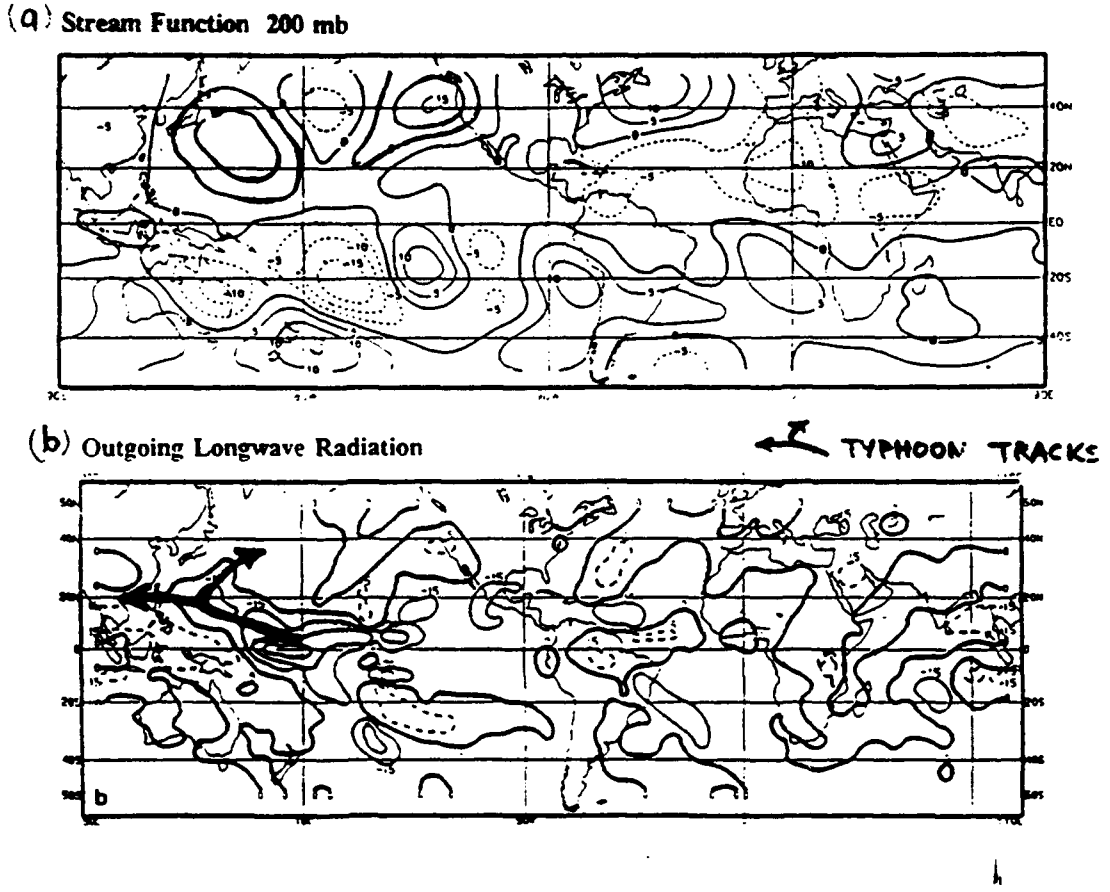

Figure 1. Monthly mean anomalies for November 1991: (a) 200 mb streamfunction, (b) OLR. Streamfunction contour interval is 5×10^6 m^2/s. OLR contour interval is 15 W/m^2 (from Kousky 1991).

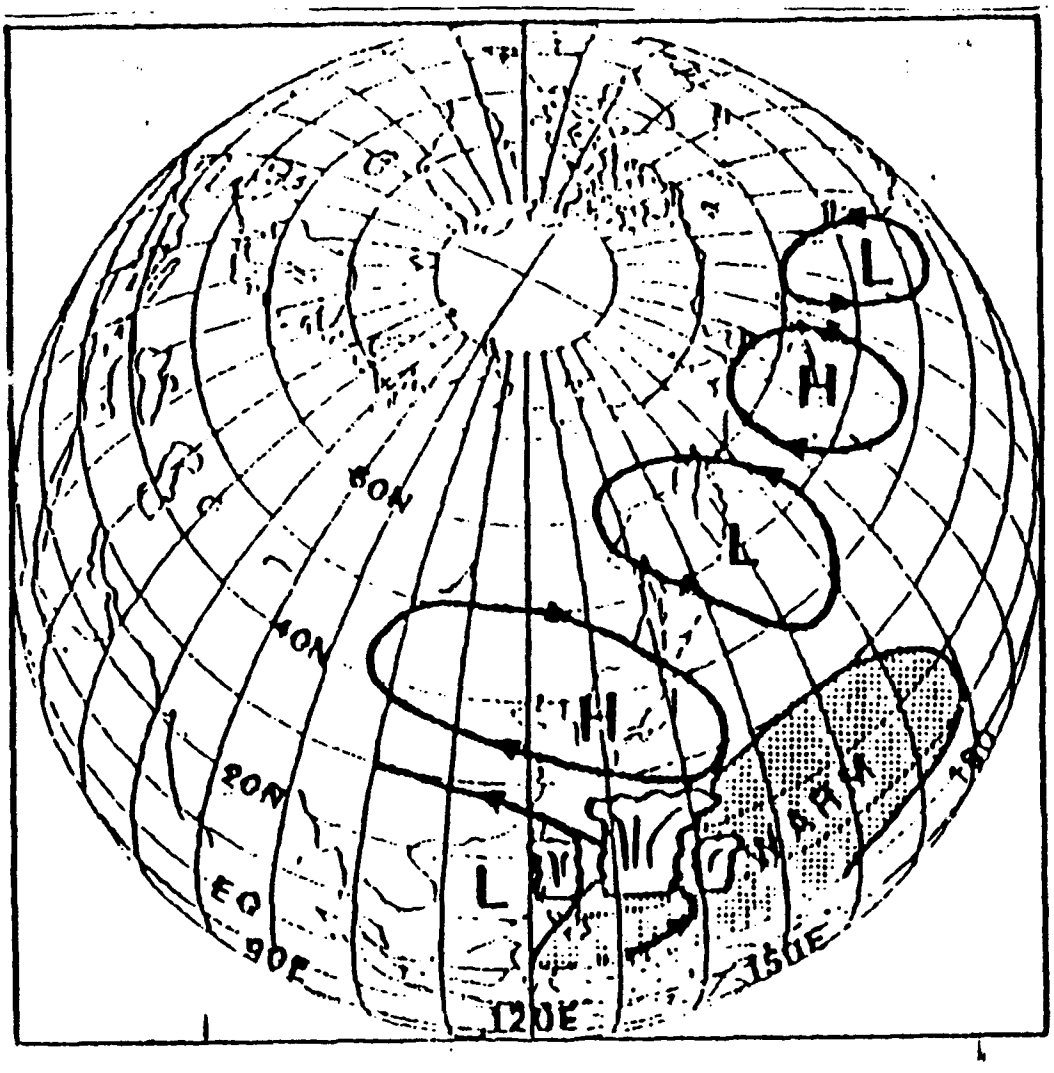

Figure 2. Schematic of 500 mb height anomalies due to increased convection during summers with warmer than normal SST in the tropical western Pacific. H denotes positive height anomaly, L denotes negative height anomaly (from Nitta 1987).

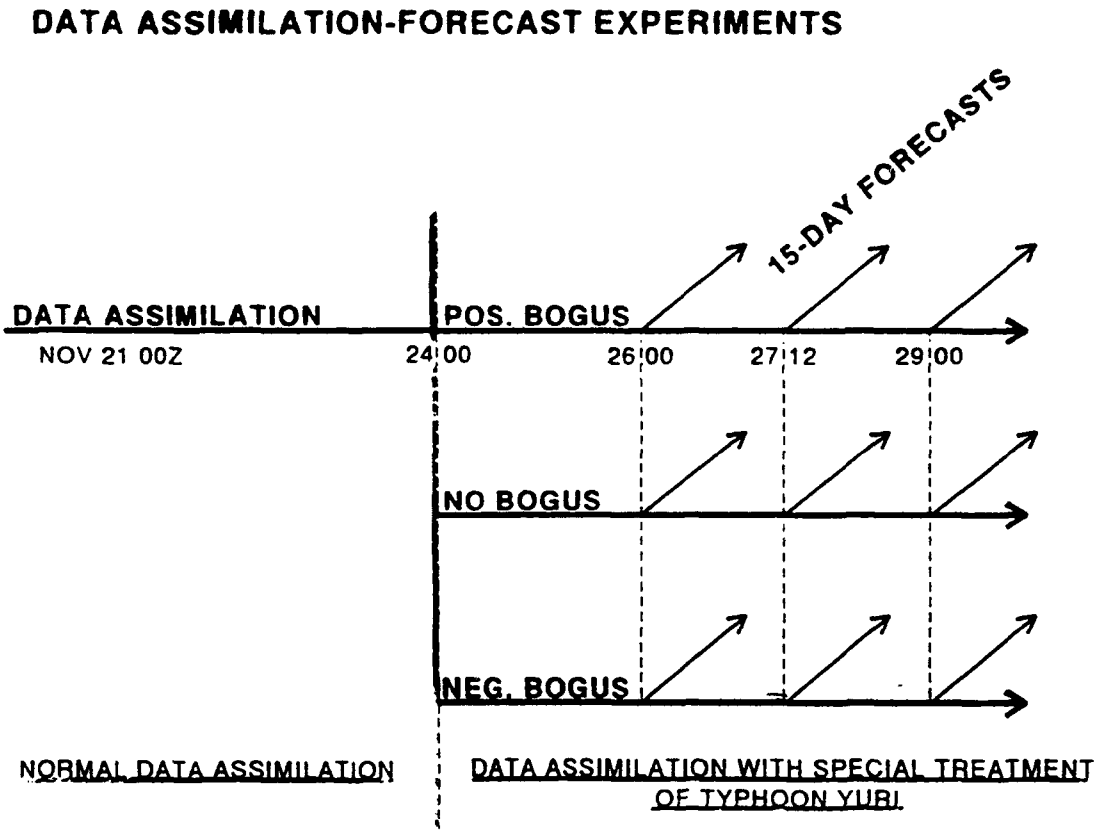

Figure 3. Schematic of the data assimilation and tropical cyclone bogusing procedures for the nine model runs. Bogusing procedures were initiated when Yuri's winds reached 18 m/s. Bogusing continued until the start of each model run.

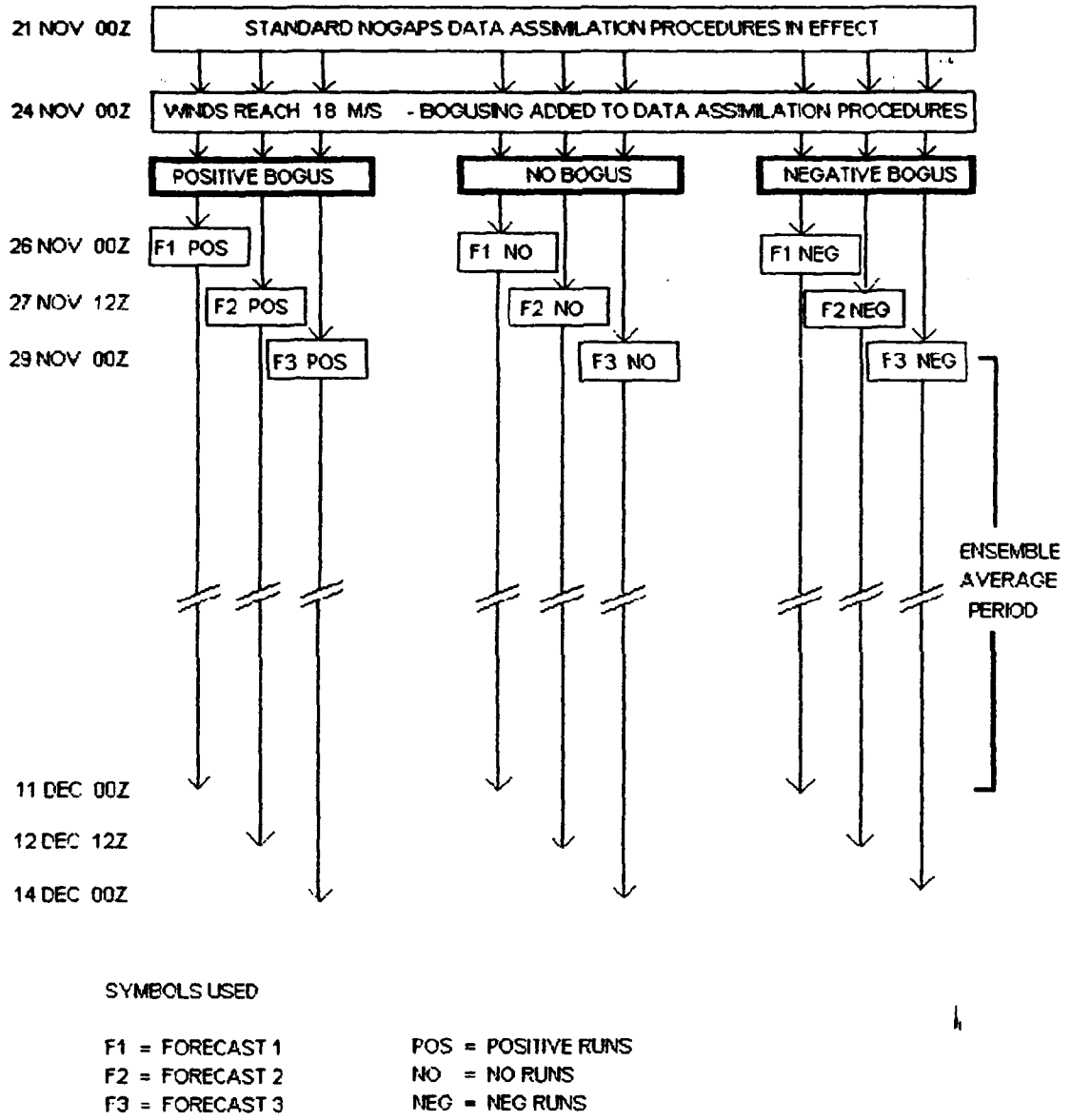

Figure 4. Schematic of nine model runs conducted, showing standard data assimilation period, modified data assimilation period, 15 day forecast period, and ensemble average period.

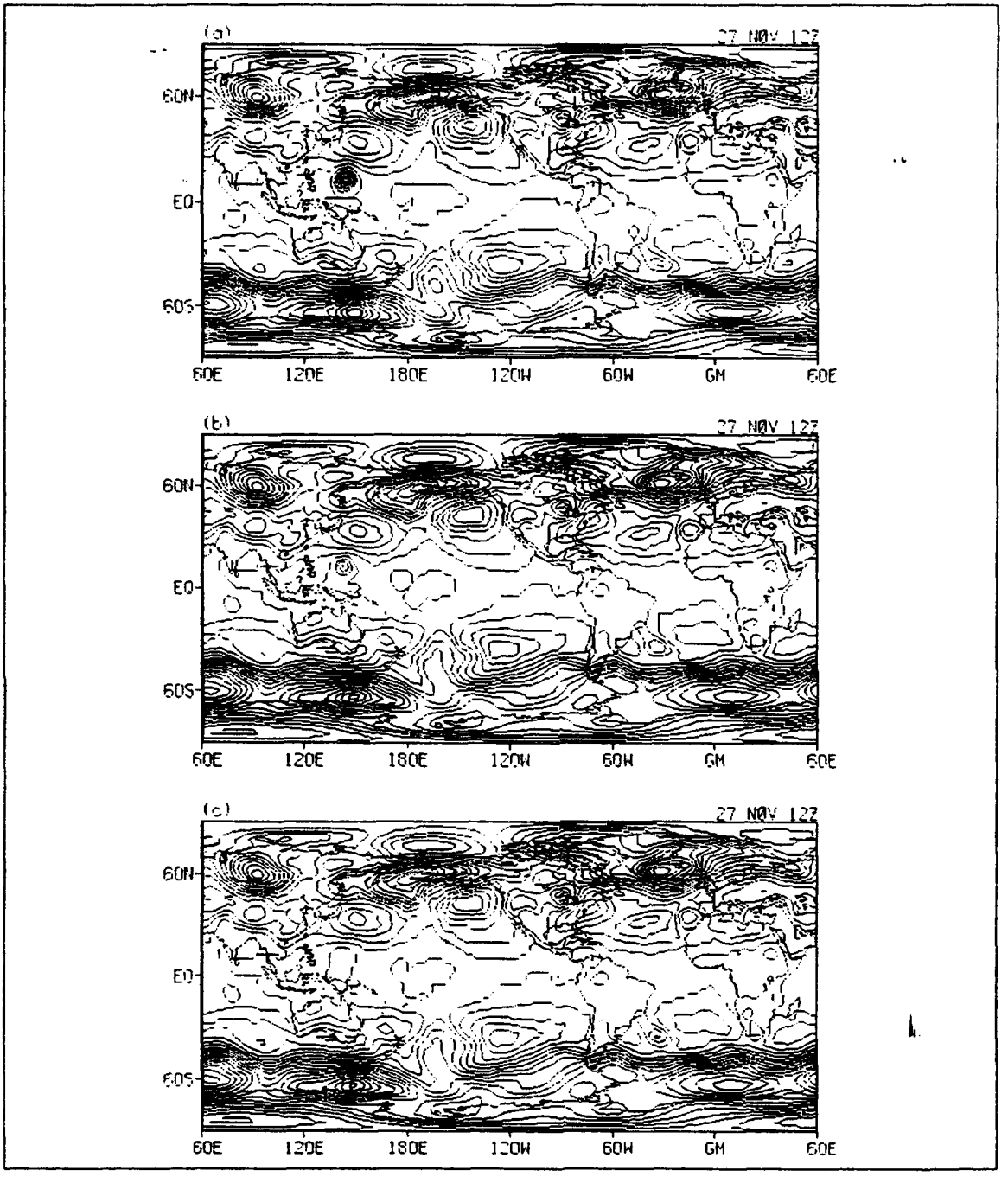

Figure 5. Sea level pressure initial conditions for Forecast 2: (a) POSITIVE, (b) NO, (c) NEGATIVE runs. Contour interval is 4 mb.

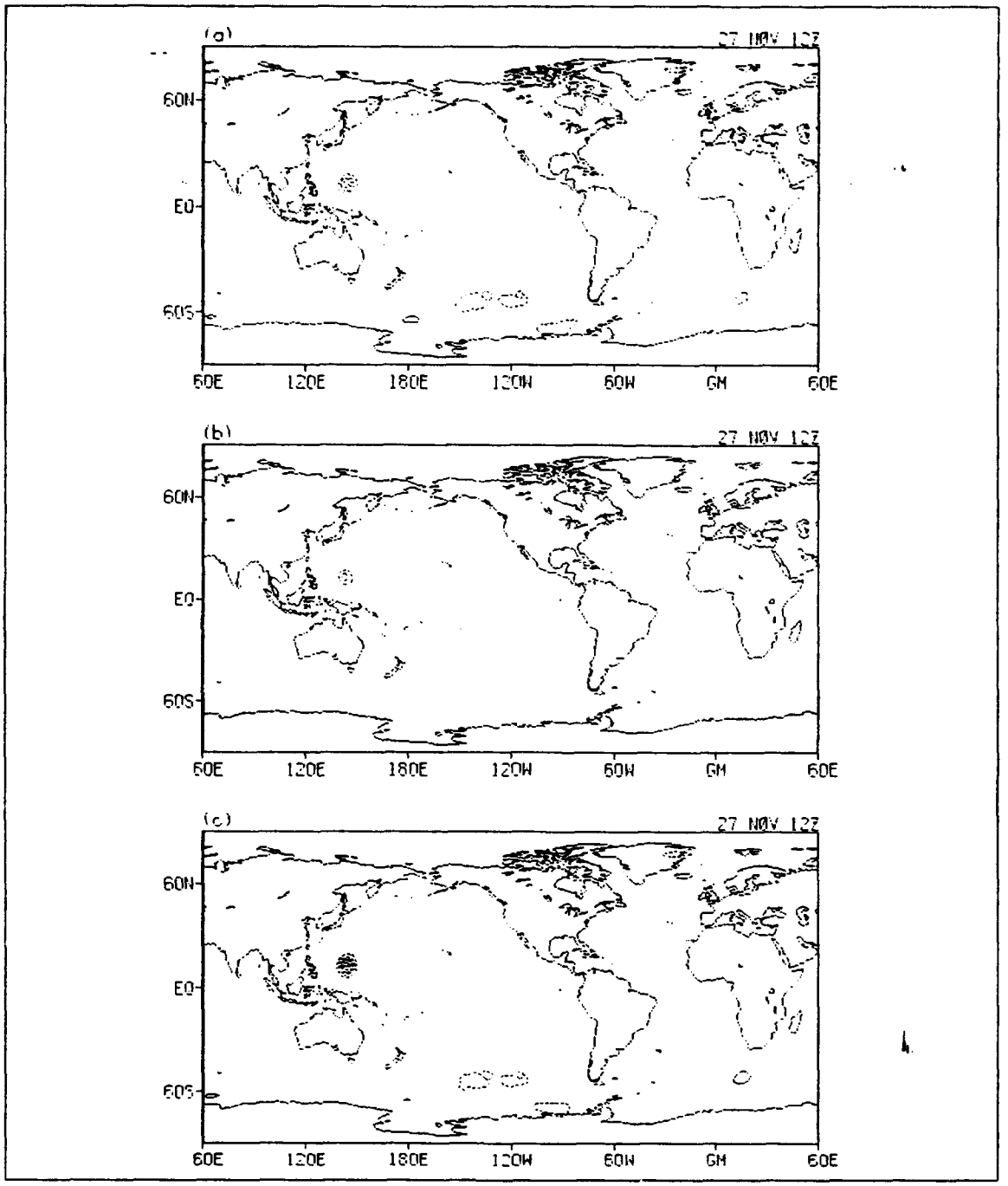

Figure 6. Differences in sea level pressure initial conditions for Forecast 2: (a) POSITIVE - NO, (b) NO - NEGATIVE, (c) POSITIVE - NEGATIVE differences. Contour interval is 4 mb.

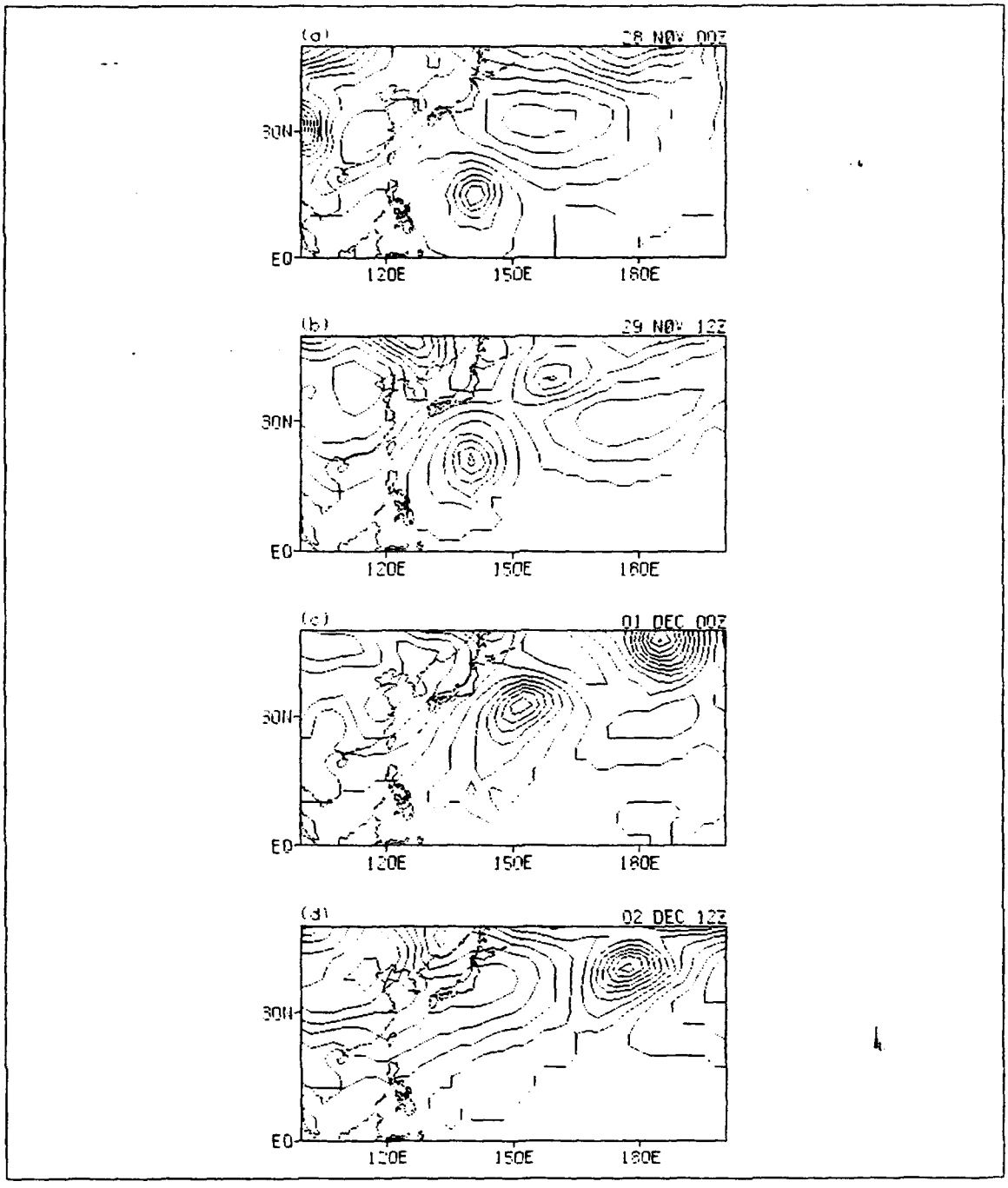

Figure 7. Sea level pressures in the western Pacific at selected times for Forecast 2 POSITIVE run. Contour interval is 4 mb.

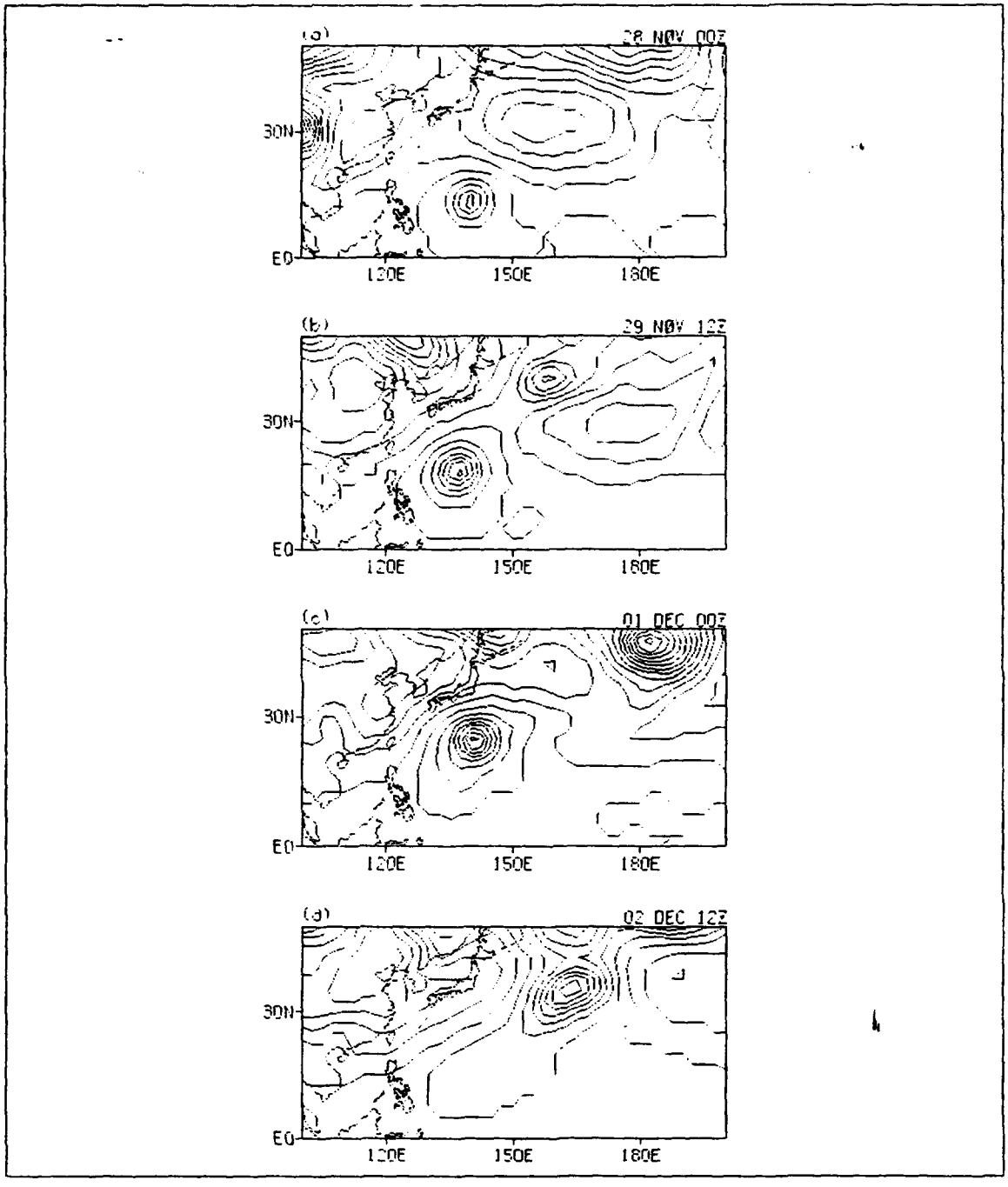

Figure 8. Sea level pressures in the western Pacific at selected times for Forecast 2 NO run. Contour interval is 4 mb.

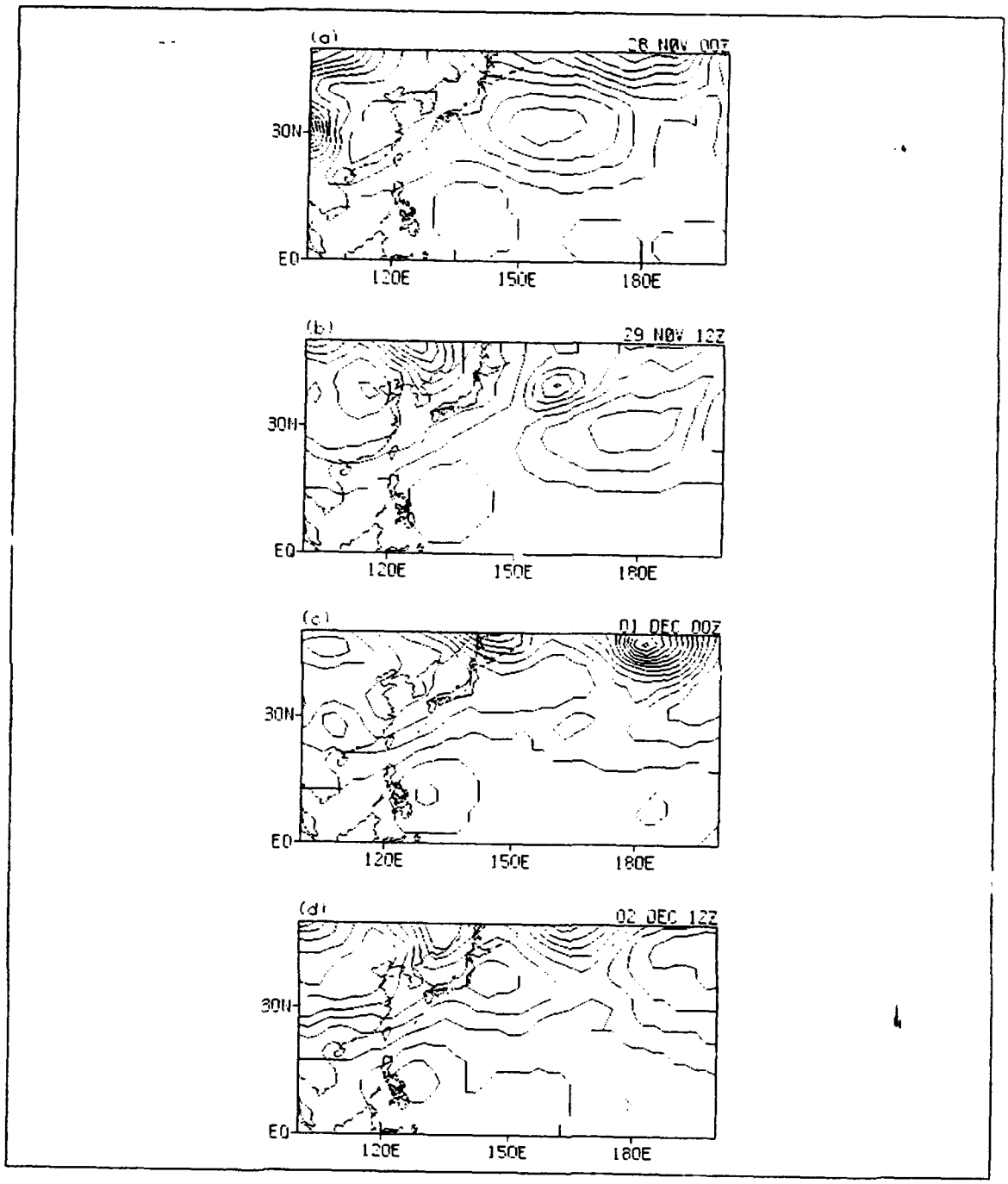

Figure 9. Sea level pressures in the western Pacific at selected times for Forecast 2 NEGATIVE run. Contour interval is 4 mb.

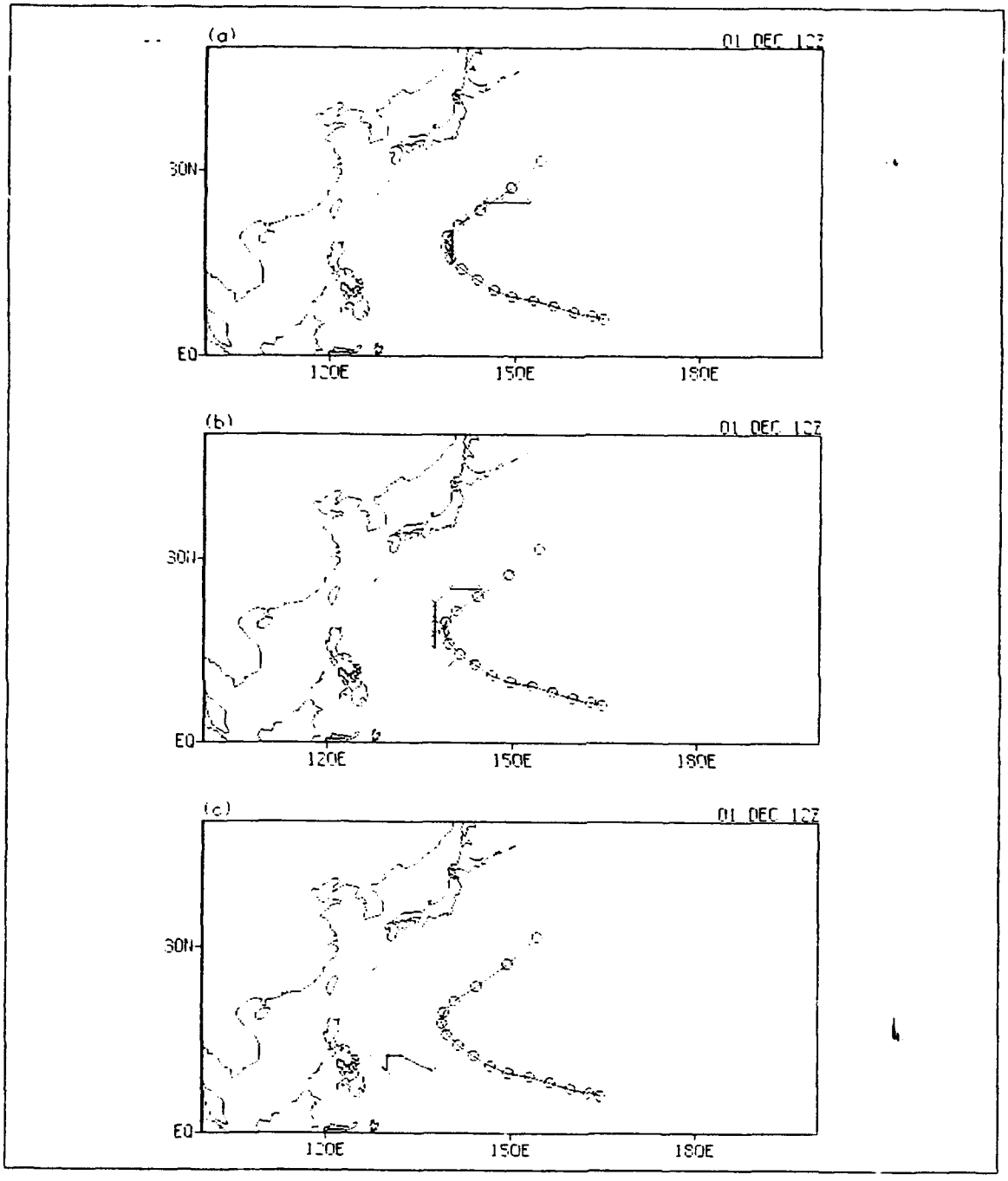

Figure 10. Yuri tracks (crosses) from Forecast 2: (a) POSITIVE, (b) NO, (c) NEGATIVE runs. Circles denote JTWC track of Yuri.

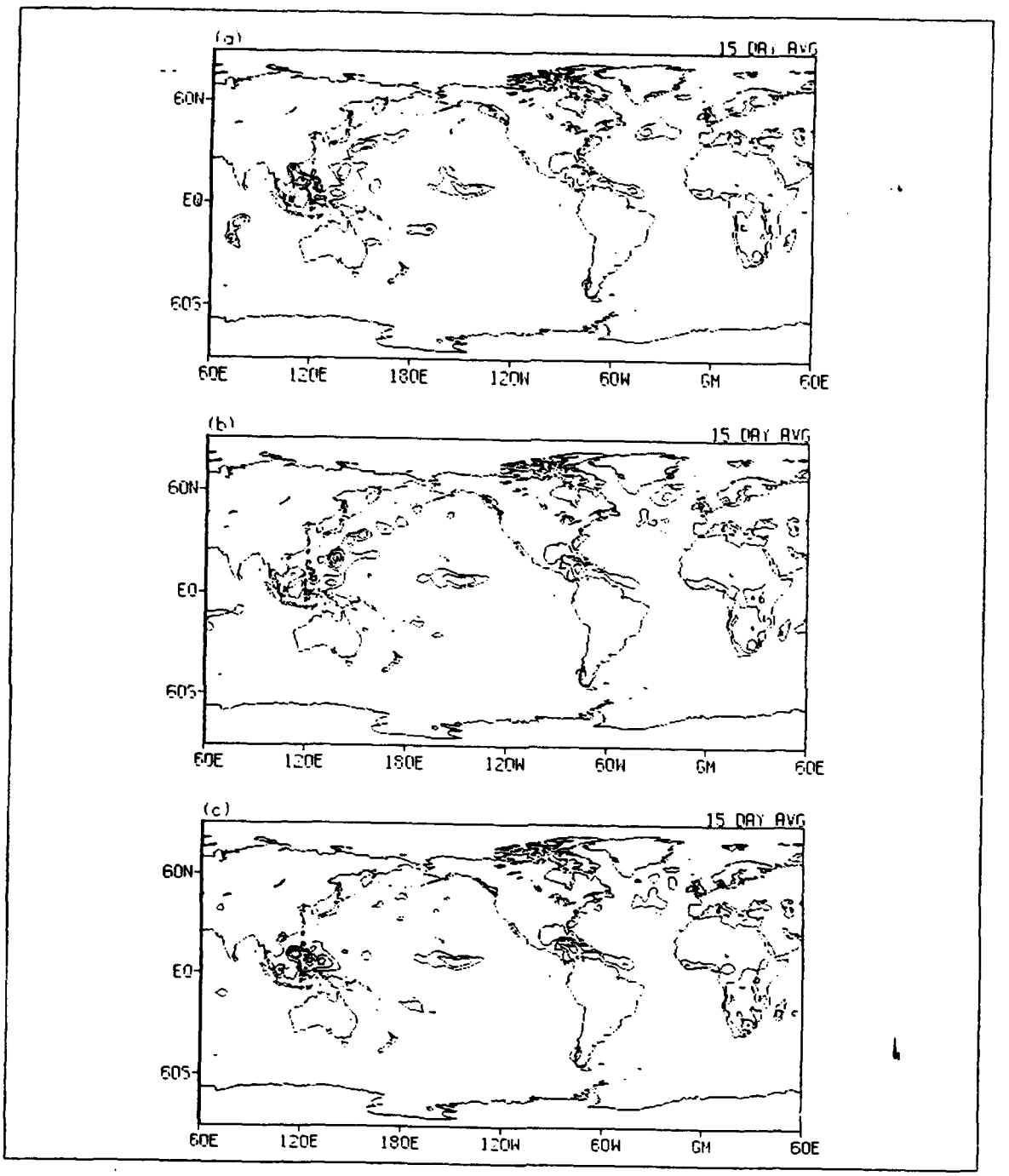

Figure 11. 15 day average atmospheric heating for Forecast 2: (a) POSITIVE, (b) NO, (c) NEGATIVE runs. Minimum contour is 2°C/day. Contour interval is 1°C/day.

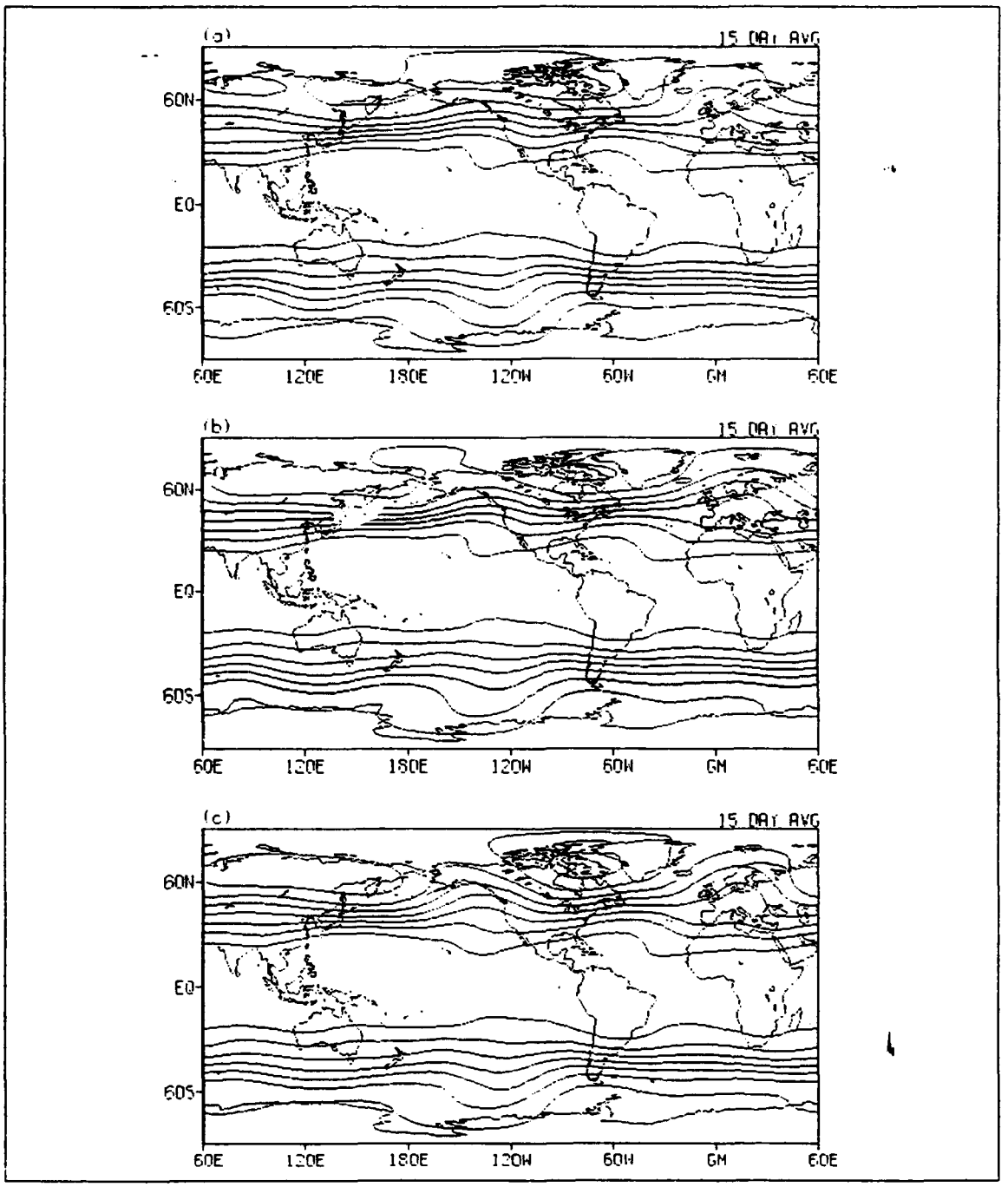

Figure 12. 15 day average 200 mb geopotential height for Forecast 2: (a) POSITIVE, (b) NO, (c) NEGATIVE runs. Minimum contour is 10500 gpm. Contour interval is 200 gpm.

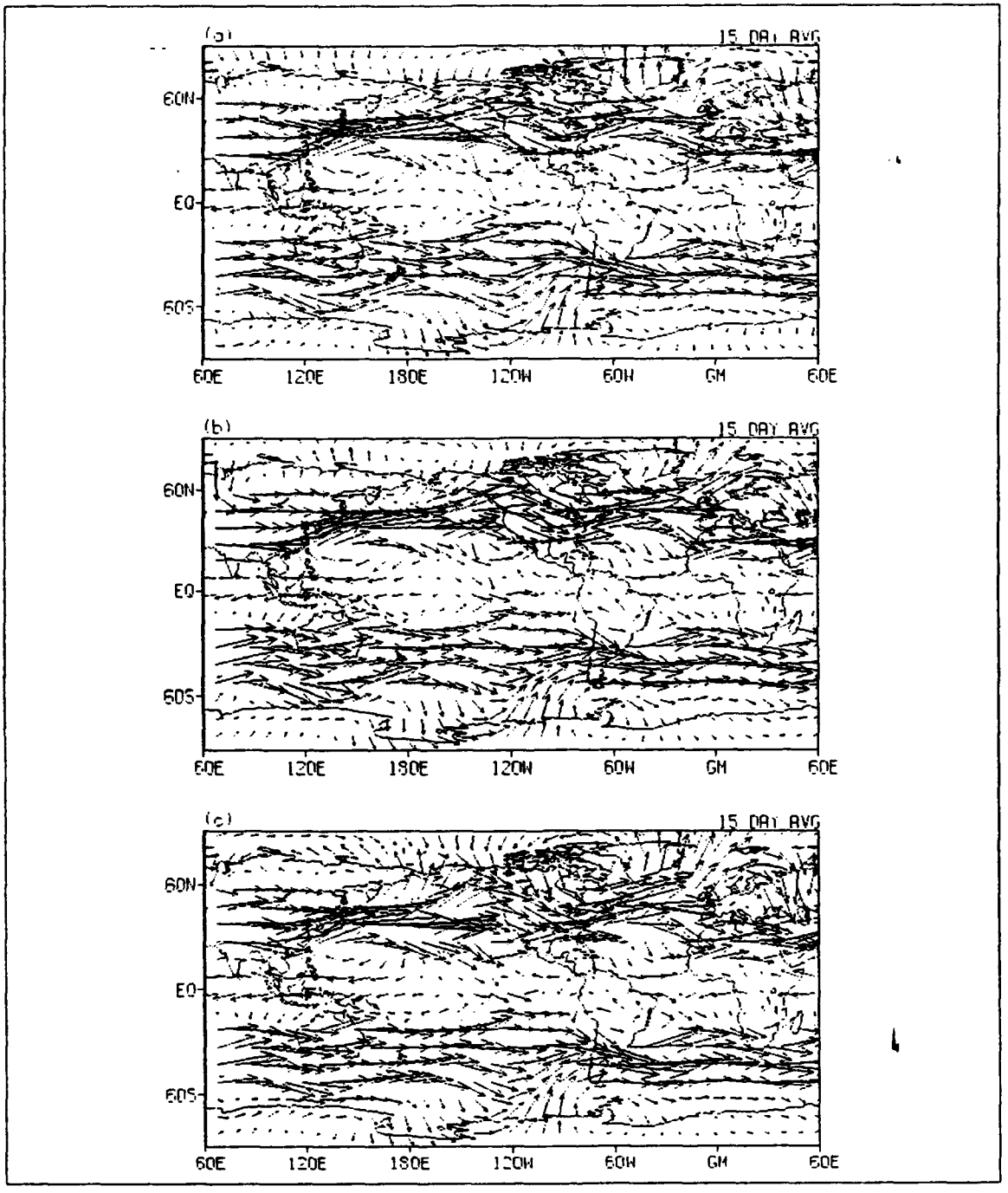

Figure 13. 15 day average 200 mb winds for Forecast 2: (a) POSITIVE, (B) NO, (C) NEGATIVE runs. Vector scale (m/s) as indicated.

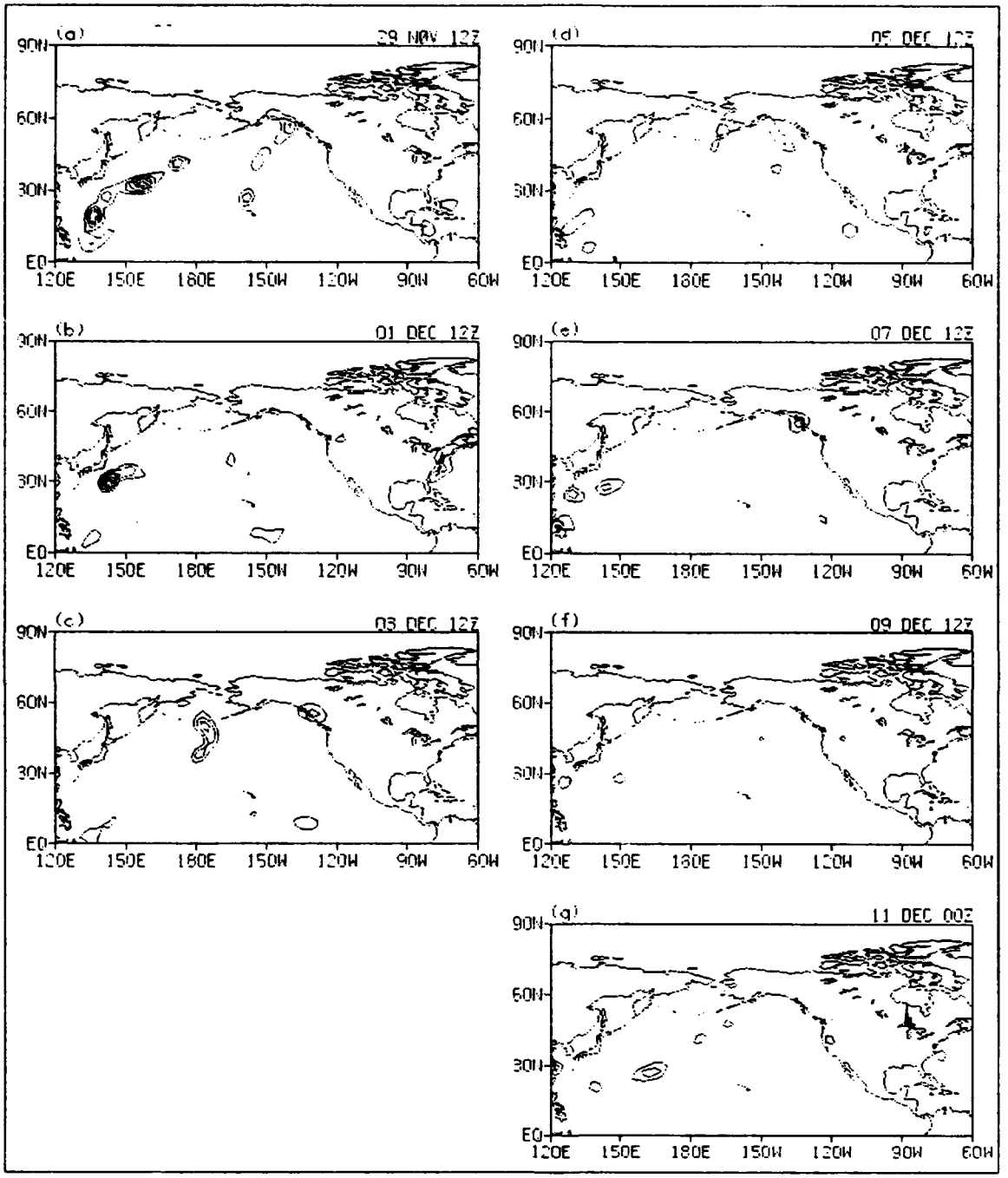

Figure 14. Atmospheric heating at selected times for Forecast 1 POSITIVE run. Minimum contour is 2°C/day. Contour interval is 1°C/day.

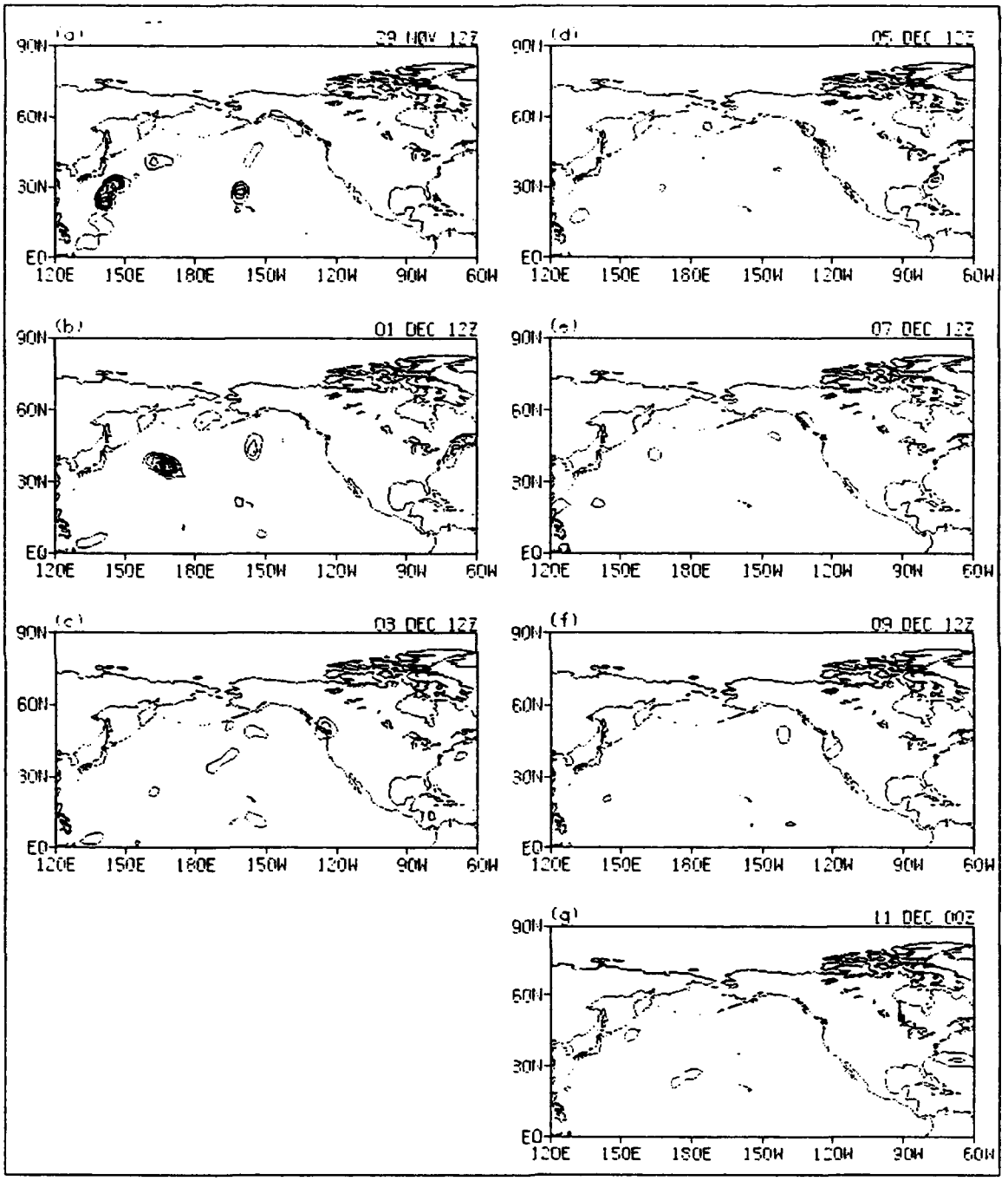

Figure 15. Atmospheric heating at selected times for Forecast 2 POSITIVE run. Minimum contour is 2°C/day. Contour interval is 1°C/day.

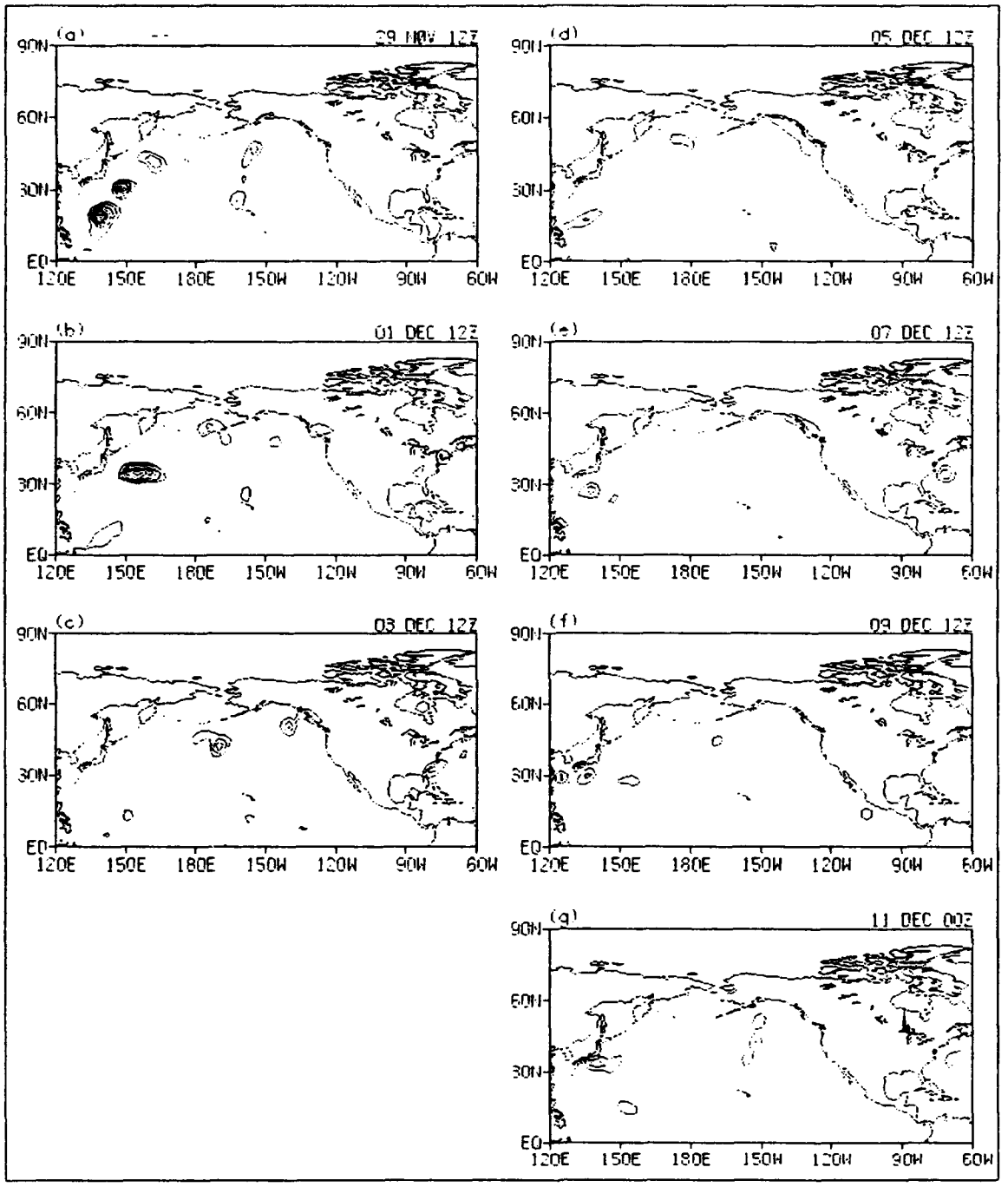

Figure 16. Atmospheric heating at selected times for Forecast 3 POSITIVE run. Minimum contour is 2°C/day. Contour interval is 1°C/day.

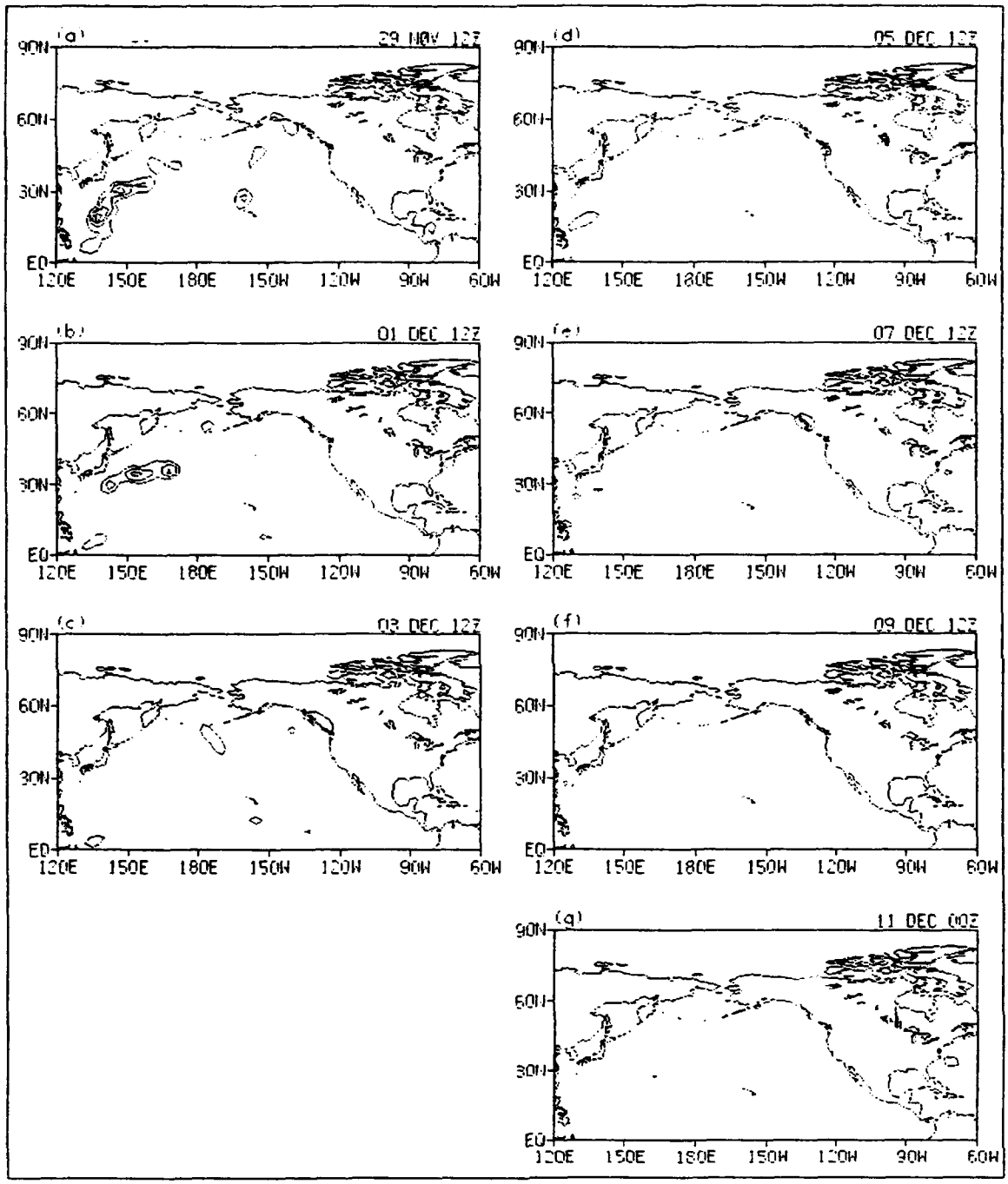

Figure 17. Atmospheric heating at selected times for Ensemble Average POSITIVE run. Minimum contour is 2°C/day. Contour interval is 1°C/day.

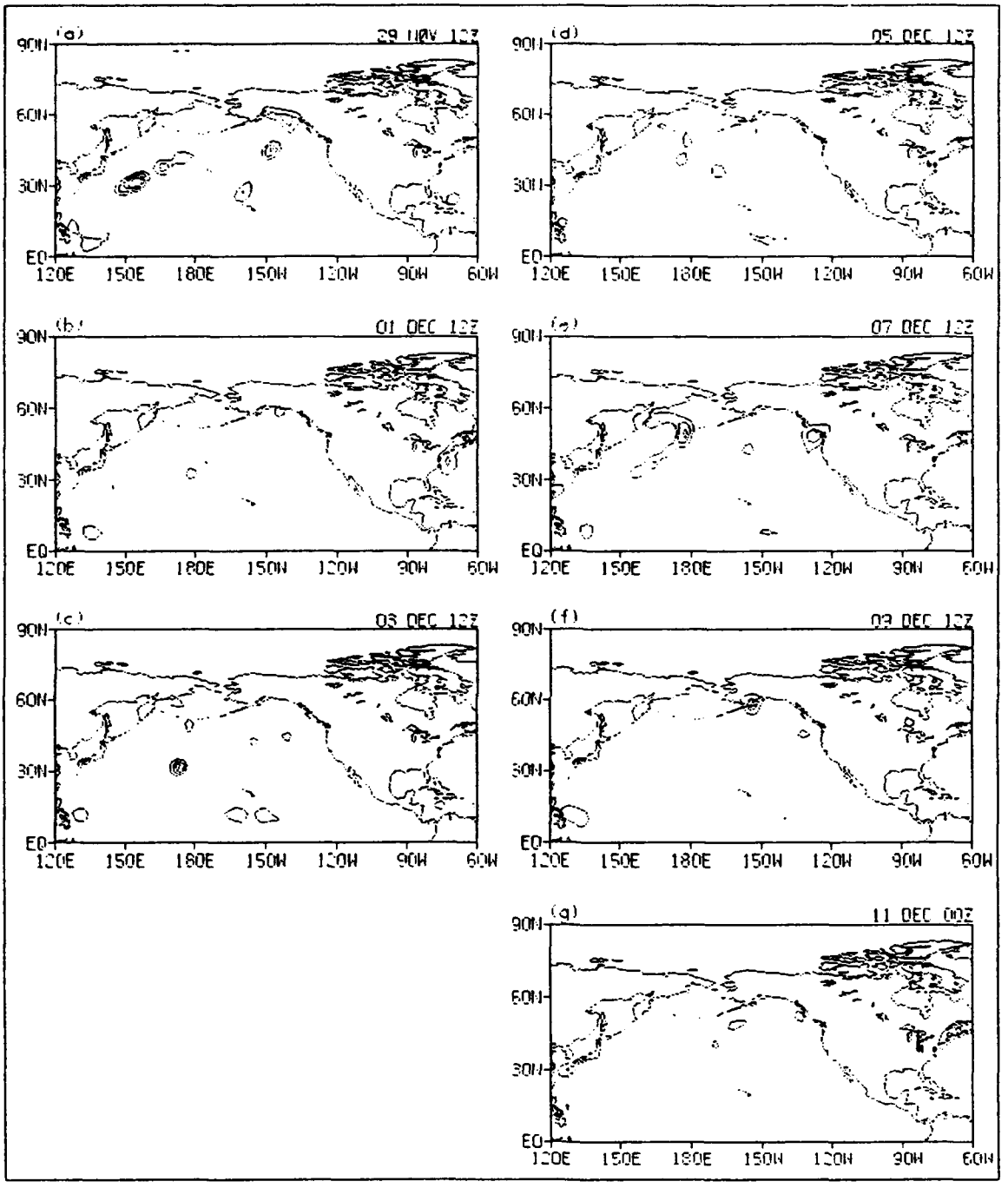

Figure 18. Atmospheric heating at selected times for Forecast 1 NEGATIVE run. Minimum contour is 2°C/day. Contour interval is 1°C/day.

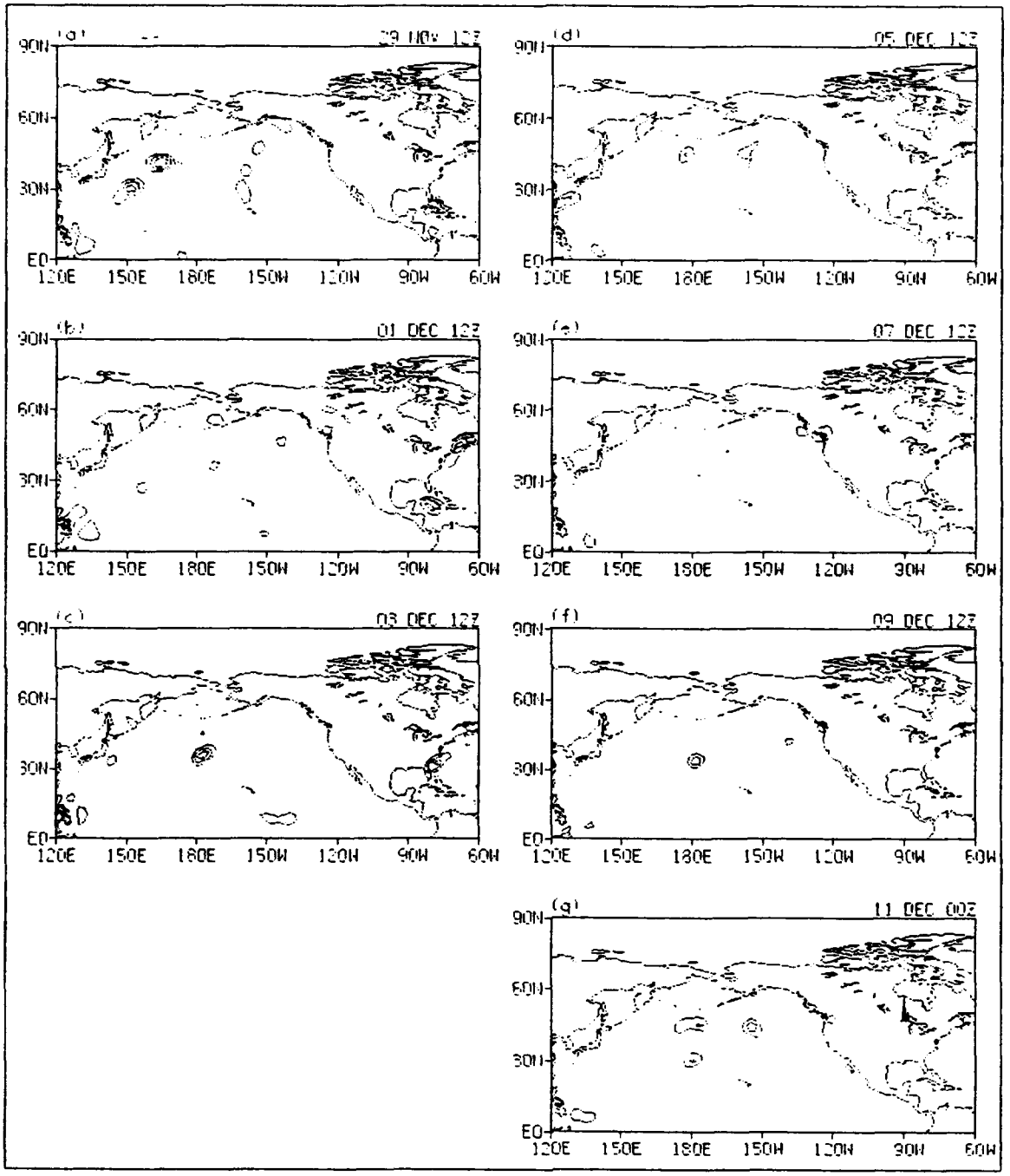

Figure 19. Atmospheric heating at selected times for Forecast 2 NEGATIVE run. Minimum contour is 2°C/day. Contour interval is 1°C/day.

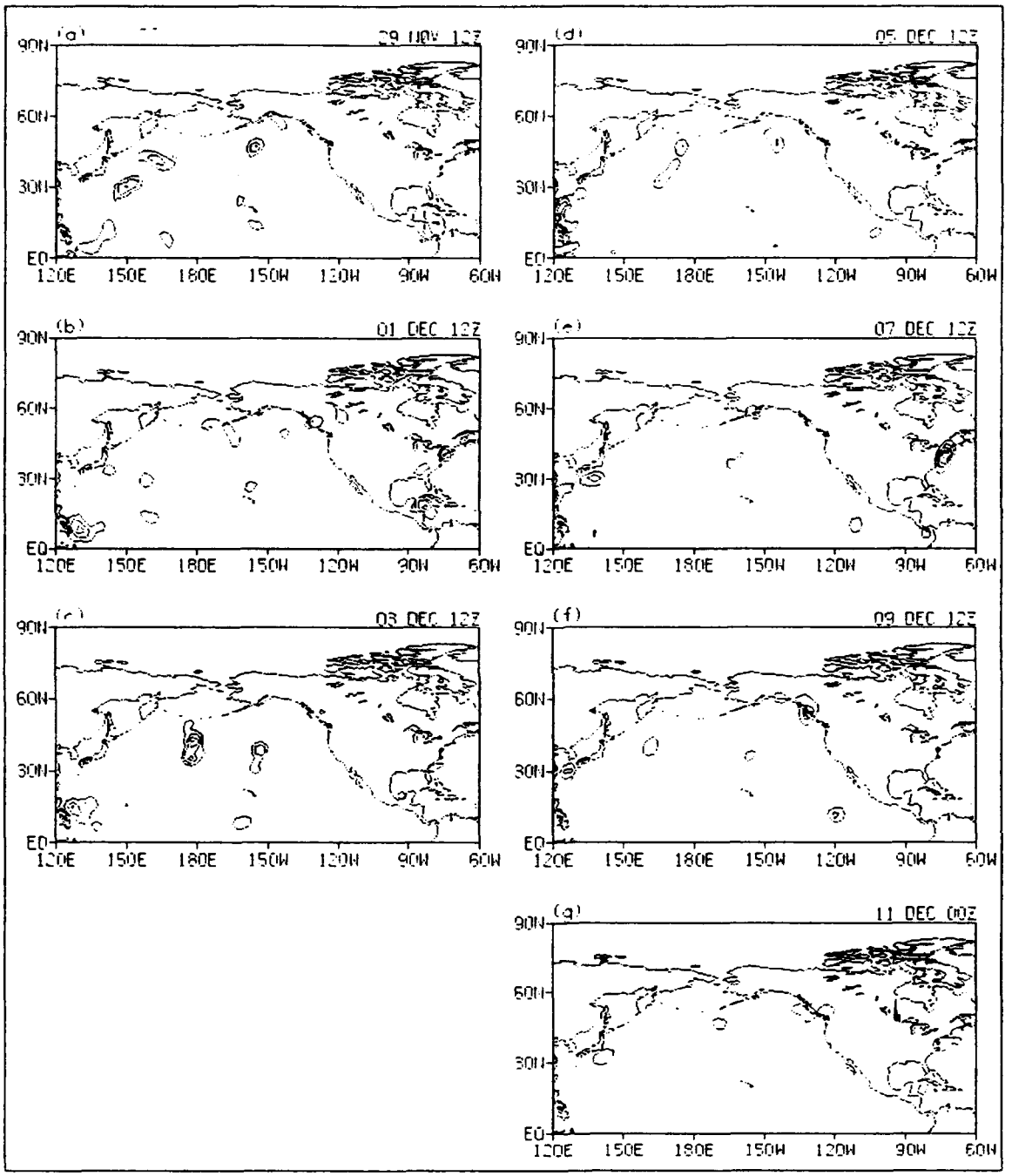

Figure 20. Atmospheric heating at selected times for Forecast 3 NEGATIVE run. Minimum contour is 2°C/day. Contour interval is 1°C/day.

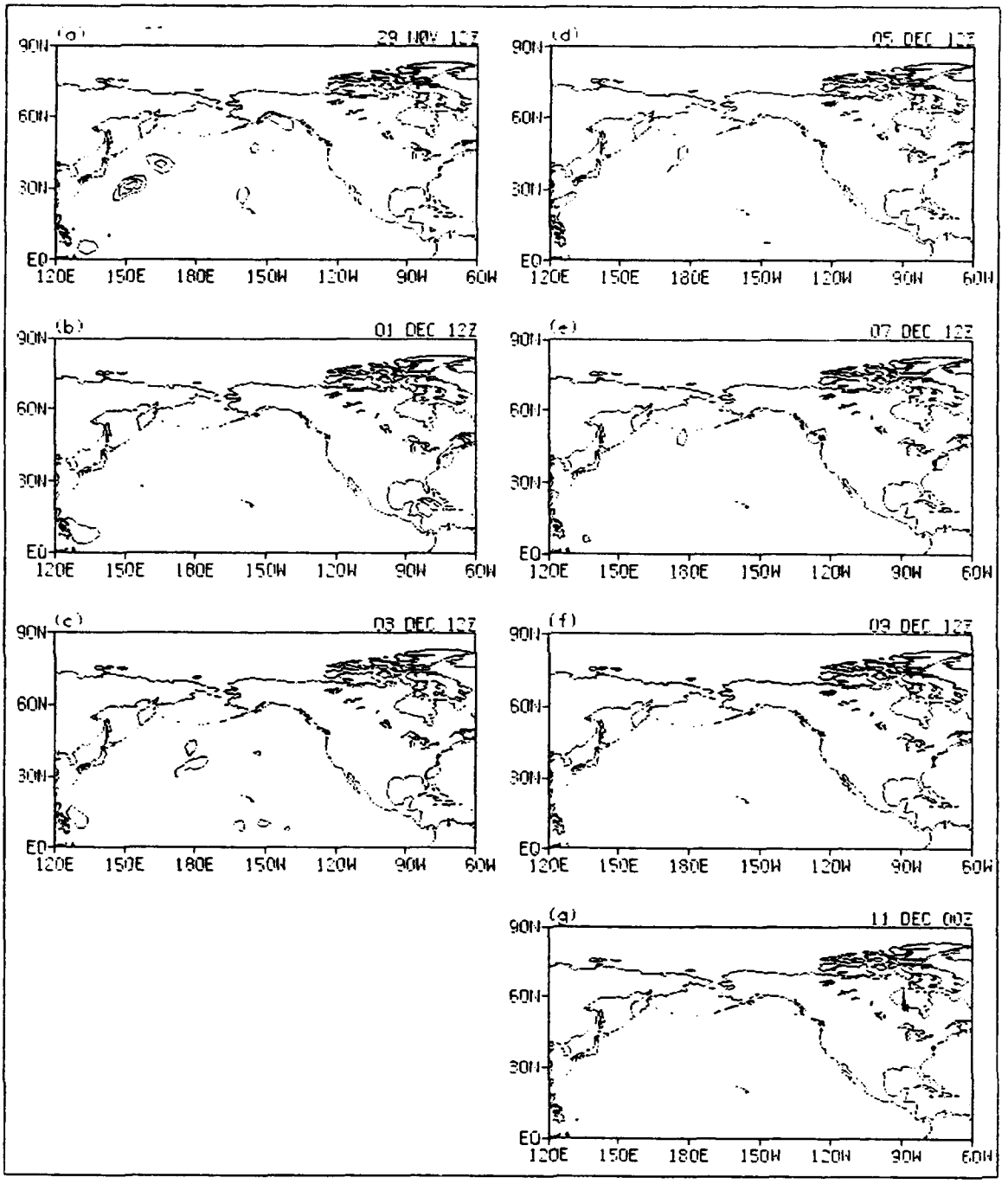

Figure 21. Atmospheric heating at selected times for Ensemble Average NEGATIVE run. Minimum contour is 2°C/day. Contour interval is 1°C/day.

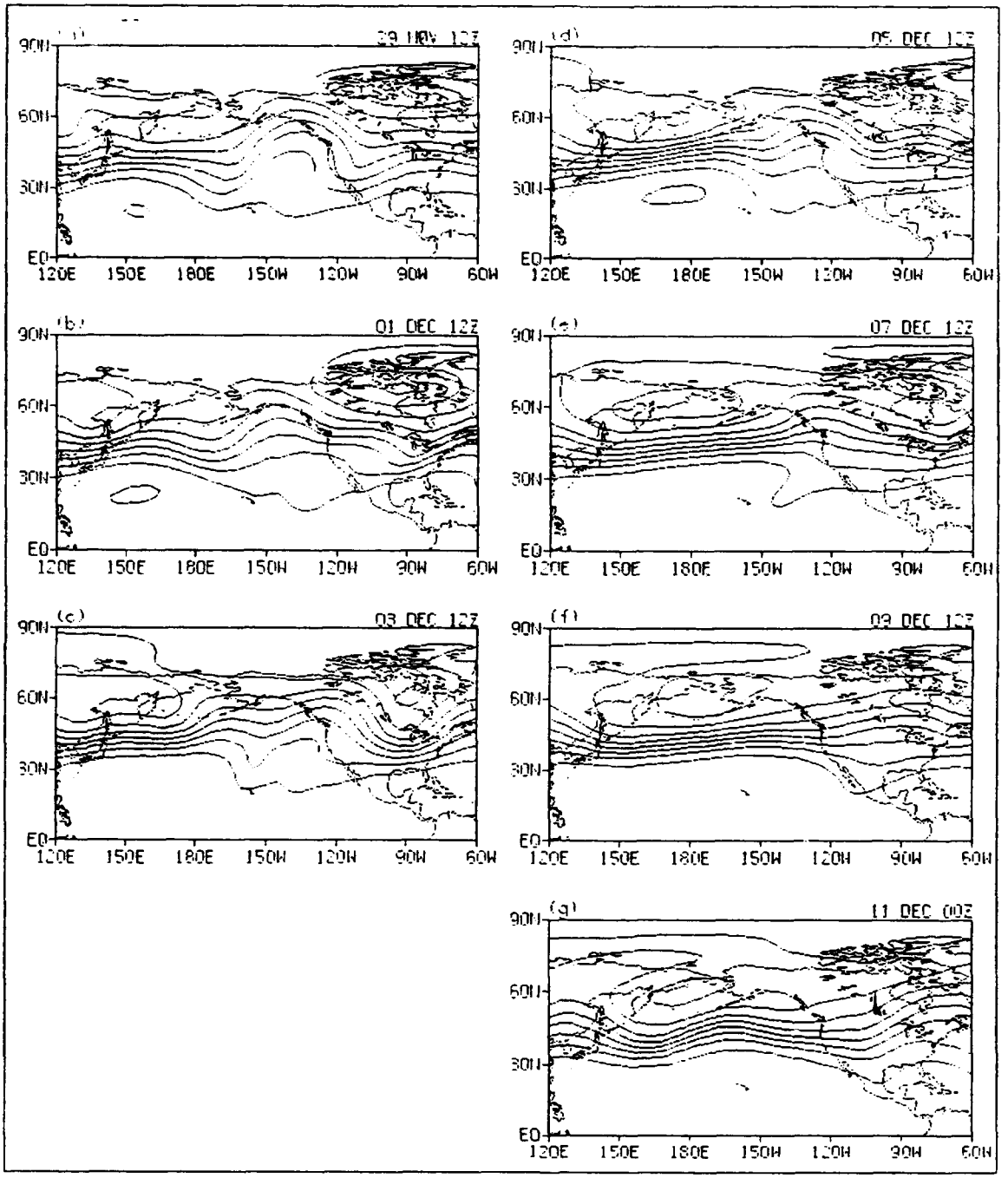

Figure 22. 200 mb geopotential heights at selected times for Forecast 1 POSITIVE run. Minimum contour is 10500 gpm. Contour interval is 200 gpm.

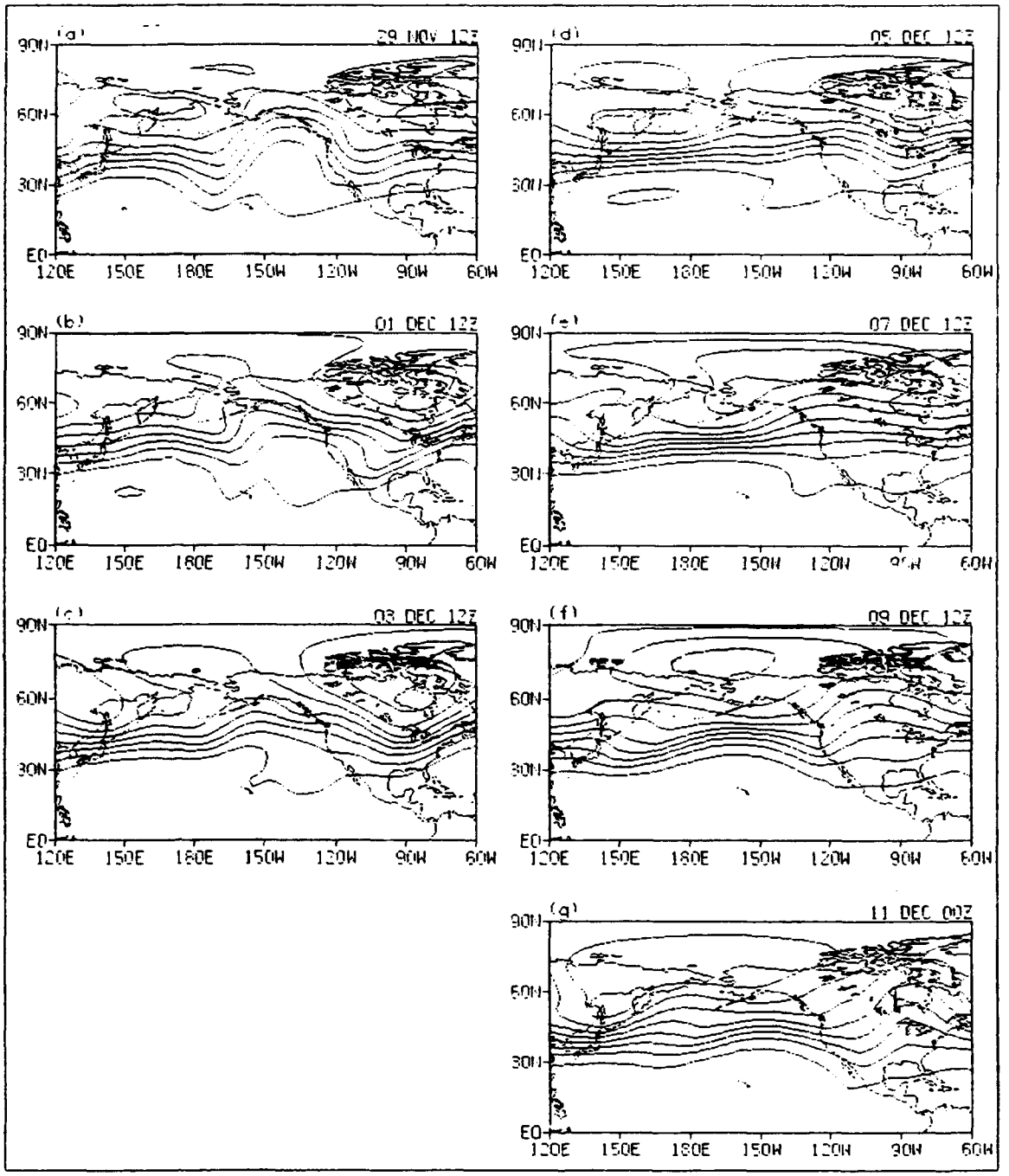

Figure 23. 200 mb geopotential heights at selected times for Forecast 2 POSITIVE run. Minimum contour is 10500 gpm. Contour interval is 200 gpm.

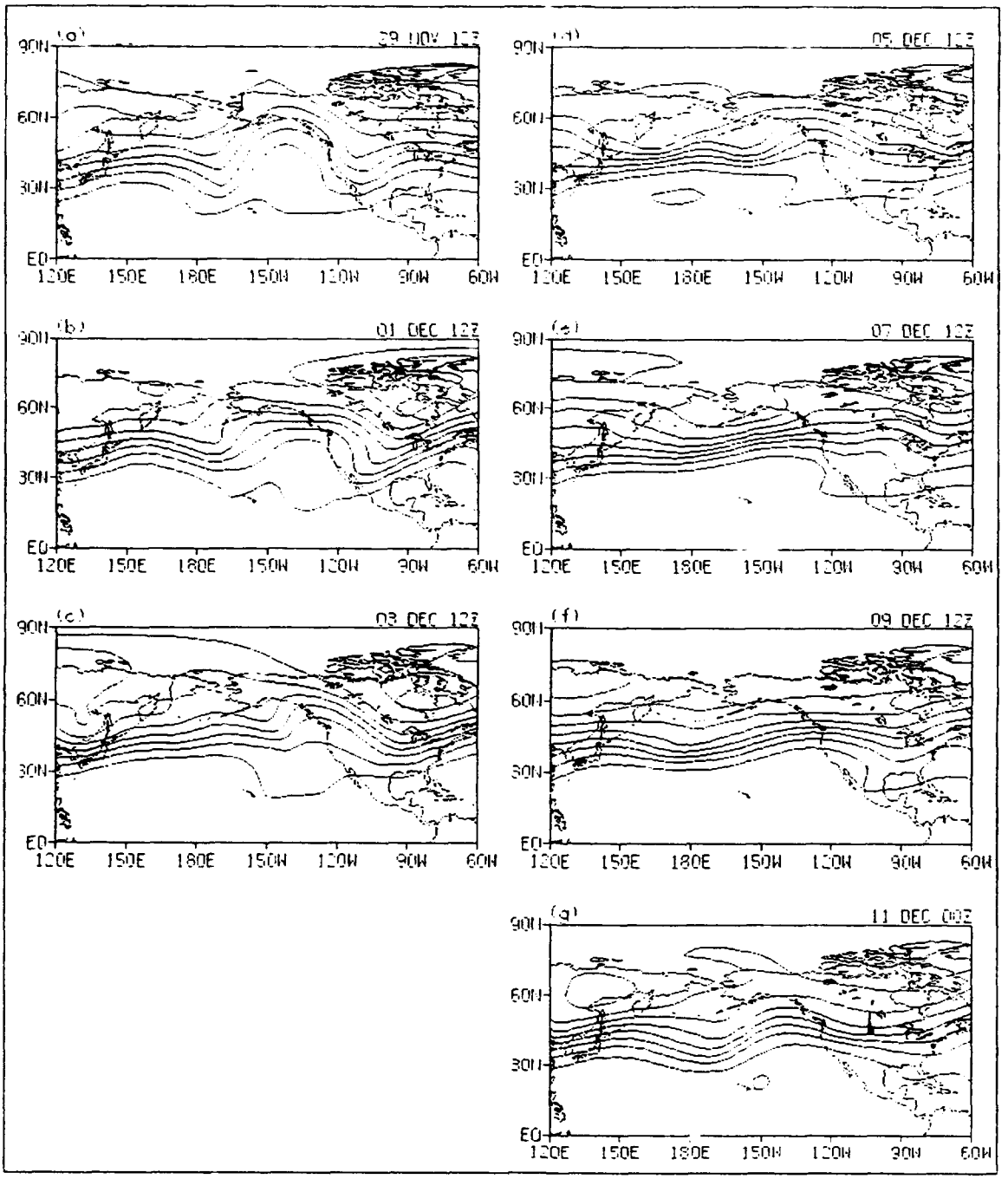

Figure 24. 200 mb geopotential heights at selected times for Forecast 3 POSITIVE run. Minimum contour is 10500 gpm. Contour interval is 200 gpm.

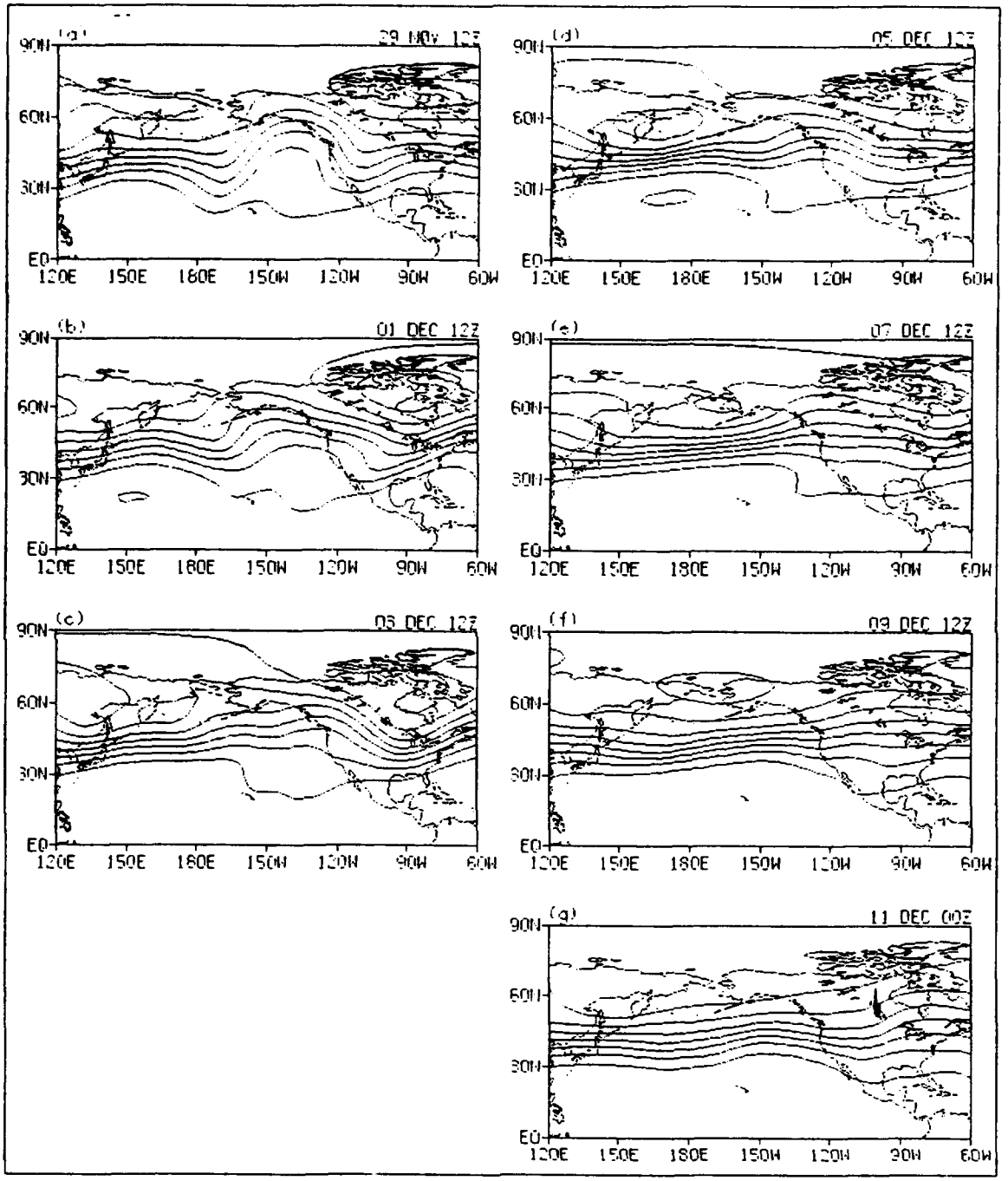

Figure 25. 200 mb geopotential heights at selected times for Ensemble Average POSITIVE run. Minimum contour is 10500 gpm. Contour interval is 200 gpm.

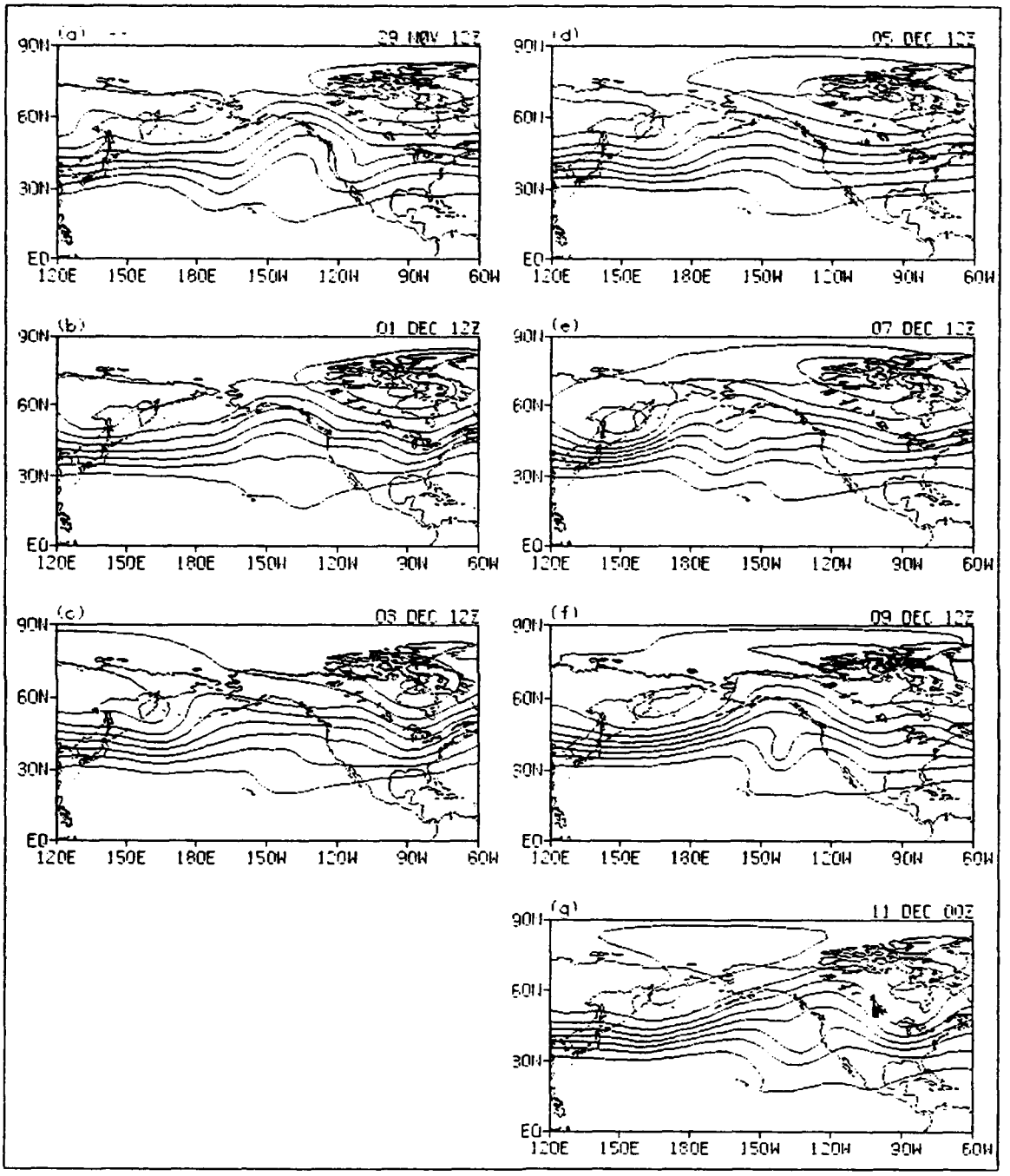

Figure 26. 200 mb geopotential heights at selected times for Forecast 1 NEGATIVE run. Minimum contour is 10500 gpm. Contour interval is 200 gpm.

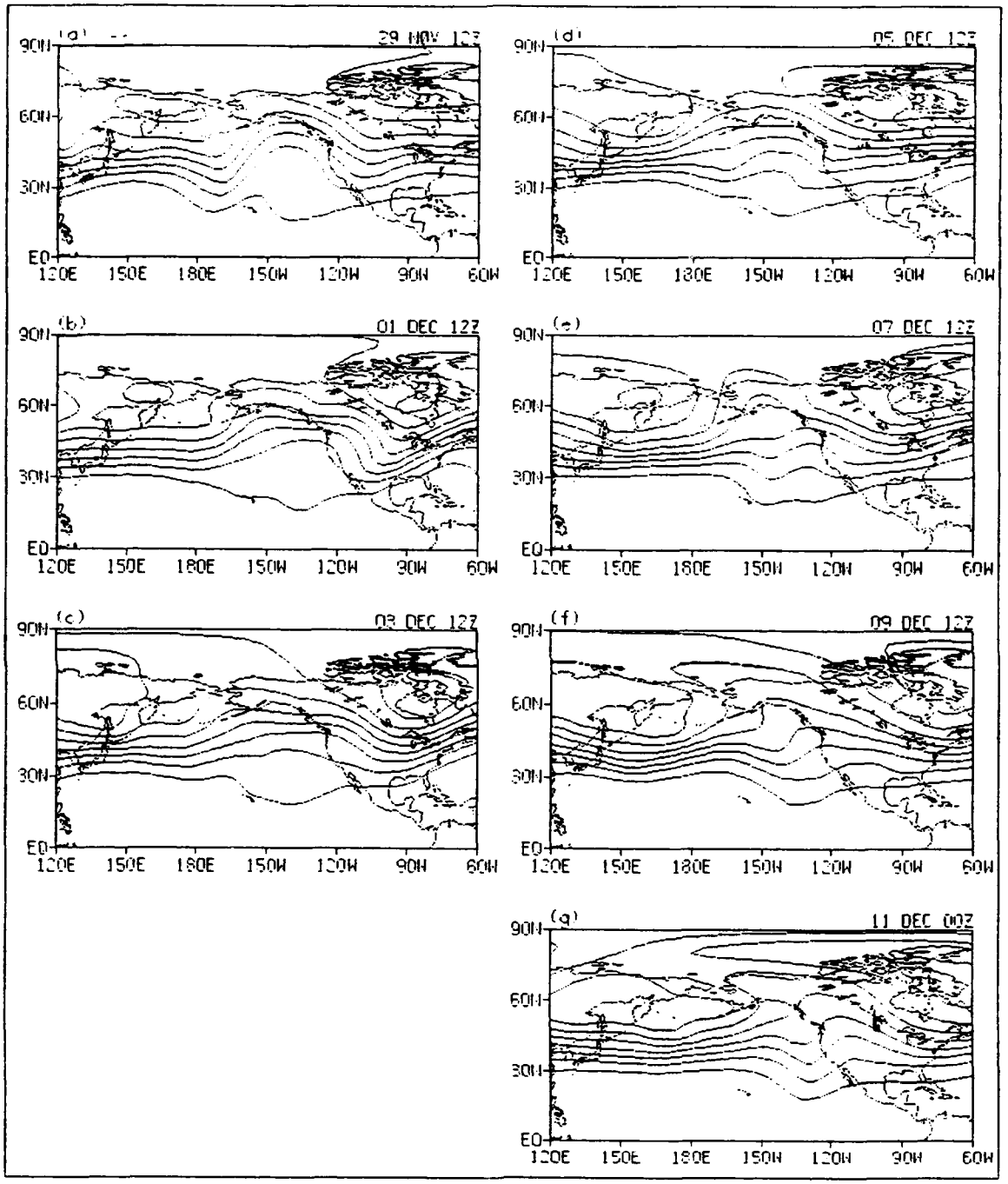

Figure 27. 200 mb geopotential heights at selected times for Forecast 2 NEGATIVE run. Minimum contour is 10500 gpm. Contour interval is 200 gpm.

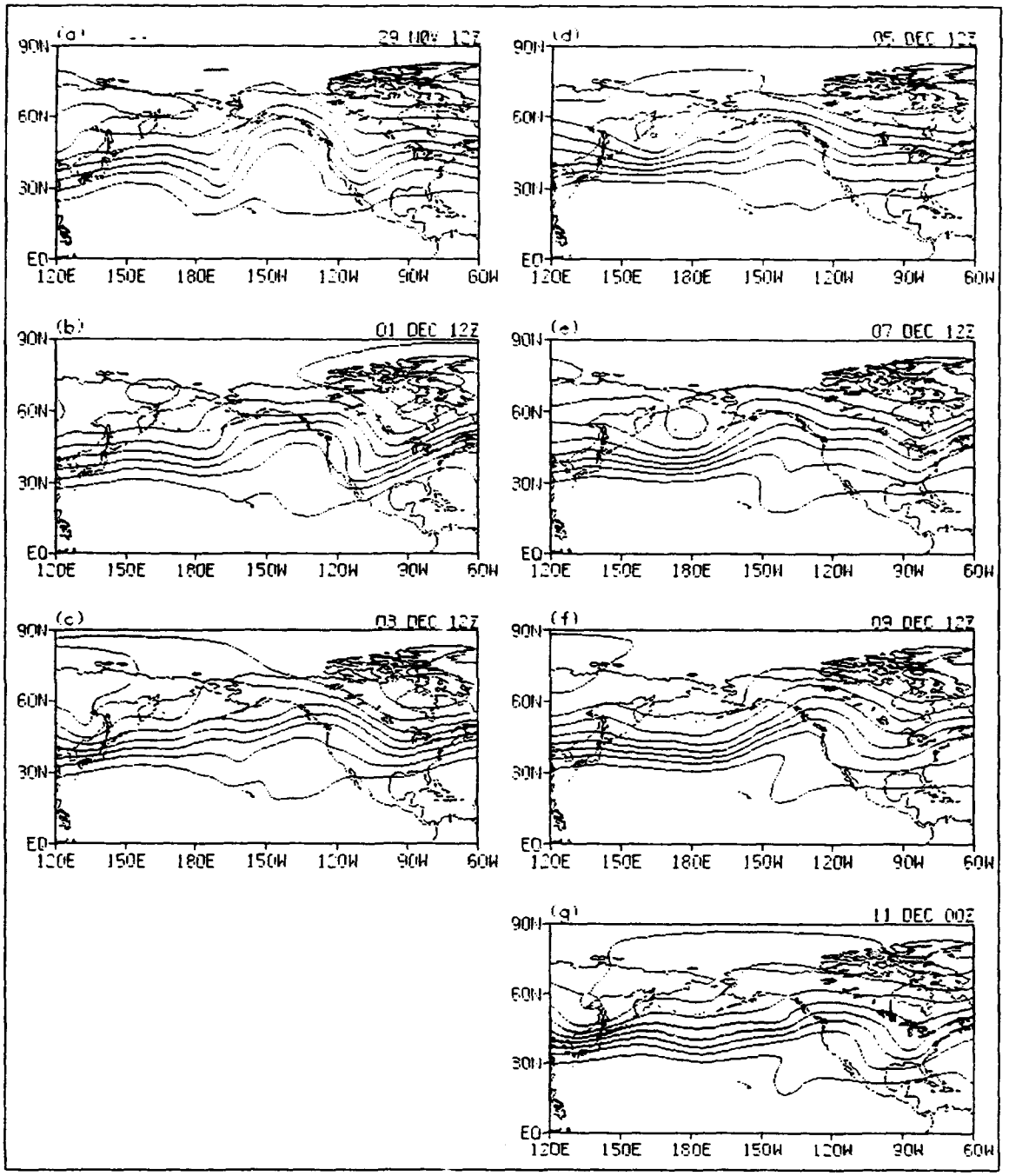

Figure 28. 200 mb geopotential heights at selected times for Forecast 3 NEGATIVE run. Minimum contour is 10500 gpm. Contour interval is 200 gpm.

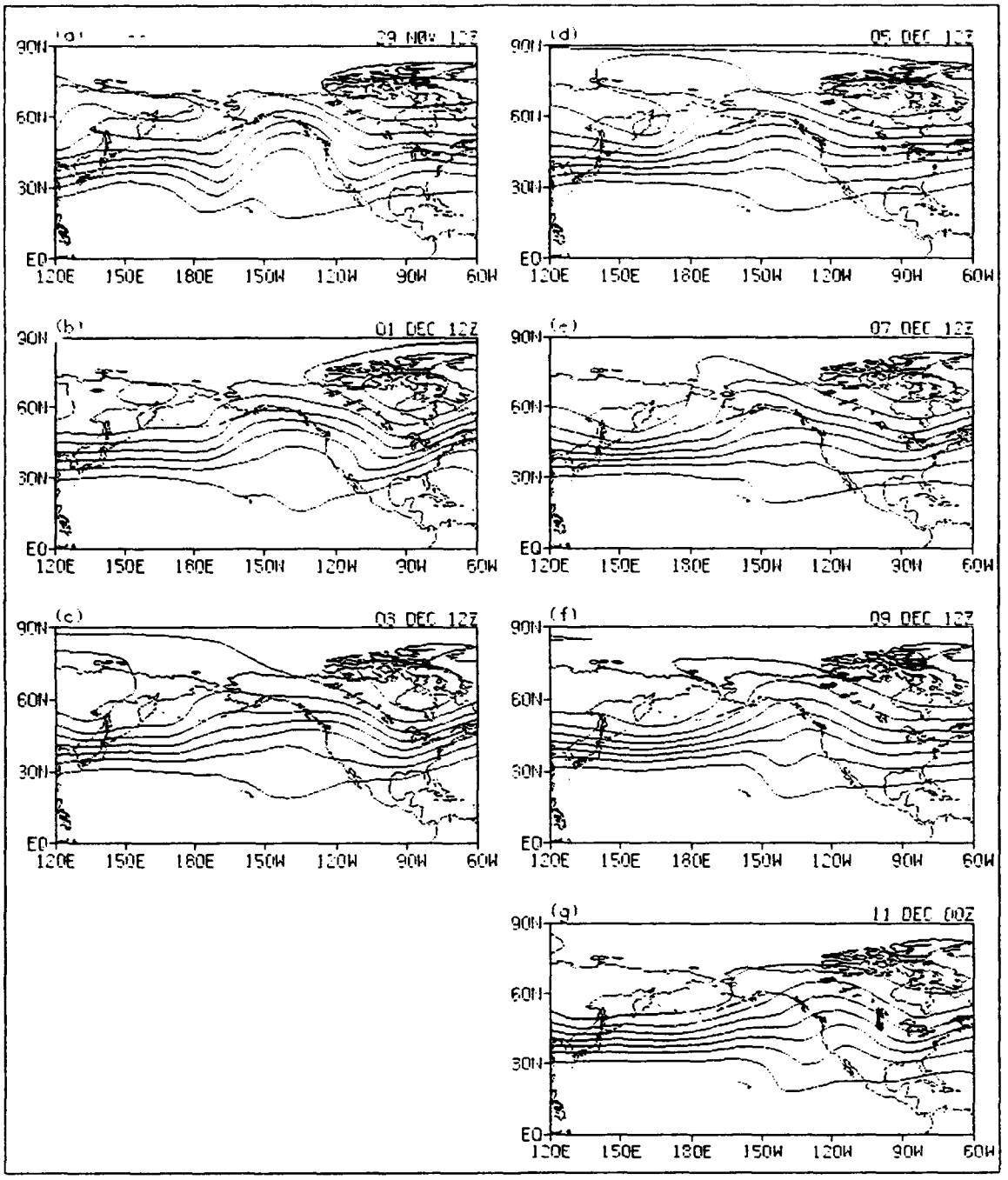

Figure 29. 200 mb geopotential heights at selected times for Ensemble Average NEGATIVE run. Minimum contour is 10500 gpm. Contour interval is 200 gpm.

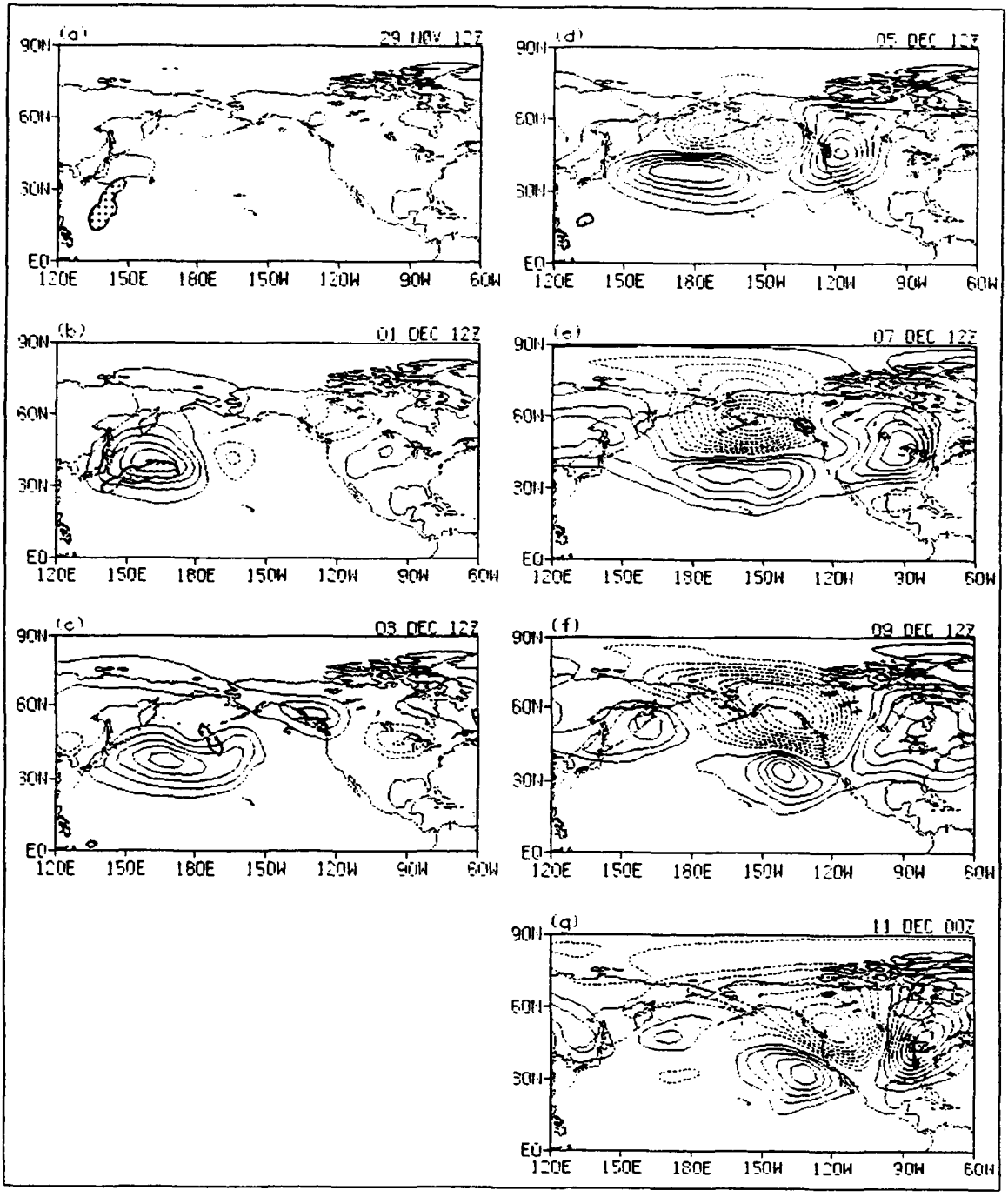

Figure 30. EA differences (POSITIVE-NEGATIVE) heating and 200 mb heights. Solid (dashed) contours represent positive (negative) height differences; contour interval is 50 gpm. Dotted areas shows heating difference > 5°C/day.

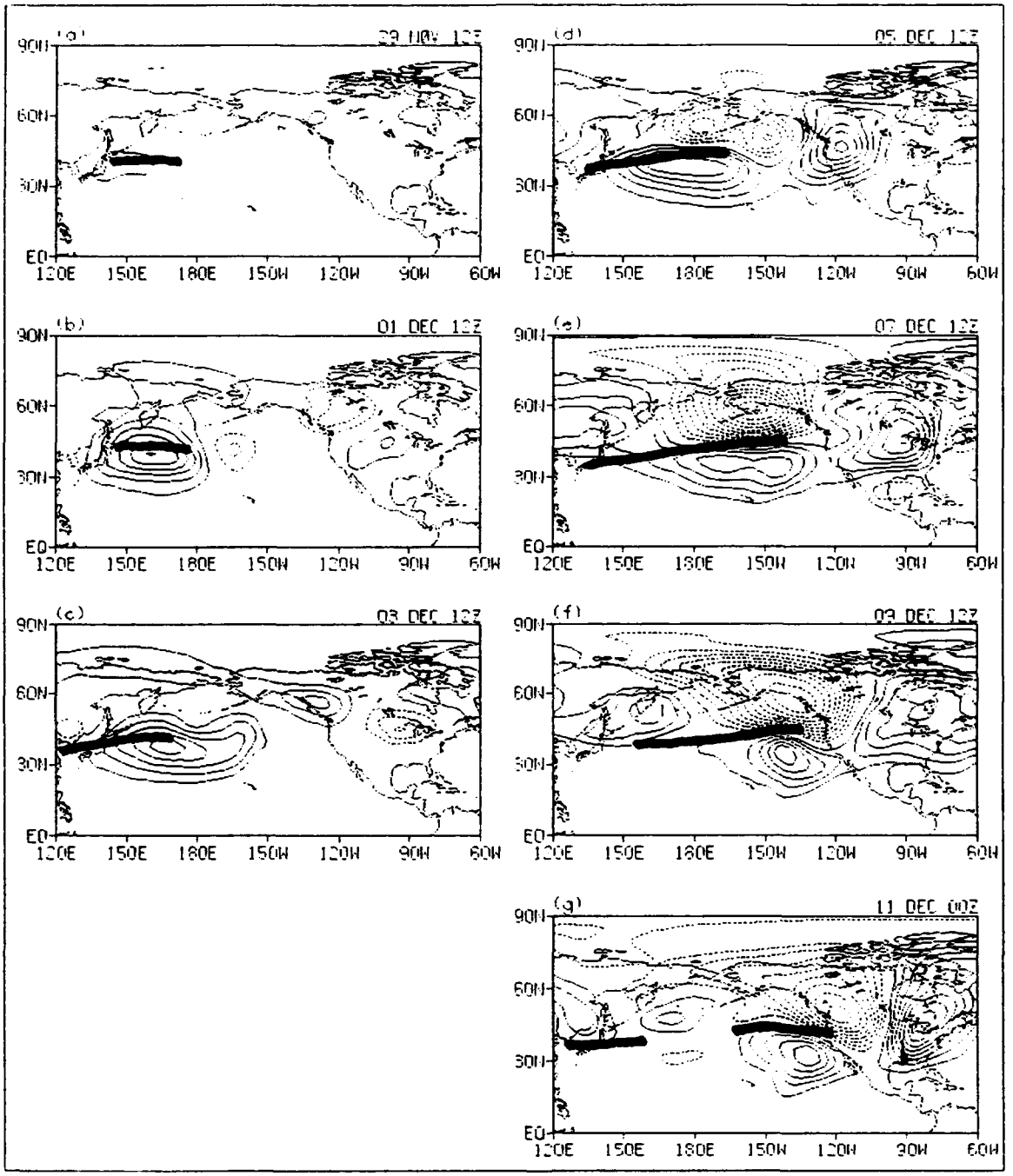

Figure 31. EA differences (POSITIVE-NEGATIVE) in 200 mb heights overlaid with POSITIVE 200 mb jet axis. Solid (dashed) contours represent positive (negative) height diffs; contour interval is 50 gpm. Jet (u >60m/s) is thick black line.

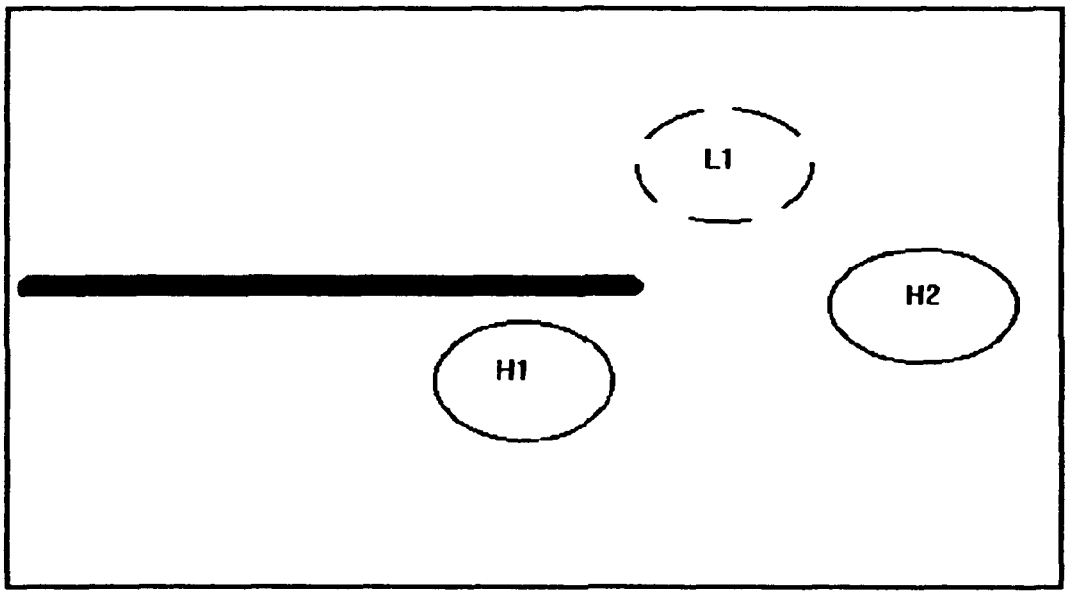

Figure 32. Schematic of 200 mb geopotential height responses (POSITIVE-NEGATIVE) and POSITIVE 200 mb jet. H1 is 1st positive height response, L1 is first negative height response, H2 is 2nd positive height response.

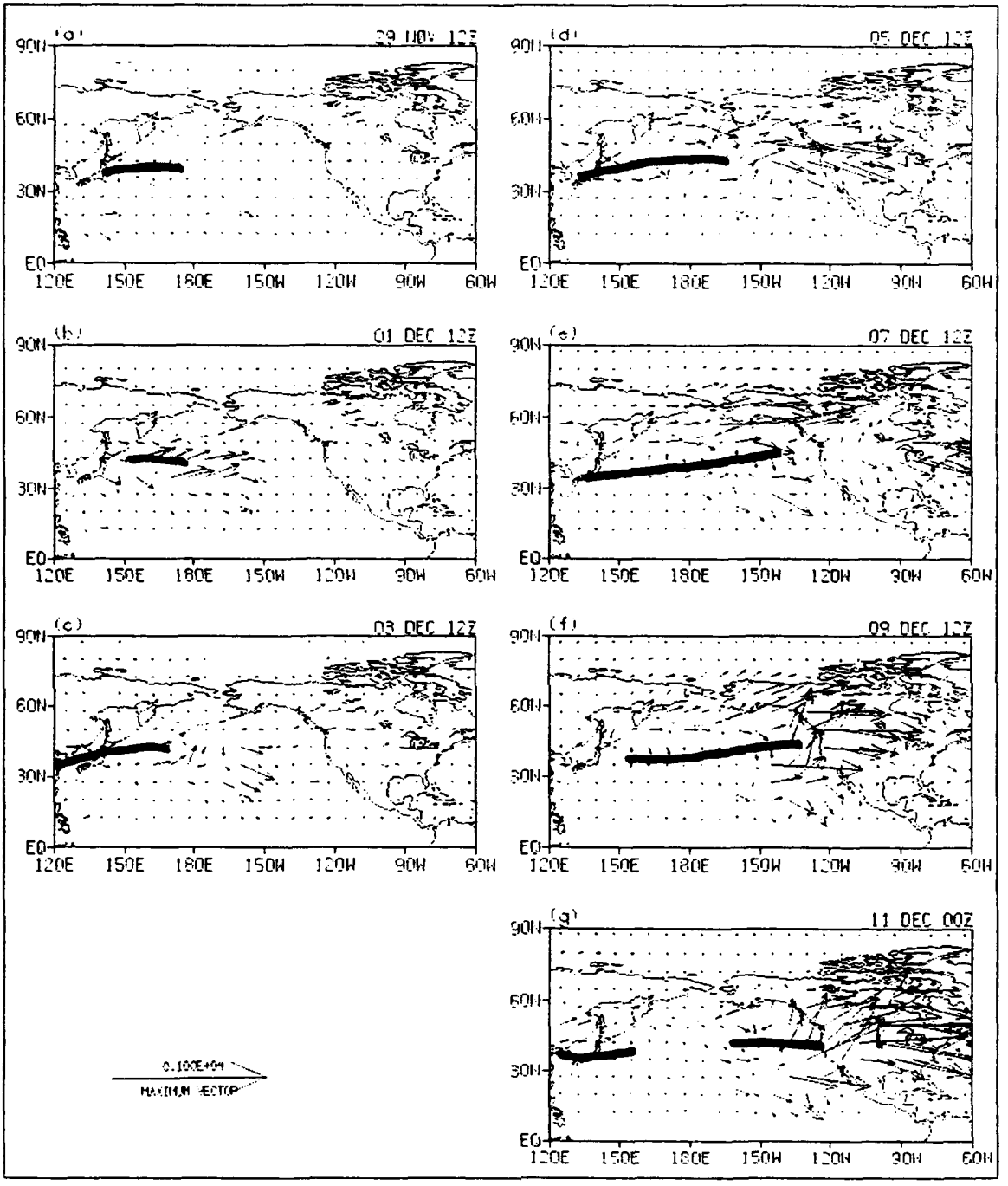

Figure 33. EA QG wave activity flux vectors (m^2/s^2) overlaid with POSITIVE 200 mb jet axis. Jet (u>60 m/s) is thick black line.

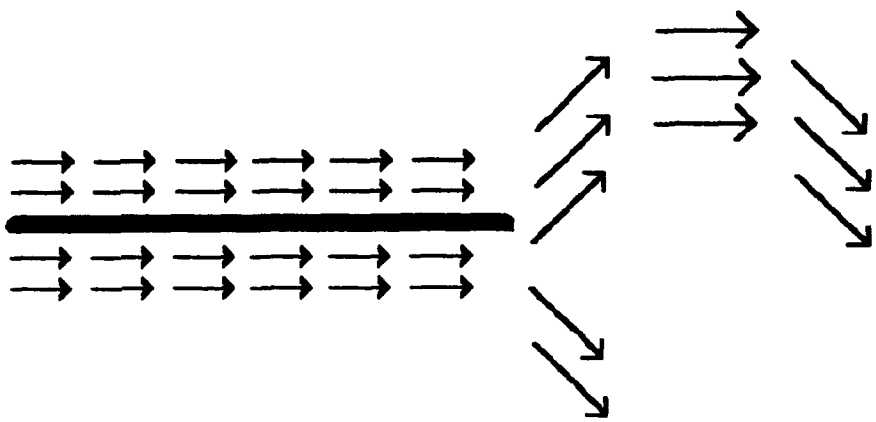

Figure 34. Schematic of waveguiding by the jet. Arrows are quasi-geostrophic wave activity flux vectors, indicating the propagation of wave energy.

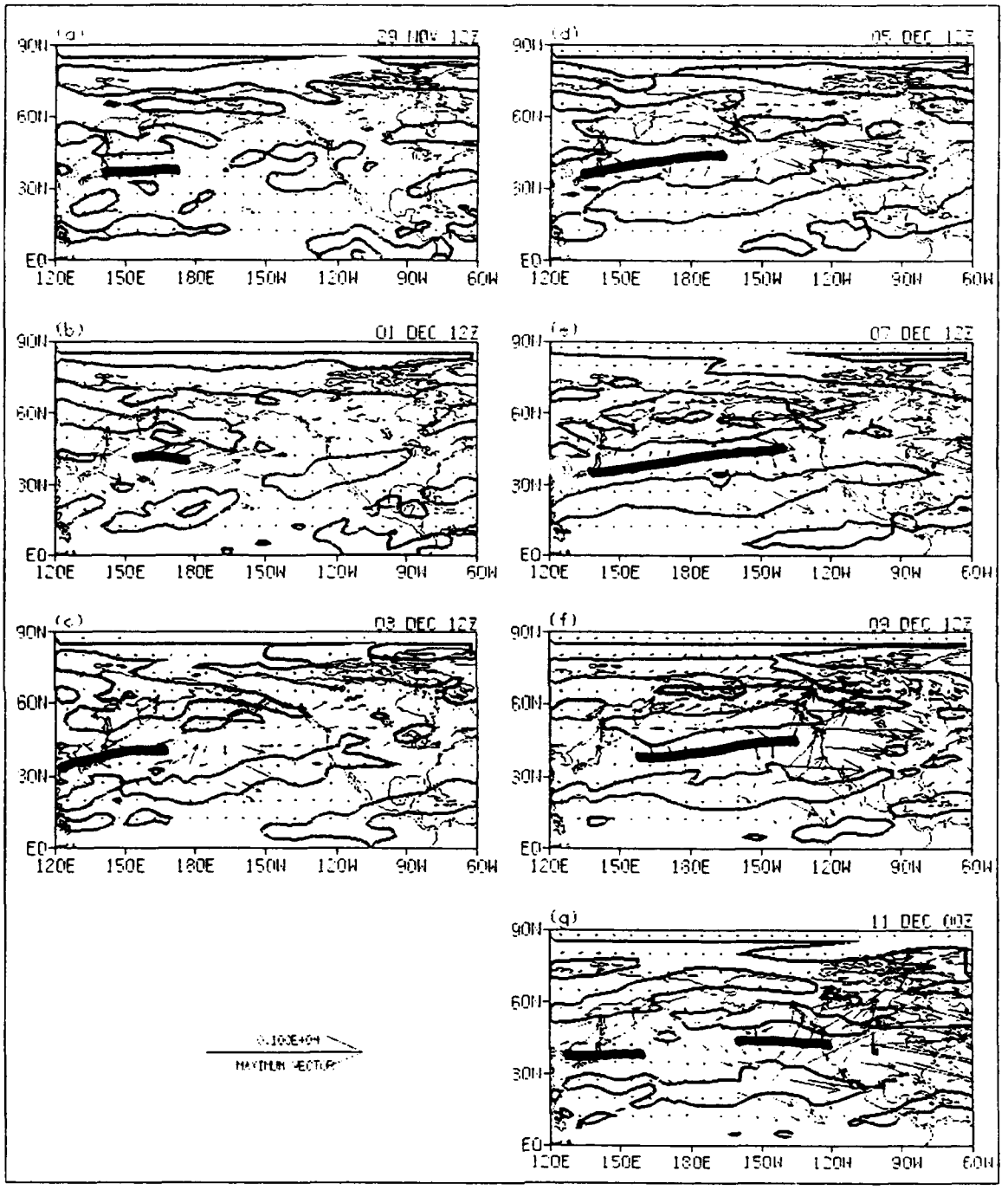

Figure 35. EA QG wave activity flux vectors (m^2/s^2) overlaid with POSITIVE 200 mb jet axis and POSITIVE 200 mb potential BTI. Jet (u>60 m/s) is thick black line. BTI contour is 0 $m^{-1}s^{-1}$.

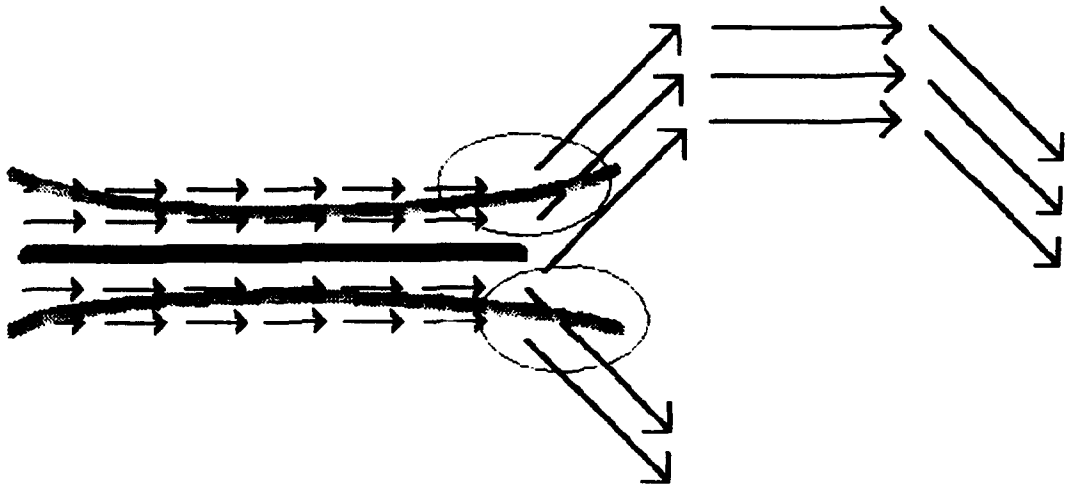

Figure 36. Schematic of wave energy amplification in areas of potential BTI. Jet is thick black line. Areas of potential BTI denoted by gray lines. Source regions denoted by oval shapes.

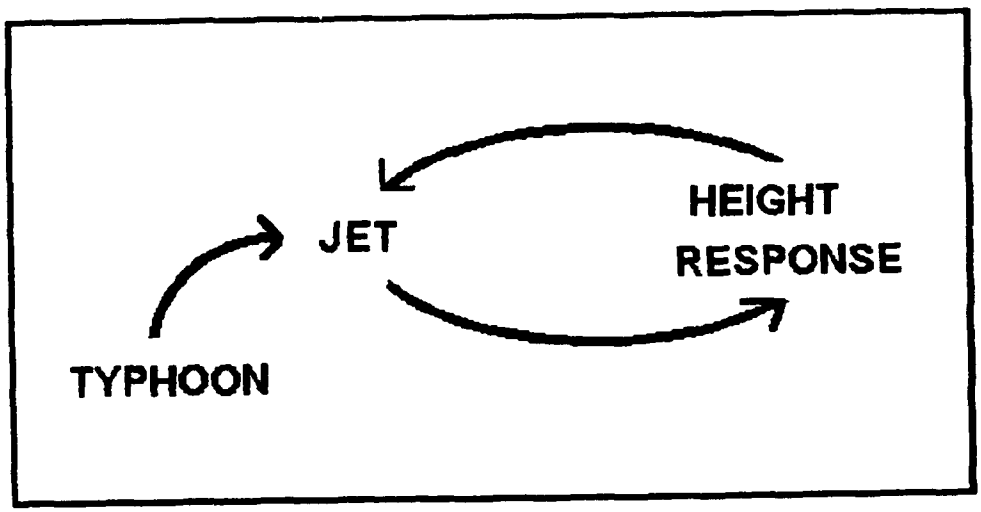

Figure 37. Schematic of feedback mechanism linking the tropical cyclones, midlatitude westerly jet, and wave/height responses.

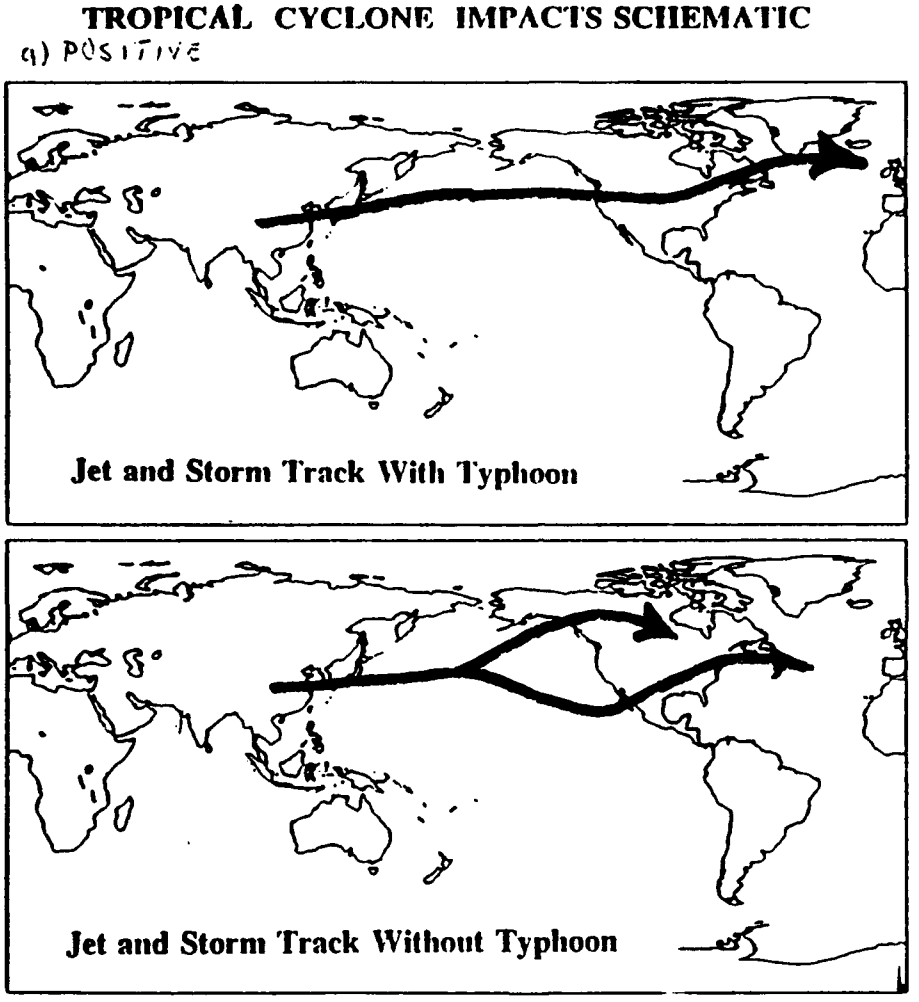

Figure 38. Schematic of forecast 200 mb jet at end of study period for: (a) POSITIVE run, (b) NEGATIVE run.

INITIAL DISTRIBUTION LIST

		No. Copies
1.	Defense Technical Information Center Cameron Station Alexandria VA 22304-6145	2
2.	Library, Code 052 Naval Postgraduate School Monterey CA 93943-5002	2
3.	Oceanography Department Code OC/CO Naval Postgraduate School 833 Dyer Rd Rm 331 Monterey CA 93943-5122	1
4.	Meteorology Department Code MR/HY Naval Postgraduate School 589 Dyer Rd Rm 252 Monterey CA 93943-5114	1
5.	Dr. James Thomas Murphree Code MR/ME Naval Postgraduate School 589 Dyer Rd Rm 252 Monterey CA 93943-5114	3
6.	Lt. Stephen C. Woll, USN 3736 Stumpy Lake Lane Virginia Beach VA 23456	1
7.	Director Naval Oceanography Division Naval Observatory 34th and Massachusetts Avenue NW Washington DC 20390	1
8.	Commander Naval Oceanography Command Stennis Space Center MS 39529-5000	1
9.	Commanding Officer Naval Oceanographic Office Stennis Space Center MS 39529-5001	1

10. Commanding Officer
Fleet Numerical Oceanography Center
7 Grace Hopper Ave Stop 4
Monterey CA 93943-0001-0120 — 1

11. Superintendent
Naval Research Laboratory
7 Grace Hopper Way Stop 2
Monterey CA 93943-5502 — 1